Geology and Geochemistry of Early Proterozoic Supracrustal Rocks from the northern Sangre de Cristo Mountains and adjacent areas, Central Colorado

by

Mark Sloan Thacker

submitted in partial fulfillment of the requirements for the degree of Master of Science in Geochemistry

New Mexico Institute of Mining and Technology

Socorro,New Mexico

May, 1988

ABSTRACT

The northern Sangre de Cristo Mountains and adjacent areas include a succession of variably deformed and metamorphosed volcanic and volcaniclastic rocks ranging in composition from basalt to rhyolite with intrusive gabbro/diabase sheets and dikes. The northern Sangre succession appears to be younger (1670-1710 Ma) than the Salida succession (1730 Ma) to the north, with the exception of the Sand Gulch area which may be the same age. The Garrel Peak-Cotopaxi (GPC) batholith (1670 Ma) intrudes this succession of supracrustal rocks along the northern side of the Arkansas River. Pendants and inclusions of the northern Sangre succession are found throughout the western margin of the batholith. Supracrustal rocks on the eastern side of the batholith, and extending as inclusions inward from the eastern margin, are migmatite-gneiss and represent remnants of the extensive early Proterozoic migmatite-gneiss complex along the Arkansas River east of Cotopaxi. This complex of dominantly clastic sediments is older (1740 Ma) than the northern Sangre succession so that it appears that the GCP batholith may have intruded along a major early Proterozoic lithologic boundary.

The supracrustal rocks of the northern Sangre

succession are metamorphosed to the amphibolite facies and the deformation increases to the southwest across the crest of the Sangre de Cristo Range. Mafic and andesitic rocks include pillow lavas, hyaloclastic breccias and gabbro/diabase sills and dikes. Felsic rocks are dominantly volcaniclastic sediments and ash-flow tuffs.

Unlike most other early Proterozoic successions of the southwest, the northern Sangre succession includes andesites that are similar in composition to modern continental-margin arc andesites. The mafic volcanics are tholeiites and when considered on tectonic discriminant diagrams such as Th-Ta-Hf, Ti-Y-Zr, Fe2O3-MgO-Al2O3 and MORB-normalized diagrams, they have affinities to modern arc-related basalts. In terms of trace element distributions and especially La/Yb-Yb, V-Zr, and Hf-Zr distributions, the northern Sangre felsic volcanics are similar to felsic rocks from continental-margin arcs and associated back-arc basins.

Geochemical modeling indicates that it is possible to relate the mafic to the intermediate rocks by fractional crystallization. The felsic volcanics appear to have been derived by partial melting of a tonalitic parent in the lower crust.

ACKNOWLEDGMENTS

There are many people to whom I owe thanks for helping make my graduate work successful and enjoyable. First I would like to thank my advisor Kent C. Condie for providing me the opportunity to do this project, partially funding the research and giving me the opportunity to present my research findings at the 1986 IGCP 217 summer field conference in Colorado. Mike Knoper and Tony Lanzirotti were very helpful with parts of the field work and in providing thought provoking discussions of Proterozoic geology. This project would not have been possible without the help and support of my parents during my undergraduate work and their continued moral support throughout the project. My fiance Lois Martin was the greatest help in dealing with the pressures of graduate life and editing this manuscript. A special thanks goes to my field assistant Socorro (pup), for his hard work and companionship throughout the field work.

TABLE OF CONTENTS

LIST OF FIGURES

LIST OF TABLES

INRTODUCTION

PREVIOUS WORK

The study area in this report has been mapped twice previously. Normand (1972) mapped the area as part of a doctoral dissertation at Texas Tech University. A reconnaissance geologic map of the Howard 7 1/2-minute quadrangle was done by Taylor etal. (1975) and a reconnaissance geologic map of the Cotapaxi 7 1/2-minute quadrangle was done by Taylor etal. (1975). Both these quadrangles were used as base maps for this study. Normand is the only geologist to do a detailed study of the northern Sangre de Cristo Mountains. His study focused primarily on the petrography and petrogenesis of the rock units. This study focuses on the geochemistry of the rocks and based on their geochemical signatures and more recent field reconnsissance by Condie, Bickford, Knoper, Lanzirotti and Thacker, the interpretation and classification of these rocks in this report is different than those of Normand.

LOCATION AND ACCESS

The study area includes approximately 15 square miles in southwest Fremont county, southern Colorado. Four 7 1/2-minute quadrangles (Howard, Bushnell Peak, Cotopaxi, Cameron Mountain) include portions of the study area (Fig.1). The best exposures of Precambrian rock occur along the crest of the northern Sange de Cristo Range from Simmons Peak southeastward to Galena Peak, the best access is from the eastern flanks of the range. The Garrel Peak Cotopaxi batholith, which contains numerous pendants and inclusions of supracrustal rocks, covers a large terrane north of the Arkansas River near Howard, Colorado, and extends eastward towards Canon City (Fig.1).

Access to the field area proved to be one of the greatest challenges of this project. To reach the best exposures of supracrustal rocks in the northern Sange de Cristo Range several backpacking trips of three to five days were required. The northwest boundary of the field area was reached by going south on Chaffee County Road 101 up Bear Creek, approximately 15 miles west of Howard. From the end of this road the Rainbow trail provides access to the Simmons Peak trail and the northwest portion of the study area. The central peaks of the range

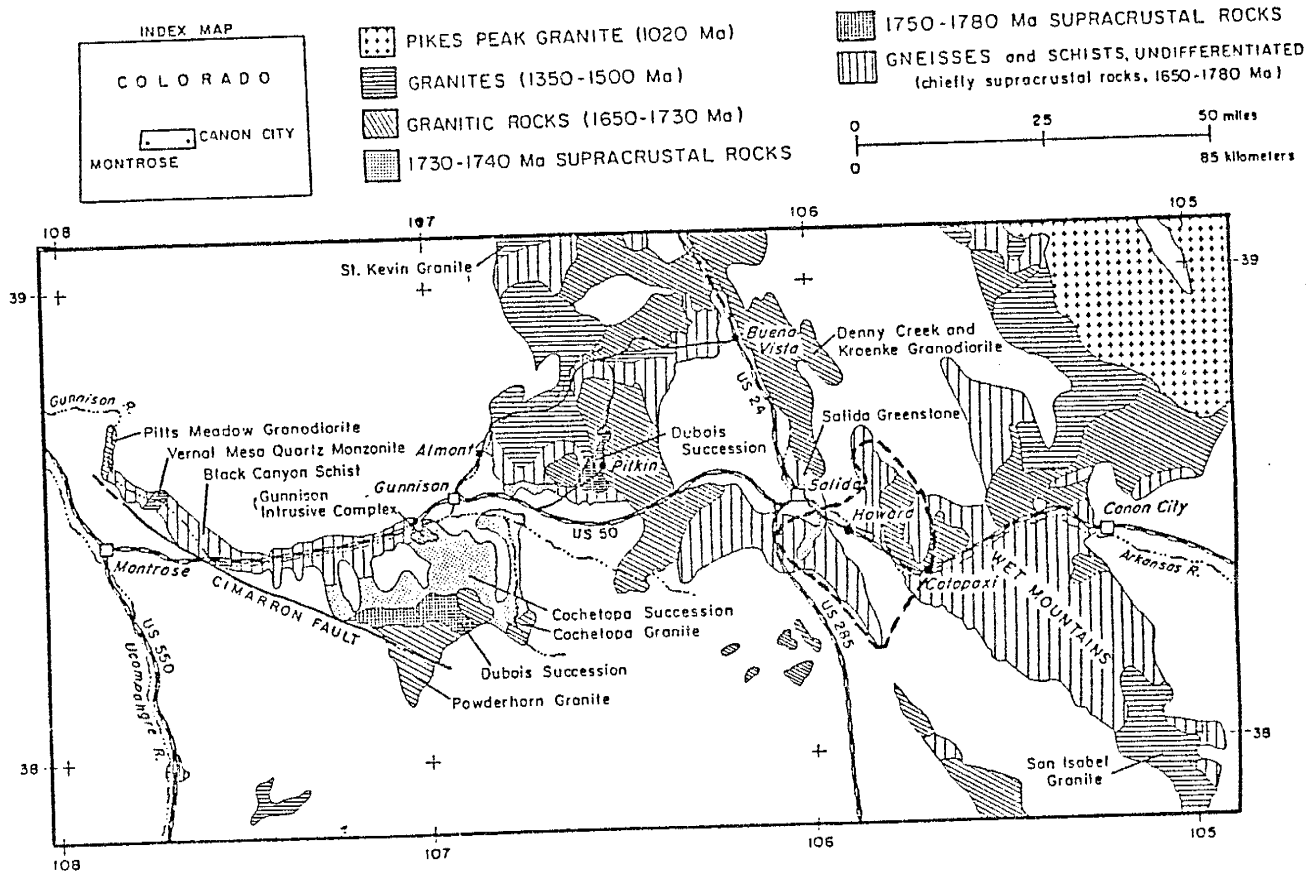

Figure 1. Generalized geologic map of Precambrian terrains in southern Colorado after Condie (1986). Dashed line: boundaries of study area.

(Hunts Peak, Red Mountain) are reached fromthe Howard Creek Road. From the parking area in the national forest, the Rainbow trail leads to the Hunts Peak trail which provides access to this portion of the field area. The southeastern section of the field area (Twin Sisters, Bushnell Peak, Galena Peak) is accessible from the Cherry Creek Road south from highway 50, approximately 2 miles east of Howard, Colorado. From the parking area take the Rainbow trail west to the Stout Creek lakes trail .

The western margin and parts of the interior of the GPC batholith are accessible from Sand Gulch north of the Arkansas River near Howard, this provides access to the areas around Copper Mountain and Burned Timber Mountain as well as Sand Gulch. Several unmarked forest roads along the northern side of the Arkansas River from Howard to Coaldale Colorado provide access to exposures of supracrustal inclusions within the batholith along Mitchell Gulch, Kiln Gulch, Alkali Gulch and Cedar Springs Gulch. The interior of the batholith is most easily reached from Bernard Creek near Cotopaxi Colorado, This approach gives access to good exposures near Park Mountain, Spruce Mountain, Indian Mountain , East Badger Creek and Gribbles Park.

GENERAL GEOLOGY

The northern Sangre de Cristo Mountains consist of approximately 2000 meters of exposed layered Precambrian metamorphic rocks. The greatest thickness of rock is exposed on the western side of the range. The eastern side of the range being essentially a dip slope which has been intensely disected by glacial and fluvial erosion. A major east-dipping normal fault crosses the range from south of Simmons Peak southwest to Red Mountain and numerous smaller faults can be recognized throughout the range (Fig.1a). Characteristic horizons within the succession can be traced across most of the Precambrian exposure. A large portion of the northern flank of Red Mountian appears to have been hydrothermally altered giving it a redish appearance. All of the units in the area strike approximately N30W and dip about 35 degrees to the northeast except were major faulting causes dips to steepen.

The metamorphic rocks in the northern Sangre succession consist of interlayered volcanic and volcaniclastic rocks ranging in composition from basalt to rhyolite with intrusive gabbro/diabase dikes and sills. Metamorphism in the area reaches amphibolite grade, as indicated by the mineralogy of the mafic rocks, and the grade of metamorphism appears to increase to the southwest or crest of the range where the rocks become

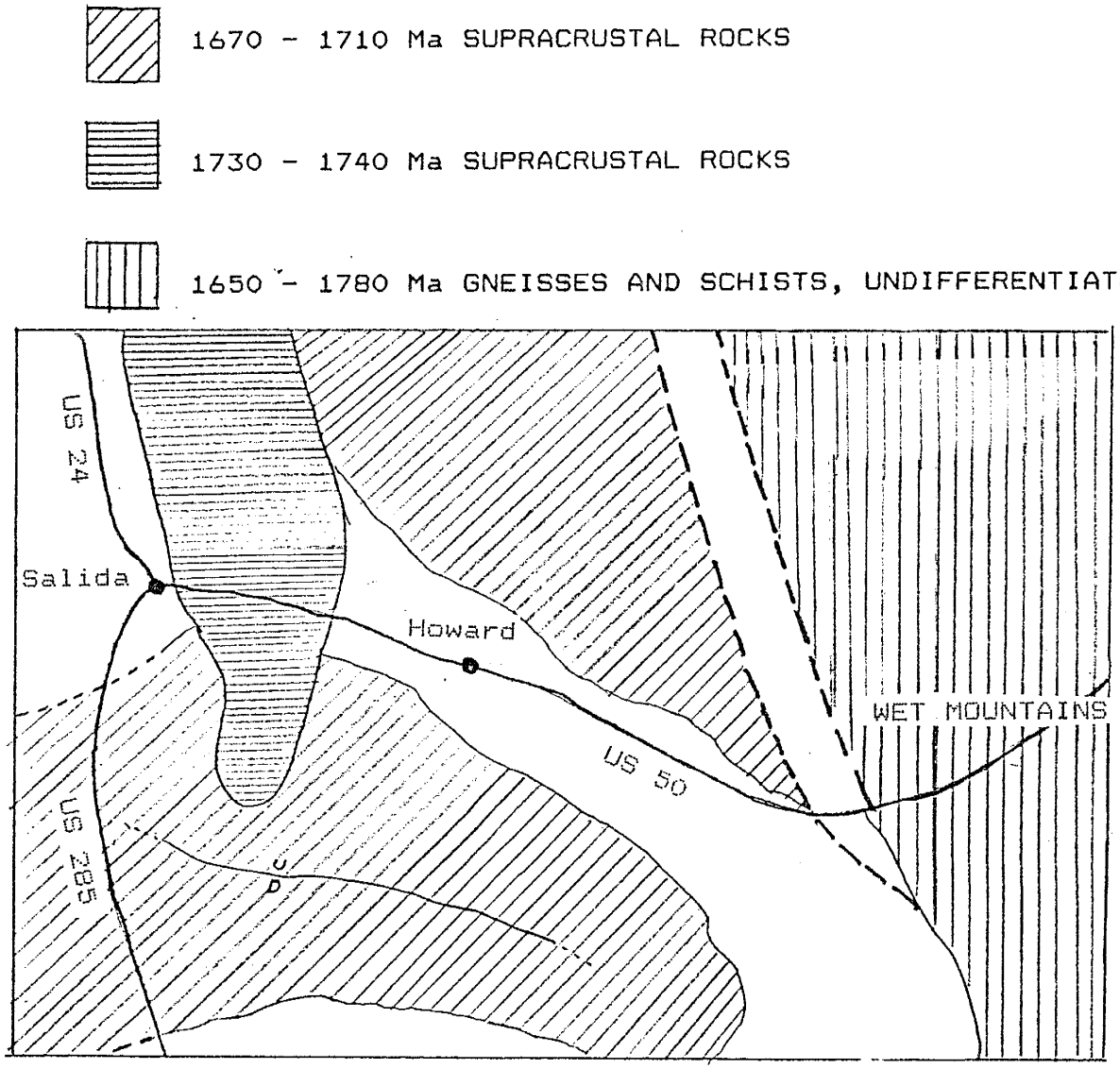

Figure 1a. Generalized geologic map of Precambrian rocks in the northern Sangre de Cristo Range and adjacent areas. Dashed lines represent possible location of lithologic boundary between clastic sedimentary terrane to the east and volcanic terranes to the west. Not shown is the GPC batholith (1670 Ma) which intrudes portions of all of these terranes.

increasingly gneissic in character. Many of the rock units have a pronounced foliation that is parrallel to compositional layering and imparts a bedded appearance to most of the outcrops.

Along the eastern side of the Arkansas river near Howord are exposures of layered Precambrian metamorphic rock, the best of which can be seen in the Sand Gulch area. Intruding into this succession of dominantly volcanigenic rocks is the Garrel Peak Cotopaxi batholith dated at 1670 Ma (Silver and Barker, 1968). The batholith ranges in composition from granodiorite to quartz monzonite and is often foliated along its margins. Throughout the batholith nuwerous roof pendants and xenoliths of the older volcanic terrrane are found. Xenoliths range in size from .25 m in diameter to over a 1 km and are widely dispersed with some areas of the batholith containing large populations of xenoliths while others areas are nearly devoid of them.

The rocks of the Sand Gulch area are also volcanic in origin and range in composition from basalt to rhyolite, with intrusive gabbro/diabase dikes and sills. These rocks have also undergone amphibolite-facies metamorphism but appear slightly less metamorphosed than similar exposures in the northern Sangres. Many of the units in the Sand Gulch area are foliated parallel to compositional layering and have a bedded appearance in outcrop. Do to the intrusion of the Garrel Peak Cotopaxi

batholith limited exposures of outcrop are available for study and tracing of units for more than 300 m is not generally possible. Major faulting or folding cannot be recognized with the limited exposure but numerous small high to low angle faults are present throughout the area. The textures and structures found in this sequence of rocks are similar to the rocks exposed in the northern Sangre de Cristos but correlation of stratigraphy is not possible between the two areas and correlation based on radiometric dates is not yet availiable.

Both the northern Sangre de Cristo and Sand Gulch successions show many similarities to the Salida volcanic terrane mapped by Boardman (1976). Despite the similarities between these terranes and the Salida terrane, radiometric dates from the Howard area by Bickford (1983), using the U-Pb method on zircons from felsic tuffs, indicate that it is younger (1670-1710 Ma) than the Salida terrane (1730 Ma). Dates are not yet available for the Sand Gulch area so that its relation to both the Sangre and Salida terranes is in question.

VOLCANIC ROCKS

GENERAL DESCRIPTION

The northern Sangre de Cristo succession is comprised of a thick sequence (more than 2000 m of exposed rock) of interlayered mafic, intermediate and felsic volcanogenic rocks along with intrusive gabbro/diabase dikes and sills. Although metamorphism and deformation have destroyed many of the primary textures, careful field studies reveal an abundance of volcanic textures which include primary bedding, hyaloclastic structures, fiame, amygdules and pillow basalts.

Along the crest of the range characteristic horizons such as the reddish horizon seen making up the northern portion of Red Mountain can be traced east-west along strike for up to 3 km, although individual lithologies within the horizons are difficult to distinguish for more than 500 m. There is a dominant NW-SE foliation in many of the units that parallels bedding or compositional layering.

The mafic rocks in the area consist of basalt flows, amygdaloidal and pillow basalts, hyaloclastic breccias and gabbro/diabase dikes and sills. Because of the degree of metamorphism and lack of primary textures, lavas and hyaloclastites are often difficult to distinguish from one another. The gabbro/diabases are distinguished by

there coarse grained nature, intrusive relationships and ophitic textures. Basalts are often fine grained gneissic rocks with pronounced foliation caused by aligned biotite; many are hornblende rich and also contain plagioclase phenocrysts. Amygdaloidal and pillow basalts are rare occuring only in the northwestern and northeastern parts of the field area. Where pillow structures occur they are small (<60 cm) and only recognizable in a few areas. Hyaloclastites, when identifiable, contained both rounded and angular volcanic fragments ranging in size from <1cm to >3 cm in a medium to fine grained, often phenocryst poor, matrix.

Andesites in the area are rare and due to the degree of metamorphism difficult to distinguish from metasediments that are andesitic in composition. Where good exposures occur andesites are fine grained, relatively non-foliated, have relic plagioclase phenocrysts. They appear to represent flows. Other units that are andesitic in chemical composition are believed to represent metasediments. They are fine grained, well foliated, micaceous, generally contain plagioclase and amphibole and often appear to have relic bedding.

Felsic rock include rhyolites, rhyodacites and dacites, many of which have been completely recrystallized. All units are characterized by adundant feldspar and quartz and contain highly variable proportions of crystal clasts, phenocrysts, lithic

clasts and matrix. The felsic rocks occur as massive ash-flow tuffs and volcaniclastic sediments. The massive tuffs are fine grained, phenocryst poor and in some cases contain fiame. The felsic volcanics are often gneissic in character and contain variable amounts of anhedral crystal clasts, euhedral phenocrysts and lithic clasts. The majority of the lithic clasts are rounded, some are angular, and most have been greatly elongated. They range in size from <1cm to >6cm and are often parallel to contacts and bedding in the host rock.

The gabbro/diabases are medium to coarse grained, hornblende rich and in some areas have relic ophitic textures preserved. Both concordant and discordant dikes and sills are seen throughout the area and occasionally chilled margins are recognized.

PETROGRAPHY

The rocks of the northern Sangre sucession can be classified into mafic (30%), intermediate (<10%) and felsic (30%) volcanic and volcaniclastic rocks with intrusive gabbro/diabase (25%) dikes and sheets. Medisedimentary rocks of intermediate composition occur but make up <5% of the section. Petrographic study of 23 thin sections showed the following alteration products were common to all of the units: (1) sericite after feldspar and (2) epidote and chlorite after biotite and hornblende. The following textures were observed during thin section study and reflect different metamorphic histories or different metamorphic effects: (1) biotite, hornblende and muscovite as alligned minerals producing a well developed foliation, (2) quartz, plagioclase, hornblende and cordierite forming granoblastic textures, (3) muscovite, hornblende, biotite and plagioclase showing poikiloblastic textures (Normand, 1972). The petrography of each group is summarized in the following sections.

Mafic Rocks

The mafic volcanic and volcaniclastic rocks comprise approximately 30% of the successions studied. Outcrops are generally continuous along strike for several hundred meters with individual flows ranging from <1 meter to over 10 meters in thickness. Flows are somewhat laterally variable as to grain size and crystal content. In hand specimen, mafic rocks range from medium to fine grained and are dominated by hornblende and plagioclase. Most of the minerals in the mafic rocks have equilibrated to amphibolite-facies conditions. Exceptions include relic plagioclase phenocrysts and late alteration and retrograde minerals such as chlorite and sericite. Hornblende is the most abundant mineral in all the mafic rocks, ranging from 30% - 70%, and often appears to be pseudomorphous after pyroxene. It generally occurs as bladed crystals ranging from .1 mm to 2 mm in length and averaging .6 mm. Fine-grained anhedral granular and poikiloblastic hornblende occurs in some sections. Plagioclase (An30) is the other dominant mineral, ranging from 10% - 40%. It occurs as tabular bladed or lath shaped, generally euhedral crystals ranging in size from .1 mm to >3 mm, averaging .4 mm, and is commonly sericitized. Occasionally relic zoning is seem in phenocrysts. Quartz occurs in amounts varying from <<10%

to ~15%, is generally <.2 mm in length and has anhedral grain boundaries. In many minerals the grain boundaries have been coroded by metamorphism. Other minerals occuring in varying amounts, generally <10% and often only as trace constituents, are cordierite, biotite, calcite, epidote, opaques, shene, garnet, microcline, pyroxene, chlorite and sericite.

In thin section, basalts are characterized by their fine-grained nature, simple mineralogy containing approximately subequal amounts of hornblende and plagioclase with other minerals making up <10% of the rock and lack of matrix. The volcaniclastic rocks have approximately the same mineralogy but are characterized by greater abundances of non-volcanigenic quartz, biotite and calcite.

Intermediate Rocks

The intermediate rocks comprise <10% of the section and occur as andesites and volcaniclastics with outcrops ranging from 1-10 meters in thickness. In hand specimen they are typically fine to medium grained and contain abundant quartz, plagioclase and biotite. Quartz ranges from 30% to 60%, generally occurs as euhedral crystals <2 mm in diameter with mozaic to granoblastic textures. Plagioclase ranges from 20% - 60%, averaging 40%, phenocrysts up to 4 mm in length are seen in some sections with the average being .2 mm and most are tabular with euhedral boundaries.Biotite ranges from 25% to 40% and occurs as lath shaped crystals up to 1 mm in length, averaging .3 mm. Other varietal and accessory minerals include calcite, opaques, garnet, epidote, hornblende, microcline, k-spar and sericite. The andesites are characterized petrographically by relict plagioclase phenocrysts and lesser abundances of biotite. The volcaniclastics have greater abundances of biotite, that in most cases defines a pronounced foliation and contain more matrix with minerals such as calcite and sericite present.

Felsic Rocks

Felsic volcanic and volcaniclastic rocks comprise around 30% of the section and occur as massive tuffs, ash flow tuffs, and volcaniclastic breccias. Individual flows range from 1 meter to over 20 meters in thickness, and are generally laterally continuous along strike for several hundred meters. Volcanic rocks show a range of textures from fine grained massive tuffs to coarse grained lithic rich breccias. All the felsic rocks contain quartz and feldspar as their dominant mineral constituients.

The massive tuffs are very fine grained with a dominantly quartz and plagioclase matrix making up 70% - 90% of the rock. Do to the fine grained nature of many of the rocks exact proportions of the matrix minerals cannot be determined but include biotite (1% - 20%), cordierite, opaques, calcite, epidote, muscovite, sphene, zircon and apatite. The matrix is generally composed of anhedral and equigranular minerals that are uniformally distributed throughout the rock. Plagioclase phenocrysts up to 2 mm in length occur in the tuffs in varying amounts (up to 50%) with most averaging <.6 mm in length. They are generally unaligned and evenly distributed throughout the rocks.

Felsic volcaniclastic rocks are mineralogically very

similar to the tuffs; they range from fine to medium grained and contain variable amounts of crystal and lithic clasts. They characteristically contain aligned biotite laths defining a foliation. Other varieties, encountered near the crest ot the Sangres range, contain rounded eye-like structures ranging from 5 mm to 5 cm in diameter that are composed dominately of fibrous needle-like masses of sillimanite formed during metamorphism from muscovite and quartz. Micaceous stringers and multigranular aggregates occur in some thin sections and reflect significant strain during metamorphism. Highly elongated lithic clasts up to 15 cm in length are observed in the field, but in thin section those of only a few millimeters are difficult to distinguish from matrix.

Gabbro/diabase Rocks

Gabbro/diabase sheets and dikes comprise up to 20% of the section. They occur as large intrusive bodies up to 1 square kilometer in diameter in the case of Simmons Peak, but are generally between 1 and 30 meters thick. They occur as sheets that are concordant with the surrounding units and are often traceable along strike; in a few cases they have recognizable chilled margins. Many smaller dikes that are discordant and pinch out are found throughout the area. In hand specimen they are medium to coarse grained and hornblende and plagioclase are the dominant minerals. Hornblende occurs as lath shaped crystals averaging .5 mm in length and varies in abundance from 40% - 60%. Plagioclase generally occurs as euhedral lath shaped crystals, up to 2 mm in length in relict ophitic textures and varies in abundance from 35% - 60%. Accessory minerals include magnetite, biotite, sphene, quartz and apatite.

GEOCHEMISTRY

GENERAL

Metamorphism to the amphibolite facies occurs throughout the area as indicated by the mineralogy of the mafic rocks which typically contain hornblende + andesine + garnet + quartz. Inferred temperatures and pressures are around 500 °C and 3.5 kb respectively. This along with diagenesis, alteration, and weathering have the potential to cause significant chemical changes, among both the major and trace elements. Samples from the northern Sangre succession have been evaluated using alteration screens such as the major element diagram proposed by Davis et al. (1979) (Fig.2). On this diagram, most of the samples fall within the boundaries of the unaltered field. This along with the fact that the parent rocks were principally of igneous origin lends confidence to the accuracy of the chemical analysis. The large ion lithophile (LIL) elements Sr, K, Rb, Ba and Th do show evidence of mobilization and were not used in geochemical modeling.

When the volcanic and volcaniclastic rocks of the northern Sangre de Cristo area samples are plotted on the Nb/Y vs. Zr/TiO2 and Nb/Y vs. SiO2 discrimination diagrams of Winchester and Floyd (1977) (Fig.3) they include rhyolites, rhyodacites, andesites, and basaltic

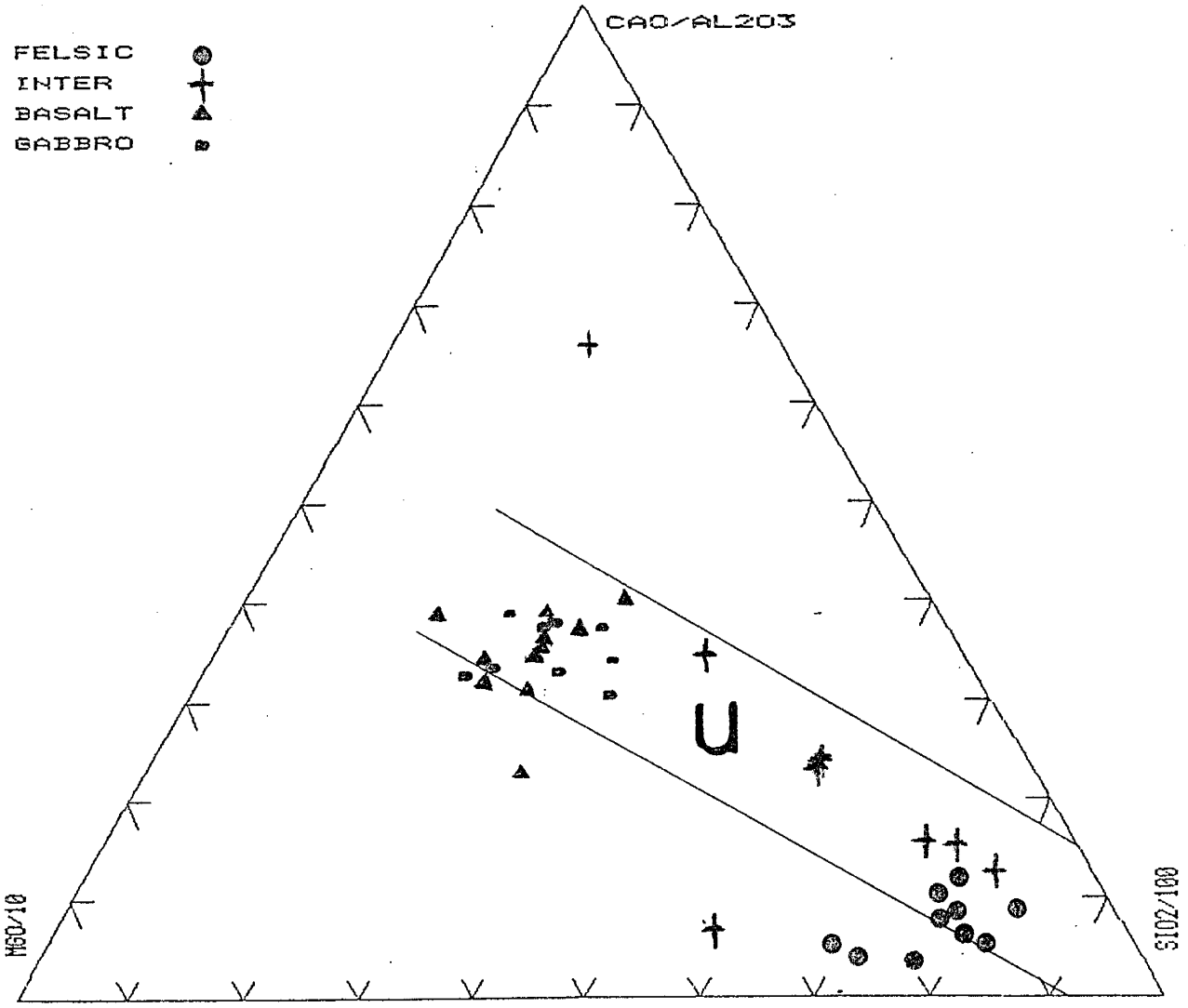

Figure 2. Distribution of northern Sangre de Cristo area samples on MgO/10 - SiO2/100 - CaO/Al2O3 alteration screen. Fields after Davis, et al. (1979), U: unaltered volcanic rocks.

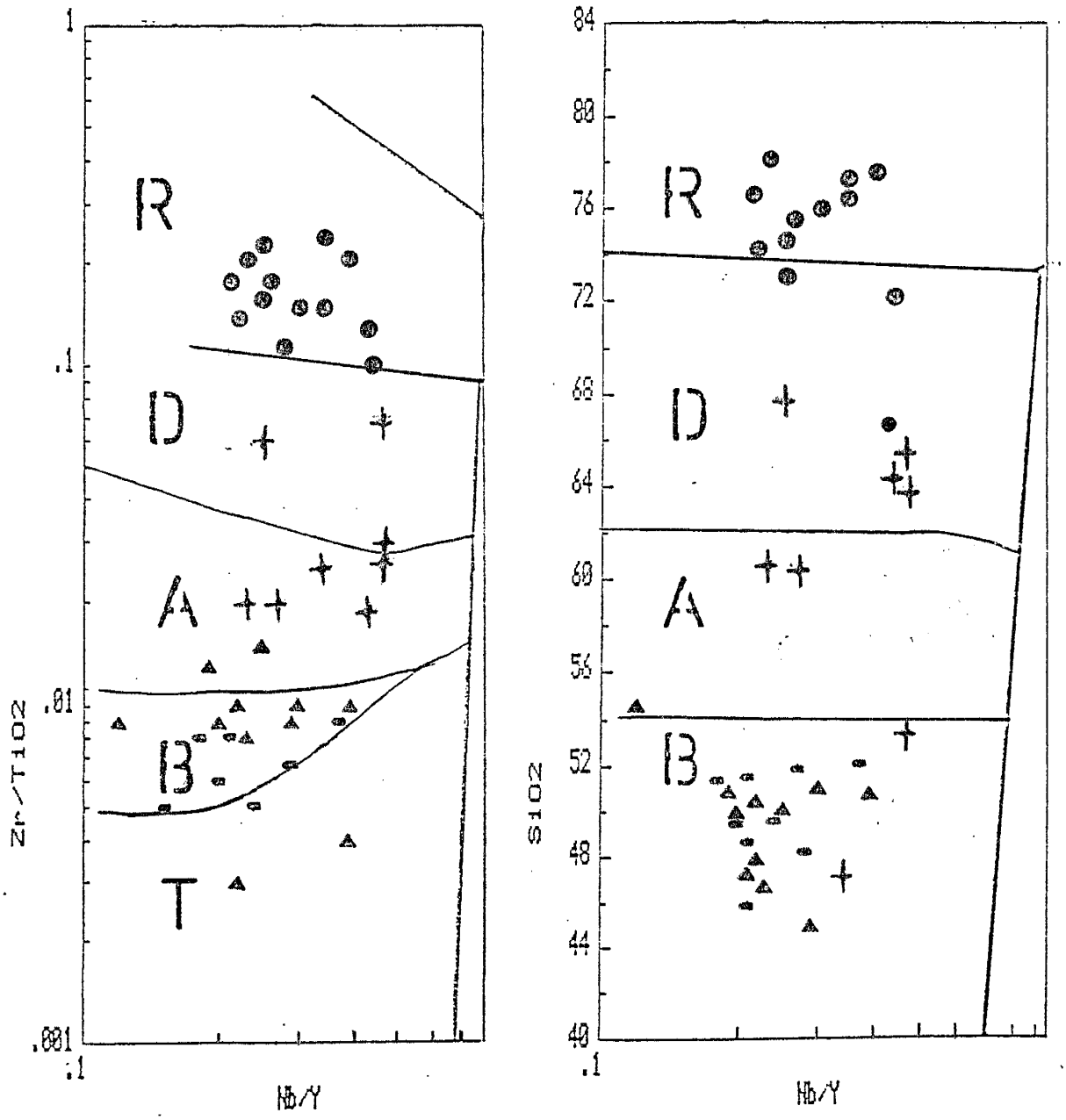

Figure 3. Classification of northern Sangre de Cristo volcanic rocks on Nb/Y vs. Zr/TiO2 and Nb/Y vs. SiO2. Fields from Winchester and Floyd (1977), R: rhoylite, D: rhyodacite, dacite, A: andesite, B: basaltic andesite, sub-alkaline basalt, T: tholeiite, ● : Felsic volcanic rocks, + : Intermediate volcanic rocks, ▬ : Basalt, ▲ : Gabbro.

andesites/subalkaline basalts. Unlike most other early Proterozoic successions in the Southwest, andesites are present in the area although minor in volume in comparison to the mafic and felsic endmembers. The mafic rocks are dominantly tholeiitic and the felsic rocks calc-alkaline on both the Jensen cation plot (Jensen, 1976; Fig.4) and the AFM plot (Irvine and Baragar, 1971; Fig.5). Figure 6 shows the suite of samples plotted on the Zr vs. TiO2 diagram of Pharoah and Pearce (1984). The mafic rocks are mostly primitive and along with the intermediate rocks show arc affinities. The felsic rocks generally fall outside of the arc field boundary showing a more within-plate character.

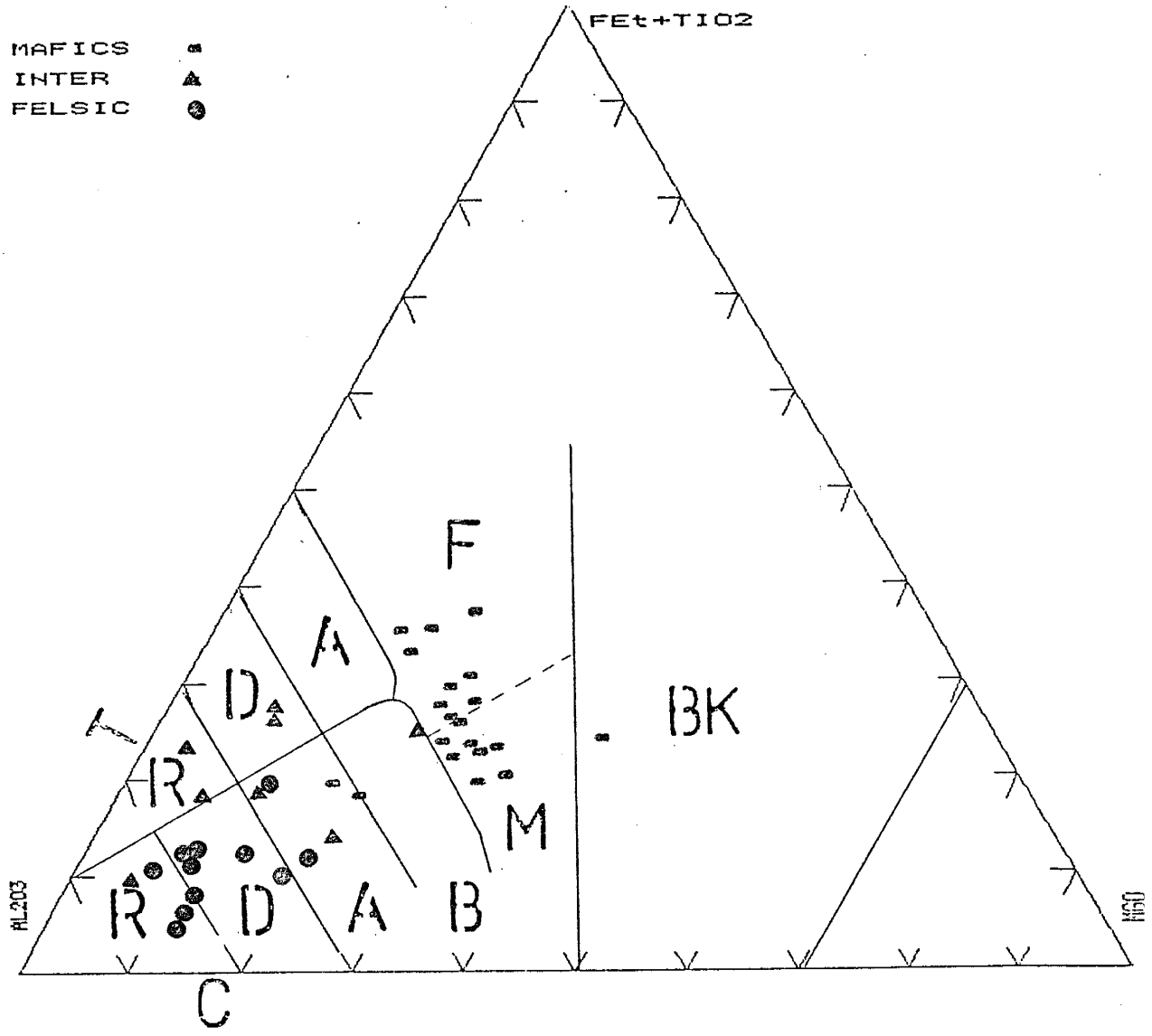

Figure 4. Distribution of northern Sangre de Cristo volcanic rocks on Jensen cation plot. Fields after Jensen (1976), R: rhyolite, D: dacite, A: andesite, B: basalt, F: high-Fe tholeiitic basalt, M: high-Mg tholeiitic basalt, T: tholeiitic, C: calc-alkaline, BK: basaltic komatiite.

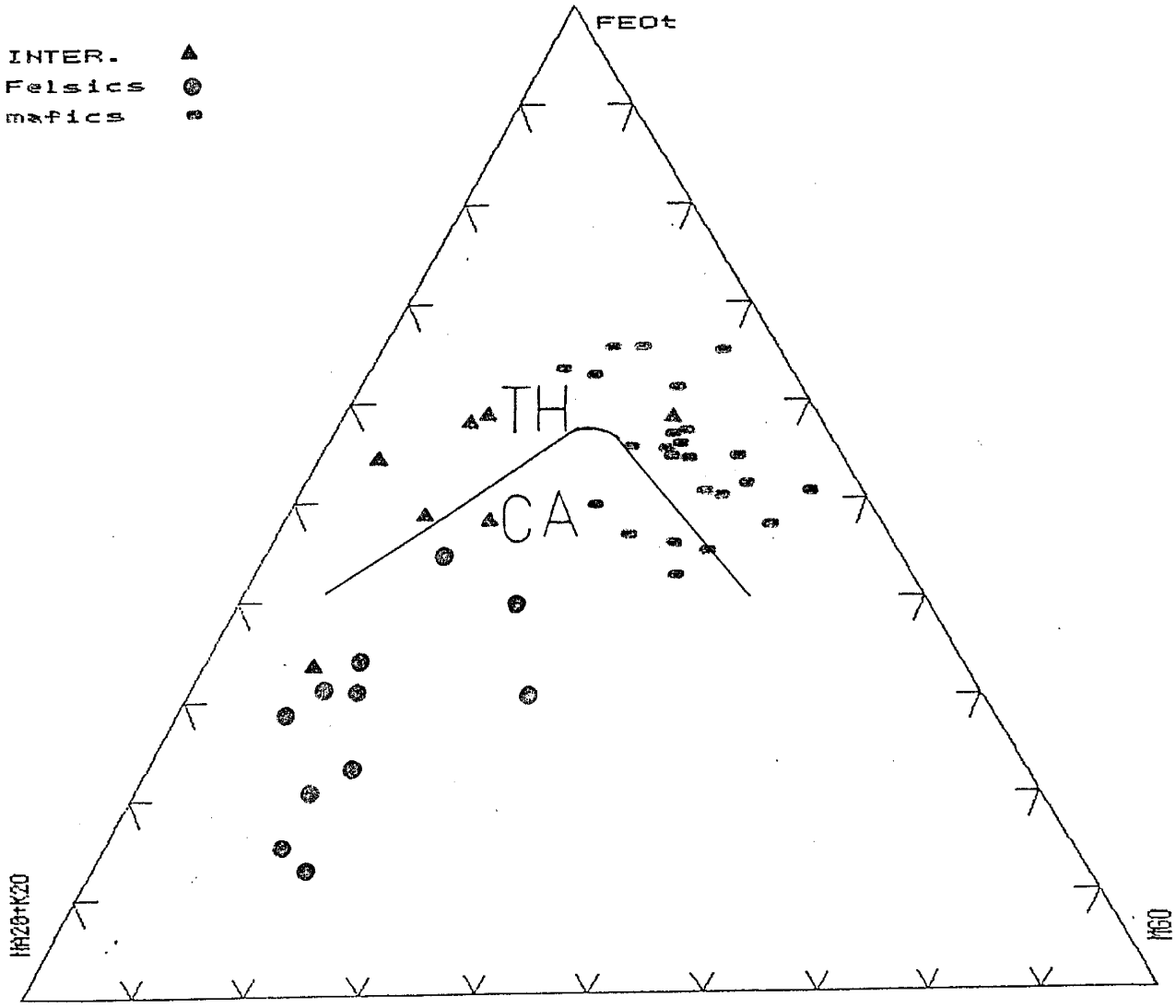

Figure 5. Distribution of northern Sangre de Cristo volcanic rocks on AFM diagram. Fields after Irvine and Barager (1971), TH: tholeiitic composition, CA: calc-alkaline composition.

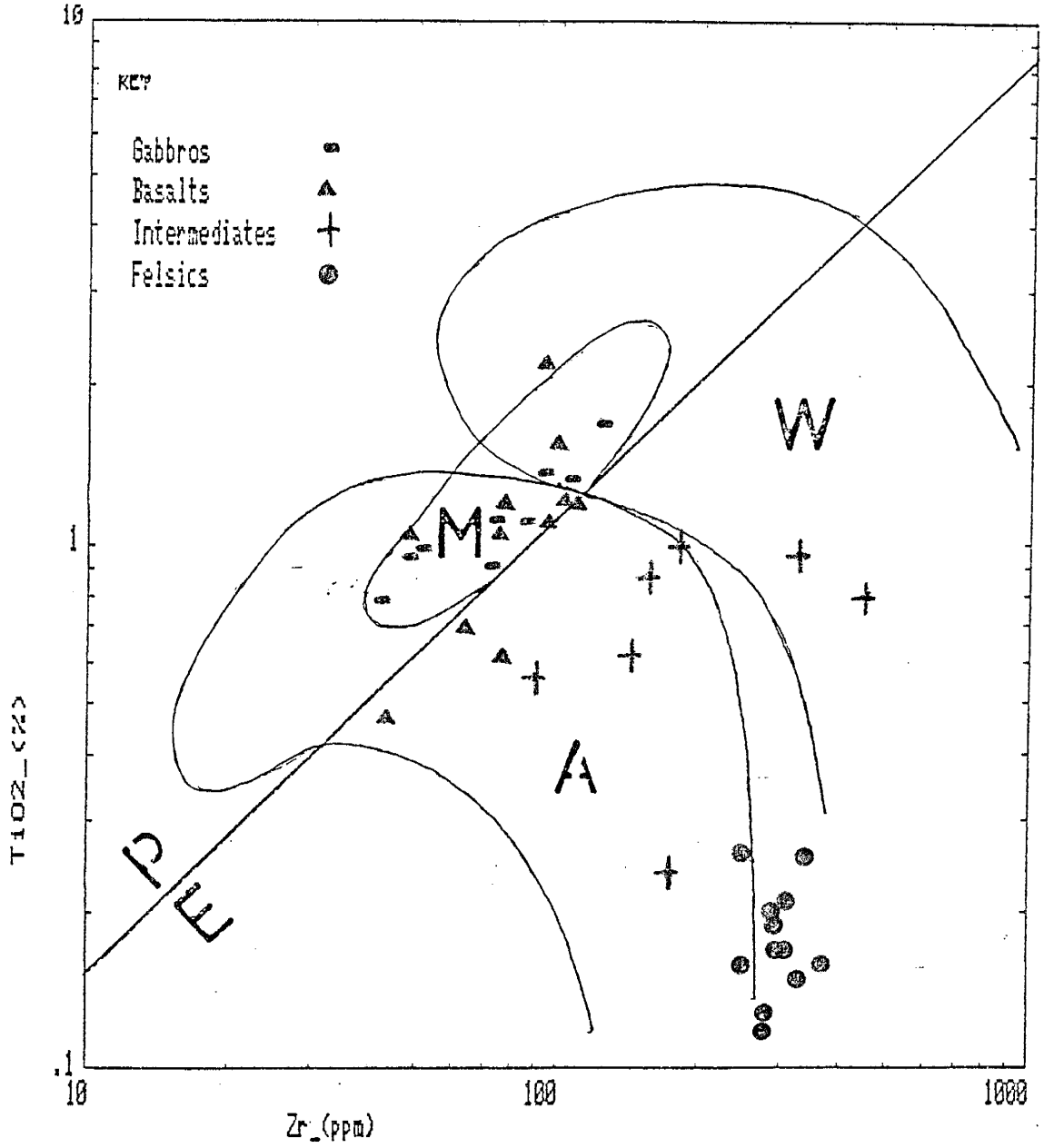

Figure 6. Distribution of northern Sangre de Cristo volcanic rocks on Zr vs. TiO2 diagram. Fields after Pharoah and Pearce (1984), M: mid-ocean ridge setting, W: within-plate setting, A: arc setting, P: primitive, E: evolved. Samples that plot in evolved field have undergone significant magnetite fractionation.

MAFIC ROCKS

Do to the degree of metamorphism and deformation and frequent lack of primary textures basalts and mafic volcaniclastics are often difficult to distinguish from one another and will be treated together in this discussion. The gabbro/diabases often can be distinguished on the basis of their textures and field relationships but are chemically similar to the basalts/mafic volcaniclastics. Both groups are dominantly tholeiitic based on the major element plot of Bravington and Taylor (1980) (Fig.7). The mean values of most of the major and trace elements are very similar for both groups (Table 1). The MG numbers for the basalt/mafic volcaniclastics have a mean value of 56 with a standard deviation of 8.1, and the mean of the gabbro/diabases is 53 with a standard deviation of 8.3. In both groups MG numbers range from 40-67 with approximately 1/3 of the samples having a MG number above 60. Those with MG > 60 are not petrologically evolved. The major and trace elements that show the greatest degree of variation among the mafic rocks are K2O, Na2O, Ba, Sr, Cr and Ni (Table 1). Some of this variation (especially among the LIL elements) is probably the result of alteration, or plagioclase and magnetite fractionation. Approximately 35% of the mafic rocks are quartz normative and 65% are

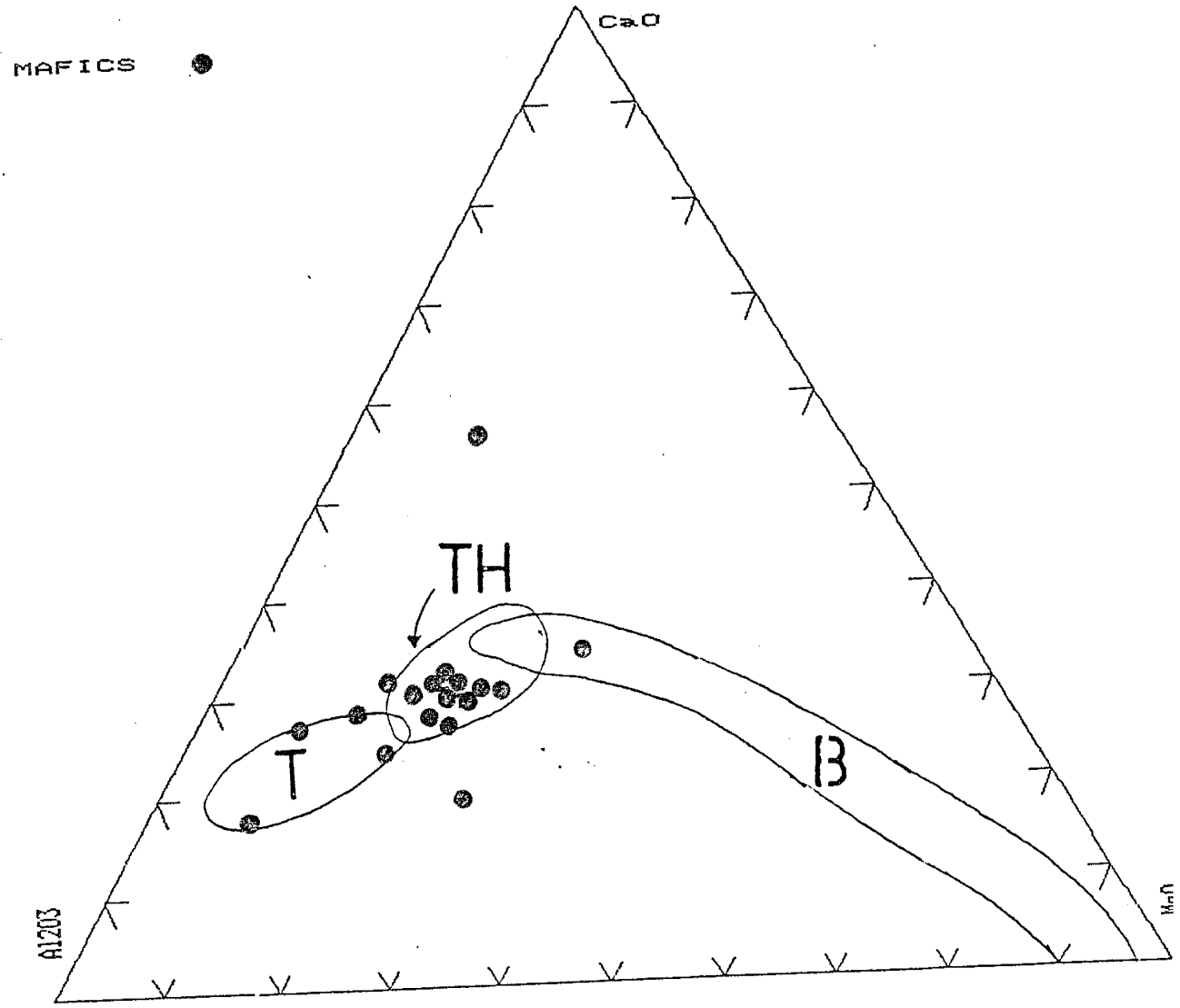

Figure 7. Distribution of northern Sangre de Cristo mafic rocks on Al2O3 - MgO - CaO diagram. Fields after Bravington and Taylor (1980), T: tonalite tronthjemite, TH: tholeiite, B: basaltic komatiite.

TABLE 1 : Chemical Composition of Mafic Rocks from the northern Sangre de Cristo Range

	BASALT	BASALT	BASALT	BASALT	BASALT	BASALT
SAMPLE	TSC-3	TSC-19	TSG-5	TSG-6	TSG-15	TSG-21
SiO2	54.4	50.5	44.9	50.0	47.9	47.3
TiO2	0.6	1.1	0.4	1.5	1.0	2.2
Al2O3	14.2	14.9	12.4	14.0	15.4	13.2
Fe2O3-T	8.4	11.7	12.9	14.7	11.2	17.0
MgO	7.3	6.3	11.2	3.9	8.3	5.8
CaO	5.3	9.4	12.5	8.4	10.6	8.9
Na2O	4.1	3.1	1.1	4.5	2.1	3.0
K2O	2.5	2.0	1.1	0.6	1.5	1.0
MnO	0.4	0.3	0.3	0.2	0.2	0.2
P2O5	0.2	0.1	0.1	0.4	0.1	0.3
LOI	0.9	0.7	1.5	0.0	1.0	0.1
TOTAL	98.8	100.5	98.8	98.7	99.7	99.5
	#	#	#	#	#	#
Rb	47.8	28.7	26.4	6.4	60.1	33.8
Ba	756.4	434.3	308.7	89.4	279.1	597.8
Cs	0.4	0.1	0.3	0.0	0.4	0.0
Sr	400.2	250.8	206.5	233.0	245.4	386.5
Pb	8.6	17.0	10.9	15.4	8.9	10.7
Th	3.1	5.3	2.5	0.7	1.7	3.8
U	3.4	2.5	3.7	1.7	2.2	5.5
Sc	27.4	50.1	37.7	52.7	37.1	50.5
V	213.2	308.4	239.2	409.9	311.2	695.2
Cr	256.0	231.0	921.0	7.9	250.0	9.5
Co	29.2	44.2	67.8	39.9	41.8	43.0
Ni	61.4	52.0	298.3	10.3	113.9	80.0
Y	41.9	33.6	17.2	36.7	23.4	36.5
Zr	77.7	95.3	44.0	99.8	48.8	94.7
Nb	5.0	7.4	4.9	7.2	5.0	7.7
Hf	2.5	2.8	1.2	3.1	1.8	3.3
Ta	0.2	0.2	0.0	0.3	0.0	0.4
La	23.1	13.5	3.6	21.6	4.5	15.9
Ce	59.5	24.3	9.3	51.0	12.9	52.2
Sm	9.5	4.3	2.3	7.5	2.7	6.2
Eu	2.2	1.1	0.7	2.4	0.9	2.6
Tb	1.4	0.7	0.2	1.1	0.5	0.9
Yb	4.6	3.3	1.3	3.2	1.7	3.3
Lu	0.6	0.5	0.2	0.5	0.2	0.5
Mg Number	66.2	54.9	66.2	37.4	62.6	43.5
K2O/Na2O	0.6	0.6	0.9	0.1	0.7	0.3
Na2O+K2O	6.6	5.1	2.2	5.1	3.6	4.0
Al2O3/TiO2	22.9	13.4	26.8	9.0	14.6	6.0
CaO/TiO2	8.5	8.5	26.9	5.4	10.0	4.0
Zr/TiO2	0.0	0.0	0.0	0.0	.0	.0

TABLE 1 : Chemical Composition of Mafic Rocks from the northern Sangre de Cristo Range

K/Rb	436.6	577.8	350.9	766.0	210.0	249.4
Ba/Sr	1.8	1.7	1.4	0.3	1.1	1.5
Rb/Sr	0.1	0.1	0.1	0.0	0.2	0.0
La/Yb	4.9	4.0	2.7	6.6	2.5	4.7
La/Sm	2.4	3.1	1.5	2.8	1.6	2.5
Sm/Eu	4.2	3.6	3.3	3.0	2.8	2.4
Ti/Zr	48.1	69.6	63.3	93.6	129.4	139.3
Zr/Nb	15.5	12.8	8.8	13.7	9.6	12.3
Nb/Y	0.1	0.2	0.2	0.2	0.2	0.2
Zr/Y	1.8	2.8	2.5	2.7	2.0	2.5
Nb/Ta	22.4	33.6	55.1	23.4	63.3	19.2
Nb/La	0.2	0.5	1.3	0.3	1.1	0.4
La/Ta	103.9	61.5	40.0	69.9	56.2	39.8
La/Th	7.2	2.5	1.4	29.7	2.5	4.1
Y/Tb	28.1	42.6	59.3	33.0	41.8	38.0
Th/Yb	0.6	1.5	1.9	0.2	1.0	1.1
Ta/Yb	0.0	0.0	0.0	0.1	0.0	0.1
Hf/Th	0.7	0.5	0.4	4.3	1.0	0.8
Ti/V	17.5	21.5	11.6	22.8	20.3	18.9
U/Pb	0.4	0.1	0.3	0.1	0.2	0.5
FeO-T/MgO	4.8	4.8	4.2	4.9	4.5	5.1
Sm/Yb	1.2	0.7	1.2	0.5	0.9	0.8
Eu/Eu*	0.6	0.1	0.3	0.0	0.2	0.0

Fe2O3-T ==> Total Fe as Fe2O3
NO ENTRY ==> No determination OR below detectability limit
MAJOR ELEMENTS ==> In weight percent
TRACE ELEMENTS ==> In parts per million
==========

TABLE 1 : Chemical Composition of Mafic Rocks from the northern Sangre de Cristo Range

	BASALT	BASALT	BASALT	BASALT	BASALT	BASALT
SAMPLE	TSG-23	THP-3	THP-P2	THC-5	THC-7	TSP-7
SiO2	50.7	51.0	46.7	50.8	50.1	50.9
TiO2	0.8	1.2	1.0	0.7	1.2	1.2
Al2O3	18.6	14.4	16.6	15.9	15.3	15.2
Fe2O3-T	7.9	12.9	12.0	11.0	11.9	12.0
MgO	5.2	6.9	8.0	6.5	6.3	6.8
CaO	11.2	9.1	10.0	9.9	9.9	8.2
Na2O	3.8	2.8	1.9	2.7	2.8	3.2
K2O	0.9	0.8	1.2	0.8	0.4	0.4
MnO	0.1	0.2	0.3	0.3	0.2	0.2
P2O5	0.2	0.1	0.1	0.2	0.2	0.2
LOI	0.3	0.4	0.9	0.4	0.7	0.9
TOTAL	100.2	100.2	99.3	99.6	99.6	99.6
	#	#	#	#	#	#
Rb	17.9	17.6	28.5	16.3	10.7	10.4
Ba	802.4	183.6	448.4	188.2	88.5	461.3
Cs	0.1	0.0	0.4	0.1	0.1	0.0
Sr	712.4	209.8	230.8	276.0	207.3	340.2
Pb	8.5	9.6	9.3	11.6	6.4	9.0
Th	1.5	1.2	5.2	5.6	0.8	3.8
U	1.2	2.7	3.8	3.7	2.3	0.8
Sc	29.2	49.9	33.3	35.6	35.1	50.3
V	311.8	315.1	320.4	247.7	314.5	320.5
Cr	109.0	233.0	3.7	108.0	154.7	241.0
Co	27.3	41.7	36.1	31.8	35.2	61.5
Ni	46.9	41.6	67.9	29.8	53.0	49.9
Y	14.7	29.7	27.9	20.0	32.9	31.7
Zr	39.3	76.9	74.9	64.2	104.2	110.3
Nb	5.8	9.0	6.3	7.8	8.1	6.0
Hf	1.4	2.0	8.5	1.8	1.8	3.0
Ta	0.1	0.3	1.3	0.2	0.2	0.3
La	12.9	6.2	5.6	14.1	8.3	11.7
Ce	30.2	18.4	119.5	32.0	20.5	29.5
Sm	3.8	3.9	2.4	5.3	3.9	4.5
Eu	1.2	1.4	0.9	1.3	1.2	1.5
Tb	0.4	0.8	0.4	0.3	0.7	0.7
Yb	1.8	3.2	2.2	1.7	2.5	3.5
Lu	0.2	0.5	0.3	0.3	0.4	0.5
Mg Number	59.6	54.5	60.0	57.1	54.2	55.8
K2O/Na2O	0.2	0.2	0.6	0.3	0.1	0.1
Na2O+K2O	4.7	3.7	3.2	3.5	3.3	3.6
Al2O3/TiO2	23.0	12.1	15.8	22.5	12.6	12.7
CaO/TiO2	13.9	7.6	9.5	14.1	8.2	6.9
Zr/TiO2	.0	0.0	0.0	0.0	0.0	0.0

TABLE 1 : Chemical Composition of Mafic Rocks from the northern Sangre de Cristo Range

K/Rb	416.1	393.1	354.9	417.2	363.9	369.8
Ba/Sr	1.1	0.8	1.9	0.6	0.4	1.3
Rb/Sr	0.0	0.0	0.1	0.0	0.0	0.0
La/Yb	7.1	1.9	2.5	8.0	3.2	3.2
La/Sm	3.3	1.5	2.3	2.6	2.1	2.5
Sm/Eu	3.0	2.7	2.5	3.9	3.1	2.9
Ti/Zr	123.5	93.2	84.1	65.7	69.7	64.9
Zr/Nb	6.7	8.5	11.9	8.1	12.7	18.3
Nb/Y	0.3	0.3	0.2	0.3	0.2	0.1
Zr/Y	2.6	2.5	2.6	3.2	3.1	3.4
Nb/Ta	35.4	30.0	4.8	35.7	29.7	17.2
Nb/La	0.4	1.4	1.1	0.5	0.9	0.5
La/Ta	78.8	20.8	4.3	64.0	30.4	33.6
La/Th	8.4	5.0	1.0	2.4	9.7	3.0
Y/Tb	32.8	37.1	59.4	54.1	42.2	43.4
Th/Yb	0.8	0.3	2.3	3.2	0.3	1.0
Ta/Yb	0.0	0.0	0.5	0.1	0.1	0.1
Hf/Th	0.9	1.7	1.6	0.3	2.0	0.7
Ti/V	15.5	22.7	19.6	17.0	23.1	22.3
U/Pb	0.1	0.2	0.4	0.3	0.3	0.1
FeO-T/MgO	4.6	4.7	4.7	4.5	4.8	4.9
Sm/Yb	2.1	0.6	0.7	1.2	0.5	0.9
Eu/Eu*	0.3	0.1	0.1	0.1	0.0	0.0

Fe2O3-T ==> Total Fe as Fe2O3
NO ENTRY ==> No determination OR below detectability limit
MAJOR ELEMENTS ==> In weight percent
TRACE ELEMENTS ==> In parts per million
==========

TABLE 1 : Chemical Composition of Mafic Rocks from the northern Sangre de Cristo Range

SAMPLE	AMPH AVG	AMPH STD
SiO2	49.6	2.4
TiO2	1.1	0.4
Al2O3	15.0	1.5
Fe2O3-T	12.0	2.3
MgO	6.9	1.7
CaO	9.5	1.6
Na2O	2.9	0.9
K2O	1.1	0.5
MnO	0.2	0.0
P2O5	0.2	0.0
LOI	0.6	0.4
TOTAL	99.5	0.5
Rb	25.4	15.2
Ba	386.5	231.1
Cs	0.1	0.1
Sr	308.2	138.1
Pb	10.5	2.8
Th	2.9	1.7
U	2.8	1.2
Sc	40.7	8.8
V	333.9	119.0
Cr	210.4	234.2
Co	41.6	11.6
Ni	75.4	71.5
Y	28.8	8.0
Zr	77.5	23.2
Nb	6.7	1.3
Hf	2.8	1.8
Ta	0.3	0.3
La	11.8	6.1
Ce	38.2	28.8
Sm	4.7	2.0
Eu	1.5	0.5
Tb	0.7	0.3
Yb	2.7	0.9
Lu	0.4	0.1
Mg Number	56.0	8.1
K2O/Na2O	0.4	0.2
Na2O+K2O	4.1	1.5
Al2O3/TiO2	13.7	3.5
CaO/TiO2	10.3	5.7
Zr/TiO2	0.0	.0

TABLE 1 : Chemical Composition of Mafic Rocks from the northern Sangre de Cristo Range

K/Rb	408.8	139.0
Ba/Sr	1.2	0.5
Rb/Sr	0.0	0.0
La/Yb	4.3	1.9
La/Sm	2.3	0.5
Sm/Eu	3.1	0.5
Ti/Zr	87.0	28.2
Zr/Nb	11.6	3.2
Nb/Y	0.2	0.0
Zr/Y	2.7	0.4
Nb/Ta	30.8	15.3
Nb/La	0.7	0.4
La/Ta	50.3	26.2
La/Th	6.4	7.5
Y/Tb	42.7	9.7
Th/Yb	1.2	0.8
Ta/Yb	0.1	0.1
Hf/Th	1.3	1.0
Ti/V	19.4	3.3
U/Pb	0.2	0.1
FeO-T/MgO	4.8	3.7
Sm/Yb	0.9	1.2
Eu/Eu*	0.1	0.1

Fe2O3-T ==> Total Fe as Fe2O3
NO ENTRY ==> No determination OR below detectability limit
MAJOR ELEMENTS ==> In weight percent
TRACE ELEMENTS ==> In parts per million
==========

TABLE 1 : Chemical Composition of Mafic Rocks from the northern Sangre de Cristo Range

	GABBRO	GABBRO	GABBRO	GABBRO	GABBRO	GABBRO
SAMPLE	TSC-4	TSC-14	TSG2-9	TSG2-4	THP-1	TSP-1
SiO2	49.6	51.3	51.94	51.5	48.6	52.0
TiO2	1.1	1.3	1.11	1.7	1.3	0.9
Al2O3	14.3	14.3	14.89	13.5	13.3	18.7
Fe2O3-T	13.2	14.1	12.29	15.0	13.2	8.3
MgO	5.9	4.5	5.92	4.6	6.0	4.4
CaO	9.6	6.1	8.18	7.9	8.8	9.3
Na2O	2.3	3.9	3.89	3.2	0.9	4.0
K2O	1.2	2.4	0.26	0.7	2.4	1.2
MnO	0.2	0.2	0.38	0.3	0.3	0.1
P2O5	0.2	0.3	0.29	0.2	0.2	0.2
LOI	1.0	0.7	0.50	0.4	3.8	0.9
TOTAL	98.9 #	99.5 #	99.66 #	99.4 #	99.3 #	100.4 #
Rb	16.5	41.7	2.18	12.3	60.7	26.1
Ba	123.6	282.2	114.59	277.0	598.7	463.8
Cs	0.2	0.1	0.17	0.0	1.1	0.2
Sr	285.8	368.9	264.57	325.7	233.8	687.0
Pb	17.4	23.0	7.85	7.3	6.1	7.7
Th	3.1	3.4	0.26	3.8	NA	1.8
U	2.2	2.5	2.22	1.7	0.8	1.9
Sc	49.5	39.1	44.3	40.7	47.3	26.0
V	363.0	396.4	302.8	533.9	388.0	334.5
Cr	61.6	26.5	46.6	5.0	155.1	60.0
Co	33.1	34.6	35.2	49.5	42.8	25.6
Ni	17.6	12.9	22.8	2.0	41.3	30.7
Y	29.8	34.9	29.1	37.4	36.9	16.0
Zr	73.7	92.8	86.1	123.4	106.2	72.5
Nb	5.8	6.4	7.9	7.8	7.6	5.8
Hf	1.6	2.4	2.2	4.2	2.9	2.1
Ta	0.1	0.2	0.3	0.3	0.2	0.2
La	9.7	14.4	12.8	12.2	11.2	11.9
Ce	23.8	34.7	32.2	30.9	26.4	30.1
Sm	3.8	5.3	5.3	5.4	4.3	3.8
Eu	1.2	1.7	1.9	1.6	1.3	1.2
Tb	0.7	1.0	0.9	1.2	0.9	0.7
Yb	2.3	3.0	3.1	3.9	3.3	1.6
Lu	0.3	0.4	0.5	0.6	0.5	0.2
Mg Number	50.3	41.7	51.9	40.9	50.7	54.5
K2O/Na2O	0.5	0.6	0.0	0.2	2.4	0.3
Na2O+K2O	3.5	6.3	4.1	4.0	3.4	5.2
Al2O3/TiO2	12.7	10.5	13.4	7.9	10.0	20.5
CaO/TiO2	8.6	4.4	7.3	4.6	6.6	10.2
Zr/TiO2	0.0	0.0	0.0	0.0	0.0	0.0

TABLE 1 : Sangre de Cristo Mafics

K/Rb	602.6	487.3	1005.1	512.4	336.3	382.2
Ba/Sr	0.4	0.7	0.4	0.8	2.5	0.6
Rb/Sr	0.0	0.1	0.0	0.0	0.2	0.0
La/Yb	4.2	4.8	4.0	3.1	3.3	7.0
La/Sm	2.5	2.6	2.4	2.2	2.5	3.0
Sm/Eu	3.2	3.1	2.7	3.3	3.1	3.0
Ti/Zr	90.9	88.3	77.3	82.7	75.1	75.5
Zr/Nb	12.5	14.4	10.7	15.7	13.8	12.3
Nb/Y	0.2	0.1	0.2	0.2	0.2	0.3
Zr/Y	2.4	2.6	2.9	3.2	2.8	4.5
Nb/Ta	40.1	26.6	21.0	25.3	28.4	23.4
Nb/La	0.6	0.4	0.6	0.6	0.6	0.4
La/Ta	66.9	59.8	33.7	39.6	41.4	47.6
La/Th	3.1	4.1	49.2	3.1	ERR	6.3
Y/Tb	39.7	34.2	32.0	30.9	38.8	20.8
Th/Yb	1.3	1.1	0.0	0.9	0.0	1.1
Ta/Yb	0.0	0.0	0.1	0.0	0.0	0.1
Hf/Th	0.5	0.7	8.7	1.0	ERR	1.1
Ti/V	18.4	20.6	21.9	19.1	20.5	16.3
U/Pb	0.1	0.1	0.2	0.2	0.1	0.2
FeO-T/MgO	4.7	5.0	4.8	5.1	4.9	4.8
Sm/Yb	0.9	0.9	0.8	0.7	0.5	1.9
Eu/Eu*	0.2	0.1	0.1	-0.0	0.0	-0.0

Fe2O3-T ==> Total Fe as Fe2O3
NO ENTRY ==> No determination OR below detectability limit
TRACE ELEMENTS ==> In parts per million
==========

TABLE 1 : Chemical Composition of Mafic Rocks from the northern Sangre de Cristo Range

	GABBRO	GABBRO	GABBRO		
SAMPLE	TKG-2	TEB-2	TTC-1	AVG	STD
SiO2	45.9	48.1	49.5	49.8	1.9
TiO2	0.9	0.7	0.9	1.1	0.2
Al2O3	16.9	16.1	14.9	15.2	1.6
Fe2O3-T	10.9	10.4	10.5	12.0	2.0
MgO	7.5	9.3	7.6	6.2	1.5
CaO	10.3	11.2	12.0	9.3	1.7
Na2O	2.9	2.1	2.6	2.9	0.9
K2O	1.8	0.4	0.4	1.2	0.8
MnO	0.2	0.1	0.1	0.2	0.0
P2O5	0.1	0.1	0.1	0.2	0.0
LOI	0.8	0.8	1.3	1.1	0.9
TOTAL	98.7 #	99.8 #	100.6 #	99.6 #	0.5 #
Rb	57.4	9.0	8.7	26.1	20.7
Ba	822.0	130.8	254.0	340.7	228.6
Cs	0.5	0.1	0.1	0.3	0.3
Sr	415.1	400.5	367.8	372.1	125.6
Pb	20.0	7.2	9.0	11.7	6.1
Th	5.4	1.0	1.9	2.3	1.7
U	3.1	0.7	2.8	2.0	0.7
Sc	46.0	48.6	57.2	44.3	8.1
V	294.5	274.3	341.2	358.7	73.2
Cr	229.0	335.0	232.0	127.8	108.3
Co	45.8	60.1	46.1	41.4	9.7
Ni	139.6	165.2	71.4	55.9	55.1
Y	20.8	14.9	21.0	26.8	8.3
Zr	48.3	42.1	51.4	77.4	25.9
Nb	4.3	4.2	5.0	6.1	1.3
Hf	1.5	2.1	2.0	2.3	0.7
Ta	0.1	0.0	0.1	0.2	0.0
La	6.5	6.2	8.4	10.4	2.7
Ce	16.9	16.6	20.6	25.8	6.3
Sm	3.3	3.1	3.9	4.3	0.8
Eu	1.2	1.1	1.3	1.4	0.2
Tb	0.4	0.4	0.7	0.8	0.2
Yb	1.7	1.6	2.2	2.5	0.7
Lu	0.2	0.2	0.3	0.4	0.1
Mg Number	60.8	66.7	62.0	53.3	8.3
K2O/Na2O	0.6	0.2	0.1	0.5	0.7
Na2O+K2O	4.7	2.5	3.0	4.1	1.7
Al2O3/TiO2	17.8	20.6	15.2	14.3	4.3
CaO/TiO2	10.9	14.3	12.3	8.8	3.1
Zr/TiO2	0.0	0.0	0.0	0.0	.0

TABLE 1 : Chemical Composition of Mafic Rocks from the northern Sangre de Cristo Range

K/Rb	262.6	398.9	449.6	493.0	204.2
Ba/Sr	1.9	0.3	0.6	0.9	0.7
Rb/Sr	0.1	0.0	0.0	0.0	0.0
La/Yb	3.8	3.6	3.7	4.2	1.1
La/Sm	1.9	1.9	2.1	2.4	0.3
Sm/Eu	2.7	2.6	2.9	3.0	0.2
Ti/Zr	117.4	111.4	114.5	92.6	16.3
Zr/Nb	11.0	9.9	10.2	12.3	1.8
Nb/Y	0.2	0.2	0.2	0.2	0.0
Zr/Y	2.3	2.8	2.4	2.9	0.6
Nb/Ta	36.6	49.7	35.3	31.8	8.7
Nb/La	0.6	0.6	0.5	0.6	0.0
La/Ta	54.8	73.0	59.7	53.0	12.5
La/Th	1.2	6.2	4.3		
Y/Tb	48.3	33.9	27.0	34.0	7.4
Th/Yb	3.1	0.5	0.8	1.0	0.8
Ta/Yb	0.0	0.0	0.0	0.0	0.0
Hf/Th	0.2	2.1	1.0		
Ti/V	19.2	17.1	17.2	18.9	1.7
U/Pb	0.1	0.1	0.3	0.1	0.0
FeO-T/MgO	4.6	4.4	4.6		
Sm/Yb	1.4	1.6	1.3		
Eu/Eu*	0.3	0.1	0.2		

Fe2O3-T ==> Total Fe as Fe2O3
NO ENTRY ==> No determination OR below detectability limit
TRACE ELEMENTS ==> In parts per million
==========

olivine normative. An iron enrichment trend is evident on the AFM diagram (Fig.5) indicating late magnetite fractionation, with the slight scattering of the data about the tholeiitic trend probably reflecting alteration.

Major element vs. MG number plots (Fig.8) show a decrease in MgO with decreasing MG number which can be explained by fractionation of olivine and/or orthopyroxene. Both Al2O3 and CaO decrease with decreasing MG number suggesting plagioclase fractionation also occurred. The major elements TiO2, Fe2O3-T and P2O5 also tend to decrease with increasing MG number. Ni decreases with decreasing MG number (Fig.9) indicating that olivine was a major fractionating ferromagnesian phase. Elements such as Ce, Zr and Y that are incompatible in the early stages of basalt crystallization increase as MG number decreases (Fig.9). The trends seen in both the major and trace elements are suggestive of crystal fractionation rather than partial melting in the formation of the mafic rocks.

Figure 10 shows the envelope of variation of chondrite-normalized rare earth element (REE) patterns for the mafic rocks. The light rare earth elements (LREE) are enriched from 15-70x chondrites and the heavy rare earth elements (HREE) are enriched from 10-30x chondrites giving a gently sloping pattern with both slightly negative and positive Eu anomalies. The mafic rocks of

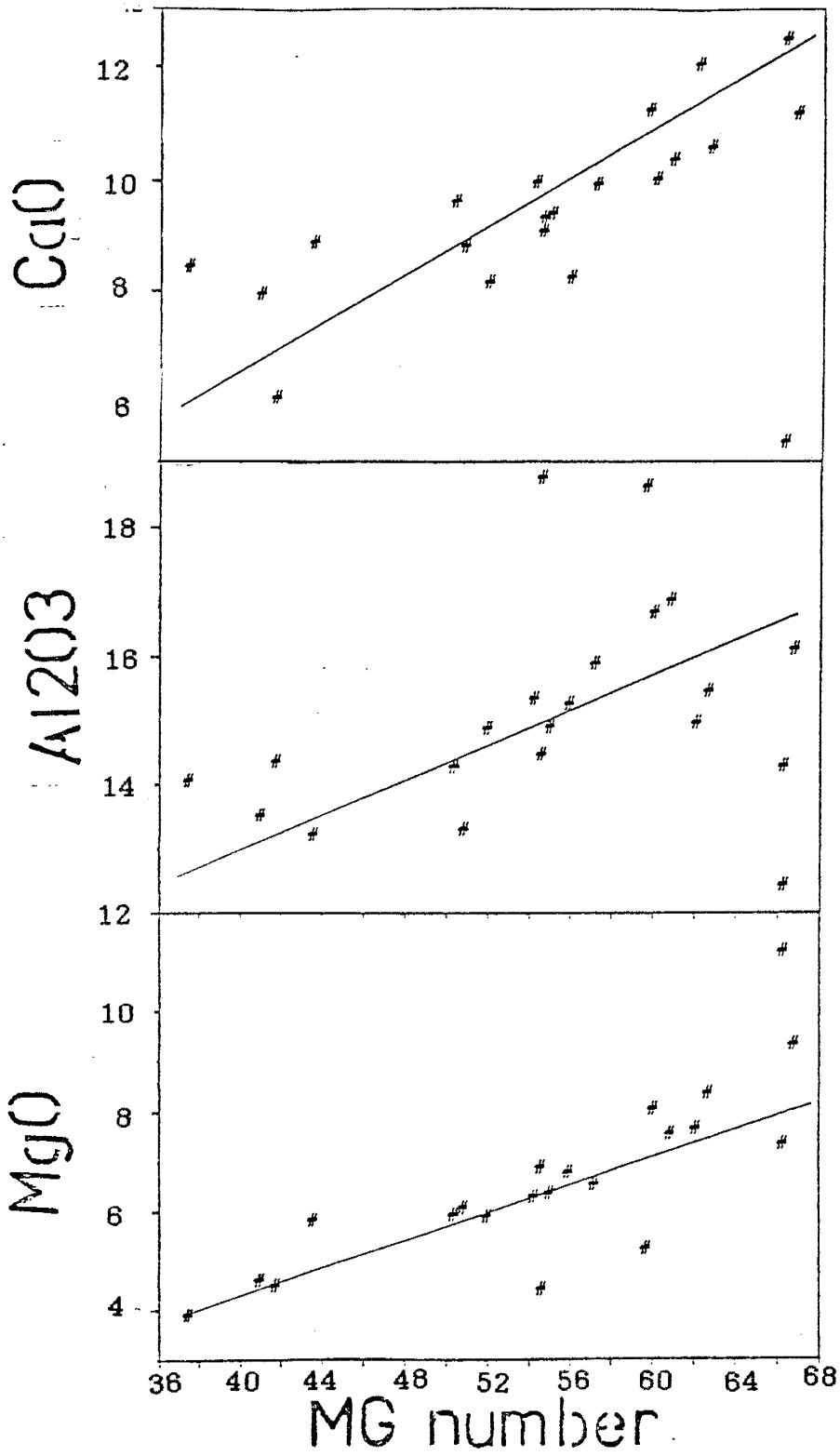

Figure 8. Major elements MgO, Al2O3, CaO vs. number plots for northern Sangre de Cristo mafic rocks showing fractionation trends.

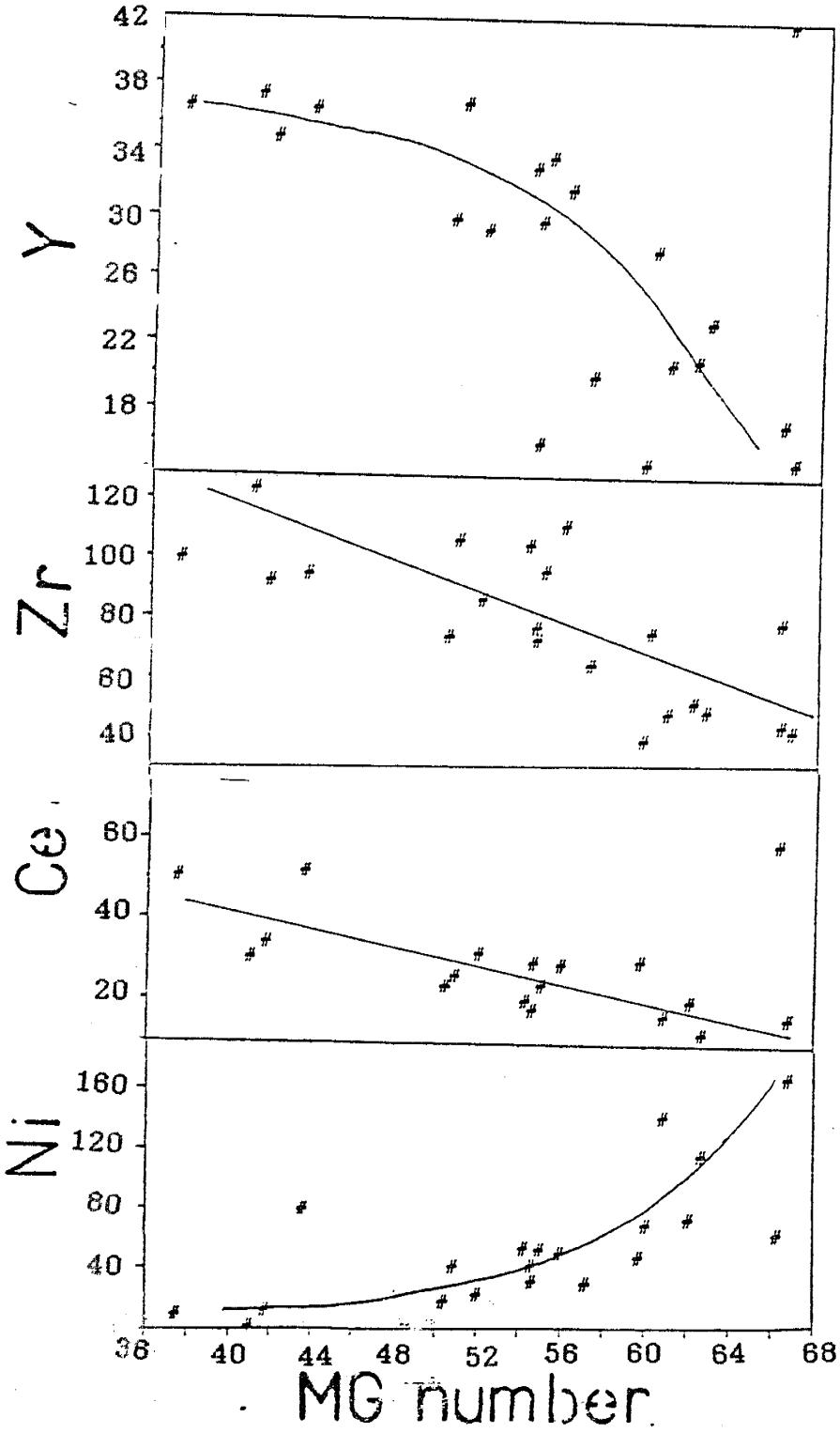

Figure 9. Trace elements Ni, Ce, Zr, Y vs. MG number plot for northern Sangre de Cristo mafic rocks showing fractionation trends.

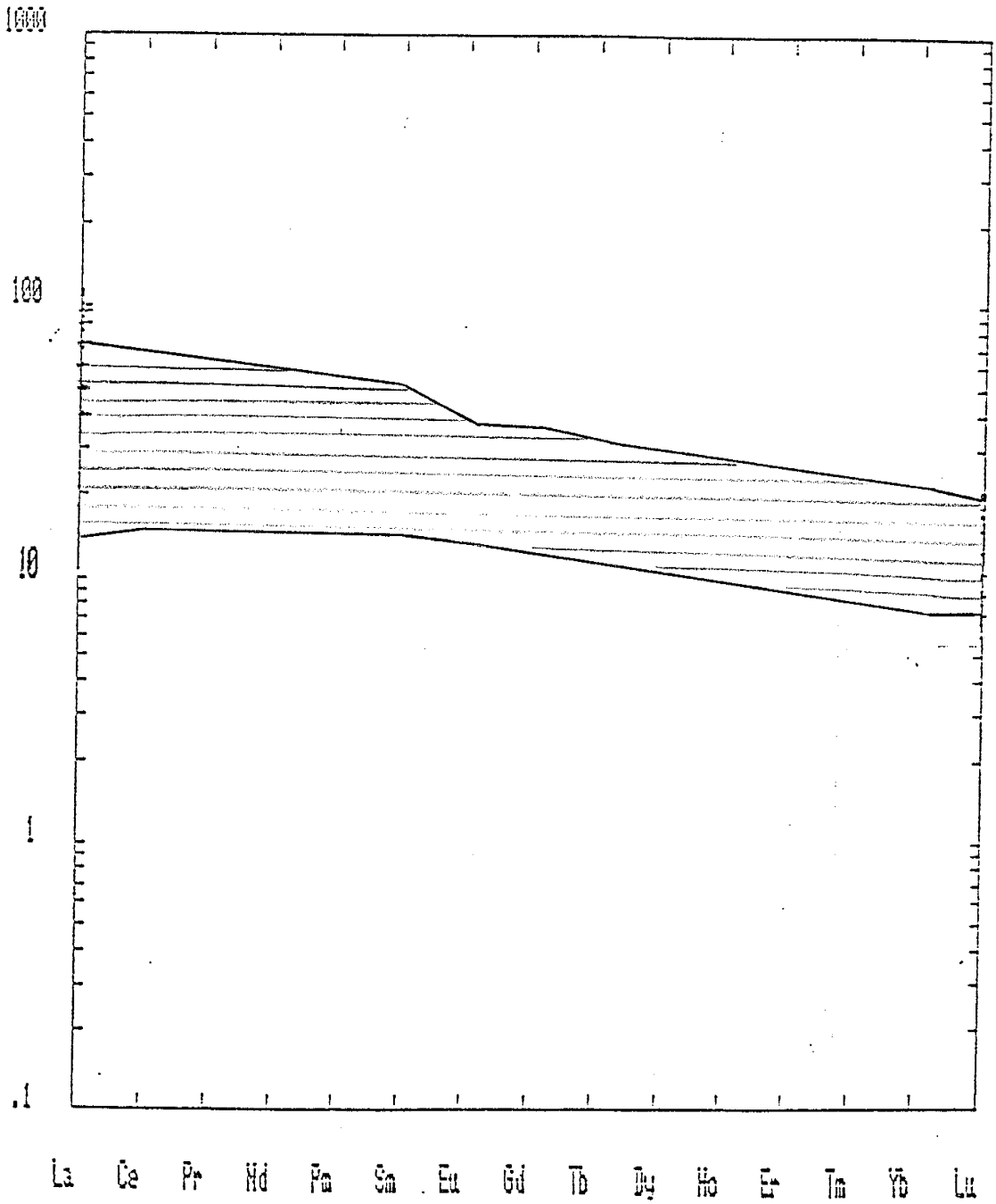

Figure 10. Chondrite-normalized REE patterns showing envelope of variation for northern Sangre de Cristo maf rocks.

the northern Sangre de Cristo area are plotted on mid-ocean ridge basalt (MORB) normalized multi-element diagrams (Pearce, 1983) to compare their patterns to the patterns of younger basalts from various tectonic settings (Fig.11). The shape of these patterns are believed to represent those of the source, with differences in geochemical evolution of the upper mantle, from fractional crystallization or partial melting, affecting the overall level of the pattern, but not greatly affecting the shape of the distributions (Pearce, 1983). For these reasons, it is suggested that comparison of Proteroizic trace element patterns to those from Phanerozoic rocks is valid (Pharoah and Pearce, 1984). Figure 11 shows the envelope of variation in these patterns for the mafic rocks of the northern Sangre de Cristo area. Most of the elements are enriched relative to MORB, with the LIL elements Sr, K, Rb, Ba, and Th showing the greatest enrichment, and the high field strength (HFS) elements, Ta, Nb, Ce, P, Zr, Hf, Sm, Ti, Y and Yb showing much less enrichment. The selective enrichment of the LIL elements relative to the HFS elements is characteristic of arc and back-arc magmas (Prarce, 1983; Saunders and Tarney, 1984). This enrichment is attributed to enrichment of LIL elements in the mantle wedge beneath the arc through volatiles transferred from the subducting and dehydrating slab. The HFS elements are retained in the subducting slab in minor

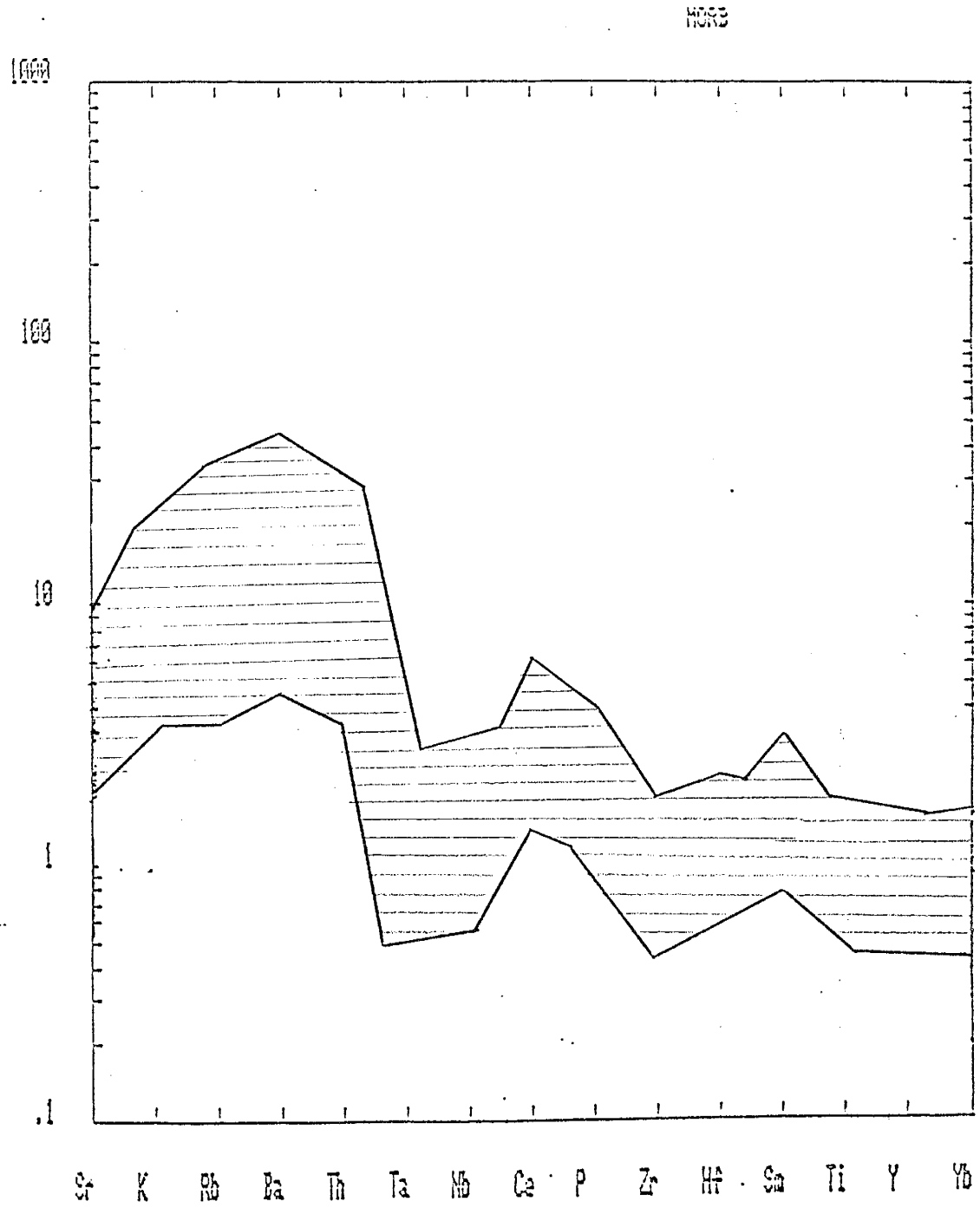

Figure 11. MORB-normalized trace element patterns showing envelope of variation for mafic rocks from the northern Sangre de Cristo Range. Normalizing values after Pearce (1983).

refractory phases such as zircon, rutile or magnetite (Saunders and Tarney, 1984). Figures 12-14 show the shapes of the MORB-normalized trace element patterns for the northern Sangre mafics relative to the patterns from modern basalts from various tectonic settings. The mafic rocks from the northern Sangres show the greatest similarity to modern basalts from continental margin arcs and evolved island arcs with their associated immature back arc basins. Both of these groups show the characteristic enrichment in the LIL's and the minimum in Ta and Nb associated with subduction zone related basalts (Fig.12). The mafic rocks from the northern Sangres are also similar to basalts from immature island arcs (Fig.13) but tend to have a slightly greater enrichment in the HFS elements. The mafic rocks of the northern Sangre de Cristo area show the least similarities to basalts from within-plate settings (Fig.14) which have a characteristic humped shaped pattern caused by the selective enrichment of both LIL and HFS elements (Pearce, 1983).

Researchers have proposed various tectonomagmatic discrimination diagrams that use trace element distributions. Particularly useful are the HFSE and HREE which are considered to be relatively immobile. The application of such diagrams which are based on data from Phanerozoic rocks, requires certain assumptions. Do the tectonic settings we see today accurately represent those

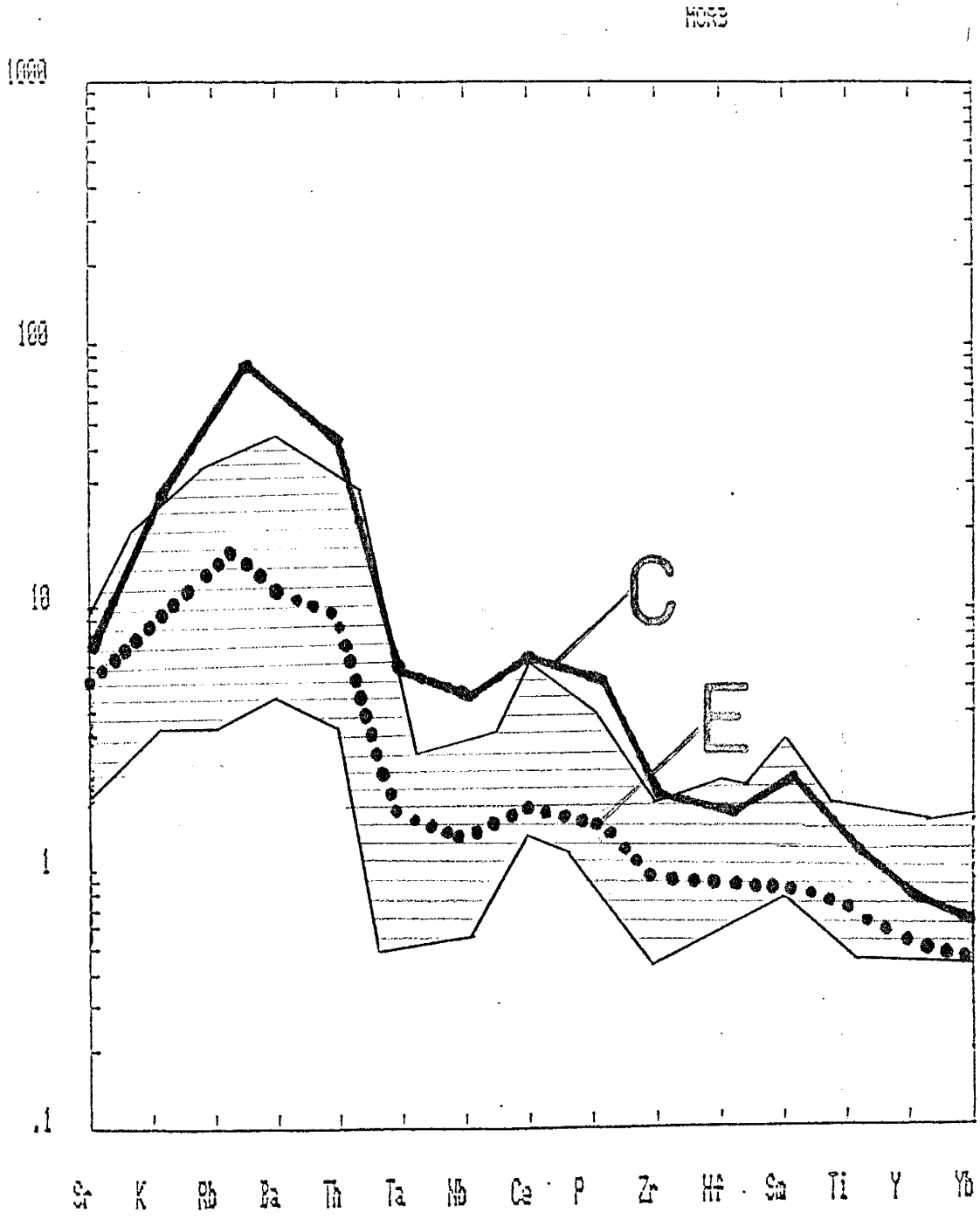

Figure 12. MORB-normalized trace element patterns for northern Sangre de Cristo mafic rocks compared to modern basalts from C: continental-margin arcs and immature back-arc basins, E: evolved island arcs and immature back-arc basins.

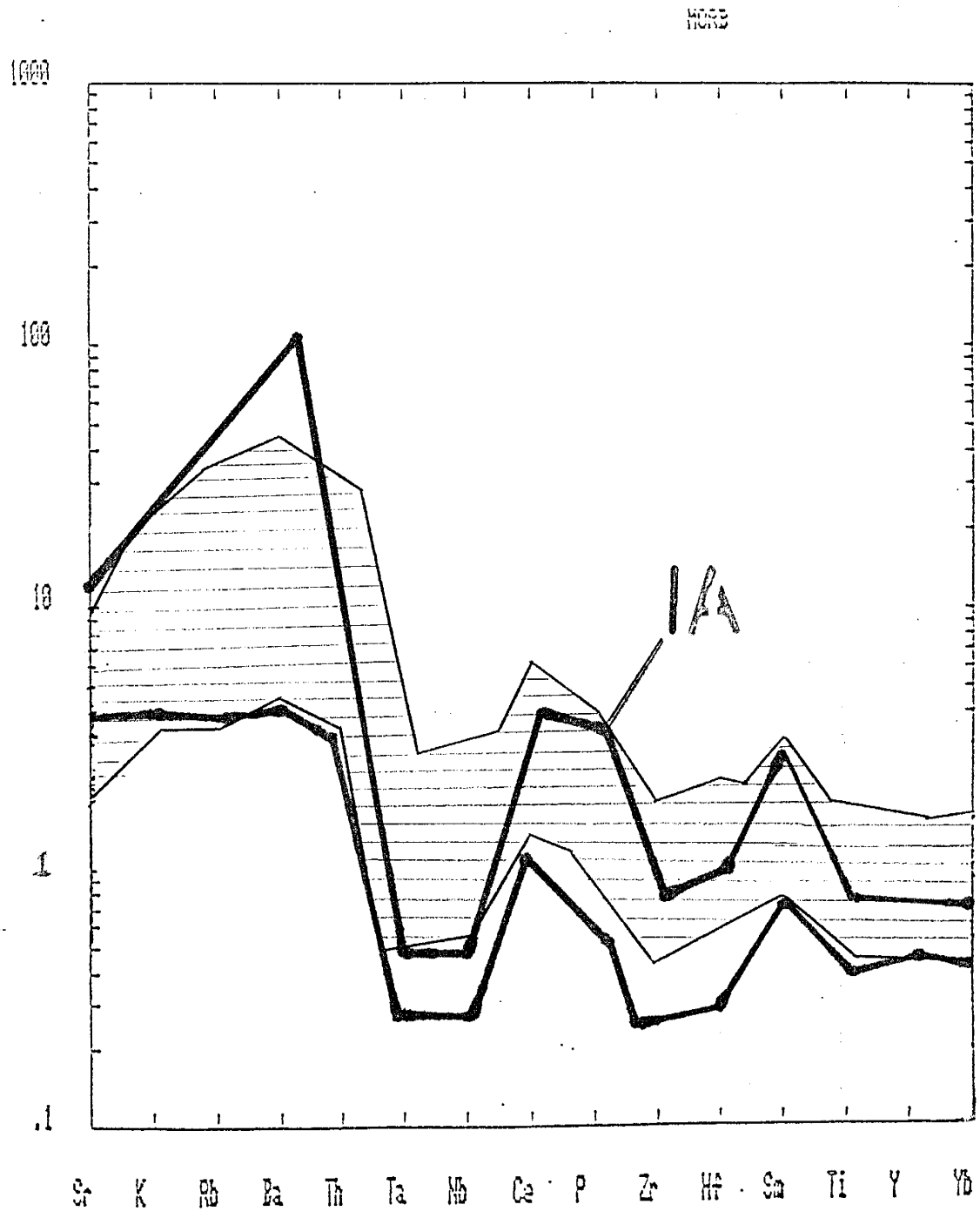

Figure 13. MORB-normalized trace element patterns for northern Sangre de Cristo mafic rocks compared to moder basalts from IA: immature island arcs, calc-alkaline basalts.

Figure 14. MORB-normalized trace element patterns for northern Sangre de Cristo mafic rocks compared to modern basalts from W: within-plate settings.

of the Proterozoic? How has the chemical composition of the mantle evolved with time? Have the processes responsible for the composition of modern basalts existed throughout geologic time? Other problems to consider when using these diagrams include that they group together all intraplate basalts, both marine and continental in origin, and that back-arc basin basalts are not distinguished. Despite these problems, the use of such discrimination diagrams provide a useful reference and are helpful in constraining origins based on similarities to modern examples.

Application of these diagrams to the mafic rocks from the northern Sangres produces consistant results. On the Th - Ta - HF/3 diagram proposed by Wood (1980) , samples plot in the destructive plate-margin basalts field with approximately half of the samples falling in the calc-alkaline subfield and the other half falling in the primitive island-arc tholeiite field (Fig.15).

When the samples are plotted on the Zr - Yx3 - Ti/100 diagram of Pearce and Cann (1973) (Fig.16), where plate margin basalts (fields A,B,C) are delineated from within plate basalts (field W), the mafic rocks plot almost exclusively in field B. This field is also the field of mid-ocean ridge basalts. Pharoah and Pearce (1984) have proposed the use of the TiO2 vs. Zr plot for delineating arc and within-plate basalts, with a MORB field that overlaps both. This diagram further

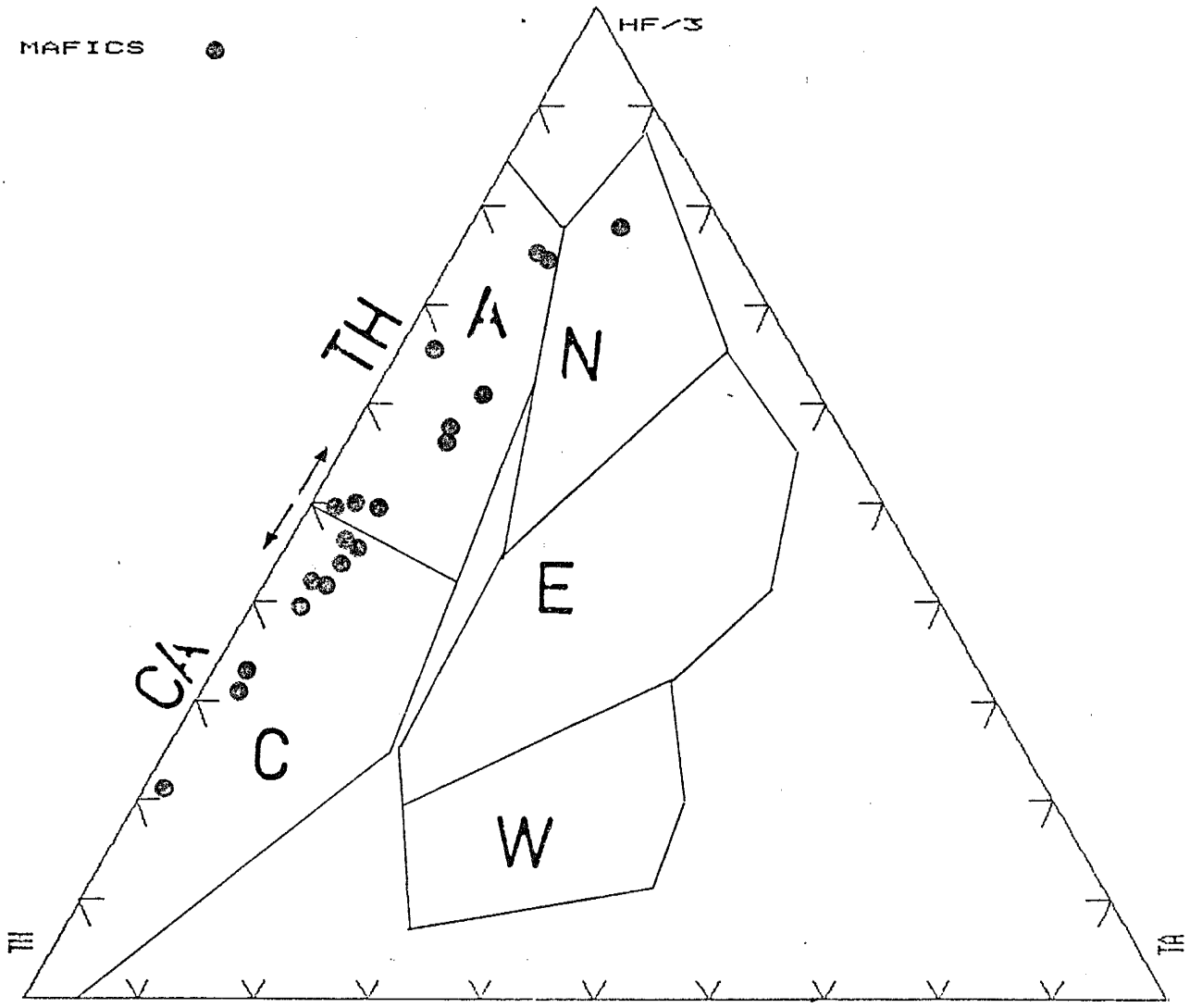

Figure 15. Distribution of northern Sangre de Cristo mafic rocks on TH - TA - HF/3 diagram. Fields after Wood (1980), CA: calc-alkaline, TH: primitive island arc tholeiite, C: subduction-zone related basalts, A: island arc basalts, N: N-MORB. E: E-MORB, W: within-plate basalts.

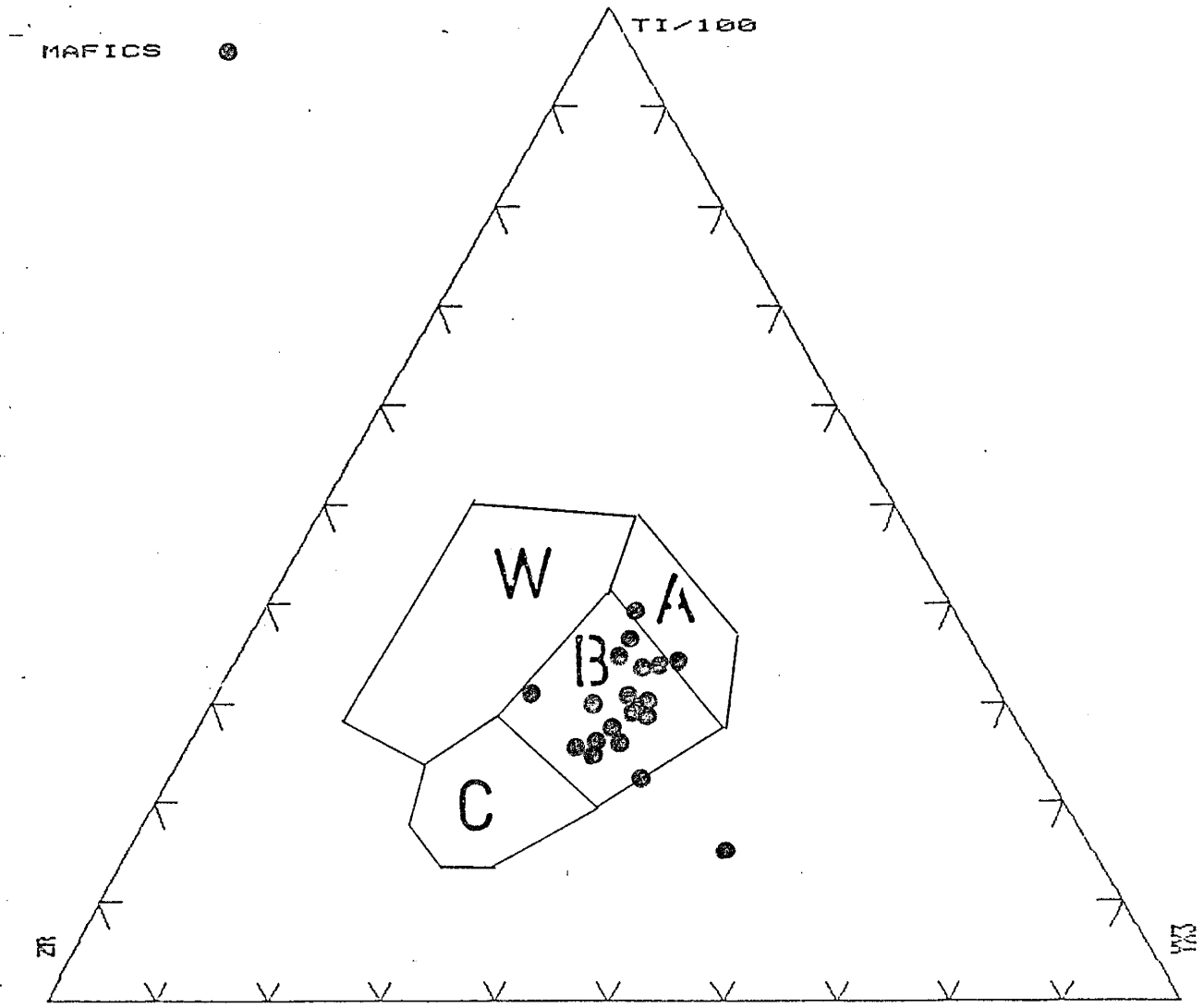

Figure 16. Distribution of northern Sangre de Cristo mafic rocks on Zr - Yx3 - Ti/100 diagram. Fields after Pearce and Cann (1973), C+B+A: plate margin basalts, B: ocean floor basalts, W: within-plate basalts.

discriminates between primitive and evolved samples. Those samples that plot on the evolved side of the diagram have undergone significant magnetite fractionation. When the samples are considered on this diagram, they plot dominantly in the arc field with most falling on the arc side of the MORB overlap field and only a few falling in the within-plate field (Fig.17). The majority of the samples plot on the primitive side of the diagram illustrating that they have not undergone significant magnetite fractionation. Most notably from the previous examples is the fact that the mafic rocks of the northern Sangre sucsession do not show a within-plate signature.

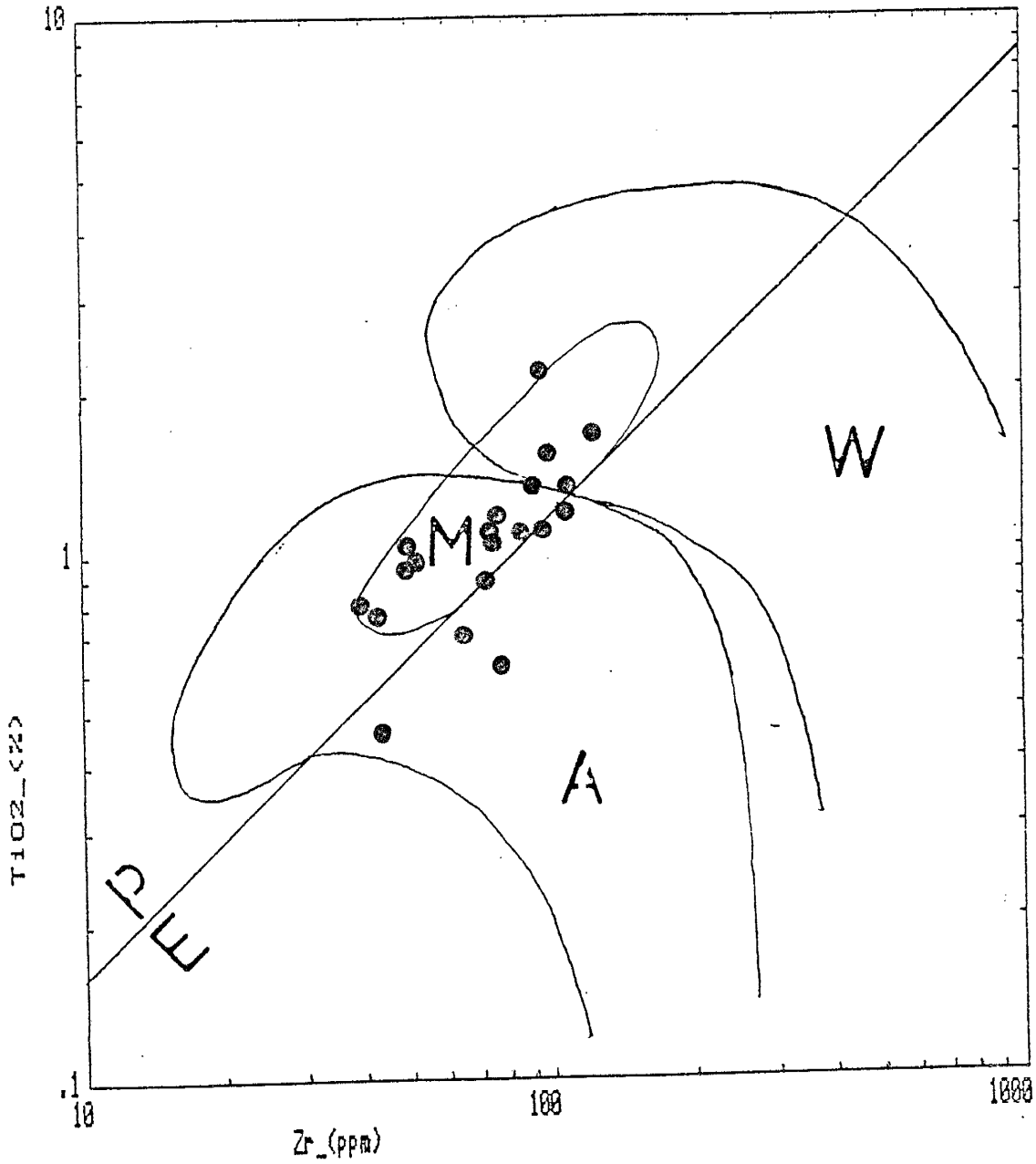

Figure 17. Distribution of northern Sangre de Cristo mafic rocks on Zr vs. TiO2 diagram. Fields after Pharoah and Pearce (1984), P: primitive, E: evolved, M: mid-ocean ridge basalts, A: arc basalts, W: within-plate basalts. Samples which plot in evolved field have undergone significant magnetite fractionation.

INTERMEDIATE ROCKS

Andesites and metasediments of andesitic composition are found throughout the field area and are almost indistinguishable in both their field characteristics and chemistry (Table 3). Their chondrite normalized REE patterns show LREE enrichment from 20-100x chondrites, very small negative Eu anomalies, and nearly flat HREE patterns (Fig.18). MORB-normalized trace element patterns for the intermediate volcanics of the northern Sangres show significant LREE enrichment relative to the HFS elements (Fig.19). These patterns also show the characteristic negative Ta and Nb anomaly which suggests they are subduction zone related rocks. The negative Ti anomaly observed in all the intermediate samples may be attributted to a subduction zone component, fractional crystallization of magnetite or result from a minor phase such as ilmenite or rutile that remains in the source. To futher characterize the Sangre andesites, MORB-normalized trace element diagrams were made for average andesites from New Hebrides and Japan and compared to the MORB-normalized trace element patterns of the northern Sangre

TABLE 2 : Chemical Composition of Intermediate Rocks from the northern Sangre de Cristo Range

	RHYDAC.	AND.	AND.	AND.	MEDSED.	MEDSED.
SAMPLE	TSG-3D	TSC-2	TSC-7	TSC-20	TKG-1	TSG-11
SiO2	67.8	60.5	60.6	65.5	63.8	47.1
TiO2	0.8	1.0	1.0	0.2	0.9	0.5
Al2O3	14.3	15.0	15.0	17.4	15.8	12.4
Fe2O3-T	4.7	8.7	9.3	3.0	7.0	9.1
MgO	1.1	1.8	1.8	0.8	0.6	4.5
CaO	2.1	3.6	3.7	2.4	1.6	22.2
Na2O	3.8	4.2	4.9	5.0	5.1	1.9
K2O	3.9	3.0	2.3	4.0	4.3	0.4
MnO	0.0	0.3	0.2	0.0	0.0	0.2
P2O5	0.2	0.3	0.3	0.1	0.2	0.1
LOI	0.5	2.1	0.2	1.0	0.0	0.7
TOTAL	99.8	101.0	99.7	99.9	99.7	99.5
Rb	183.3	61.7	42.1	121.7	69.1	23.3
Ba	907.5	1208.4	1187.9	1544.5	1946.9	164.5
Cs	6.8	0.3	0.7	1.2	0.3	0.4
Sr	152.3	178.4	306.6	870.6	189.9	215.6
Pb	26.0	20.2	17.6	12.2	38.0	10.2
Th	7.0	5.8	3.3	2.1	5.0	5.8
U	5.0	3.0	2.4	2.4	1.6	3.0
Sc	10.5	20.9	16.2	2.1	10.2	17.9
V	67.6	85.8	101.3	17.6	28.9	108.7
Cr	1.3	4.5	1.9	2.3	8.0	333.0
Co	5.4	9.6	10.8	1.6	5.0	24.1
Ni	ND	ND	ND	ND	ND	149.6
Y	111.3	43.1	41.9	15.2	29.9	19.4
Zr	453.3	180.2	182.6	174.3	324.9	89.7
Nb	27.5	11.7	9.6	6.9	14.1	6.5
Hf	18.5	5.5	3.8	3.8	7.9	2.7
Ta	1.7	0.6	0.6	0.4	0.5	0.2
La	37.1	36.7	26.6	22.9	42.0	15.7
Ce	144.6	84.4	60.8	44.3	95.6	37.1
Sm	17.4	9.1	7.6	3.5	10.4	4.4
Eu	2.4	2.5	1.7	0.9	2.2	1.4
Tb	3.3	1.4	1.1	0.4	0.9	0.5
Yb	8.7	4.2	3.5	1.3	2.1	1.6
Lu	1.3	0.6	0.5	0.2	0.3	0.3
Mg Number	35.6	32.3	30.4	40.0	17.5	52.6
K2O/Na2O	1.0	0.7	0.4	0.8	0.8	0.2
Na2O+K2O	7.8	7.2	7.3	9.0	9.4	2.4
Al2O3/TiO2	17.8	15.0	15.0	73.1	16.6	22.1
CaO/TiO2	2.6	3.6	3.7	10.0	1.7	39.6
Zr/TiO2	0.0	0.0	0.0	0.0	0.0	0.0
K/Rb	180.5	402.4	468.8	273.3	519.1	165.2

TABLE 2 : Chemical Composition of Intermediate Rocks from the northern Sangre de Cristo Range

Ba/Sr	5.9	6.7	3.8	1.7	10.2	0.7
Rb/Sr	1.2	0.3	0.1	0.1	0.3	0.1
La/Yb	4.2	8.7	7.5	17.2	19.4	9.4
La/Sm	2.1	4.0	3.4	6.3	4.0	3.5
Sm/Eu	7.1	3.5	4.3	3.7	4.6	3.0
Ti/Zr	10.6	33.1	32.9	8.2	17.5	37.4
Zr/Nb	16.4	15.3	18.9	25.1	22.9	13.6
Nb/Y	0.2	0.2	0.2	0.4	0.4	0.3
Zr/Y	4.0	4.1	4.3	11.4	10.8	4.6
Nb/Ta	15.8	16.9	14.6	16.1	24.8	24.4
Nb/La	0.7	0.3	0.3	0.3	0.3	0.4
La/Ta	21.3	53.1	40.3	53.3	73.6	58.2
La/Th	5.2	6.2	7.9	10.4	8.4	2.7
Y/Tb	33.5	30.8	37.0	33.8	32.1	34.1
Th/Yb	0.8	1.4	0.9	1.6	2.3	3.4
Ta/Yb	0.2	0.1	0.1	0.3	0.2	0.1
Hf/Th	2.6	0.9	1.1	1.7	1.6	0.4
Ti/V	71.3	69.7	59.3	81.1	196.9	30.9
U/Pb	0.1	0.1	0.1	0.2	0.0	0.3
FeO-T/MgO	3.6	4.2	4.6	3.0	9.4	1.8
Sm/Yb	2.0	2.1	2.1	2.7	4.8	2.6
Eu/Eu*	0.4	0.8	0.7	0.8	0.7	1.0

Fe2O3-T ==> Total Fe as Fe2O3
NO ENTRY ==> No determination OR below detectability limit
MAJOR ELEMENTS ==> In weight percent
TRACE ELEMENTS ==> In parts per million
==========

TABLE 2 : Chemical Composition of Intermediate Rocks from the northern Sangre de Cristo Range

	MEDSED.	AND.		
SAMPLE	TGP-4	THP-P1	AVG	STD
SiO2	53.3	64.3	60.4	6.4
TiO2	0.8	0.6	0.7	0.2
Al2O3	19.0	15.1	15.5	1.8
Fe2O3-T	7.4	4.6	6.7	2.2
MgO	2.7	3.9	2.2	1.3
CaO	8.2	1.1	5.6	6.5
Na2O	5.2	1.7	4.0	1.3
K2O	1.6	4.4	3.0	1.3
MnO	0.1	0.2	0.1	0.0
P2O5	0.5	0.1	0.2	0.1
LOI	0.1	1.7	0.8	0.7
TOTAL	99.3	98.0	99.6	0.7
Rb	43.6	64.0	76.1	48.7
Ba	755.9	2090.5	1225.8	593.6
Cs	1.2	0.3	1.4	2.0
Sr	784.1	89.1	348.3	283.1
Pb	17.2	12.9	19.3	8.5
Th	0.9	4.2	4.3	1.9
U	3.1	2.1	2.8	0.9
Sc	14.2	8.9	12.6	5.5
V	137.2	52.4	74.9	38.4
Cr	21.1	2.0	46.7	108.3
Co	16.7	5.9	9.9	6.8
Ni	11.9	ND	20.2	49.0
Y	25.2	27.4	39.2	28.7
Zr	156.6	144.1	213.2	110.0
Nb	11.9	11.7	12.5	6.1
Hf	4.1	3.3	6.2	4.8
Ta	0.4	0.6	0.6	0.4
La	30.8	23.4	29.4	8.2
Ce	70.4	50.0	73.4	32.7
Sm	7.2	5.1	8.1	4.1
Eu	1.7	1.2	1.8	0.5
Tb	0.9	0.7	1.1	0.8
Yb	2.1	1.7	3.1	2.2
Lu	0.3	0.2	0.5	0.3
Mg Number	45.4	65.8	40.0	13.8
K2O/Na2O	0.3	2.6	0.8	0.7
Na2O+K2O	6.9	6.1	7.0	2.6
Al2O3/TiO2	21.9	24.5	25.7	18.2
CaO/TiO2	9.4	1.9	9.1	11.9
Zr/TiO2	0.0	0.0	0.0	0.0
K/Rb	316.7	574.5	362.6	143.3

TABLE 2 : Chemical Composition of Intermediate Rocks from the northern Sangre de Cristo Range

Ba/Sr	0.9	23.4	6.7	7.0
Rb/Sr	0.0	0.7	0.3	0.3
La/Yb	14.1	13.5	9.2	3.6
La/Sm	4.2	4.5	3.6	1.9
Sm/Eu	4.1	4.1	4.5	7.5
Ti/Zr	33.2	25.6	24.8	10.5
Zr/Nb	13.1	12.2	17.2	4.4
Nb/Y	0.4	0.4	0.3	0.1
Zr/Y	6.2	5.2	6.3	2.8
Nb/Ta	26.4	19.6	18.5	14.6
Nb/La	0.3	0.5	0.4	0.7
La/Ta	68.4	39.1	43.5	19.5
La/Th	33.1	5.5	9.9	9.0
Y/Tb	27.7	37.0	33.1	33.5
Th/Yb	0.4	2.4	1.3	0.8
Ta/Yb	0.2	0.3	0.2	0.1
Hf/Th	4.4	0.7	1.7	1.2
Ti/V	37.9	70.6	77.2	48.0
U/Pb	0.1	0.1	0.1	0.0
FeO-T/MgO	2.4	1.0	2.7	1.5
Sm/Yb	3.3	2.9	2.5	1.8
Eu/Eu*	0.7	0.7	0.6	0.3

Fe2O3-T ==> Total Fe as Fe2O3
NO ENTRY ==> No determination OR below detectability limit
MAJOR ELEMENTS ==> In weight percent
TRACE ELEMENTS ==> In parts per million
========== 0.00 0.00

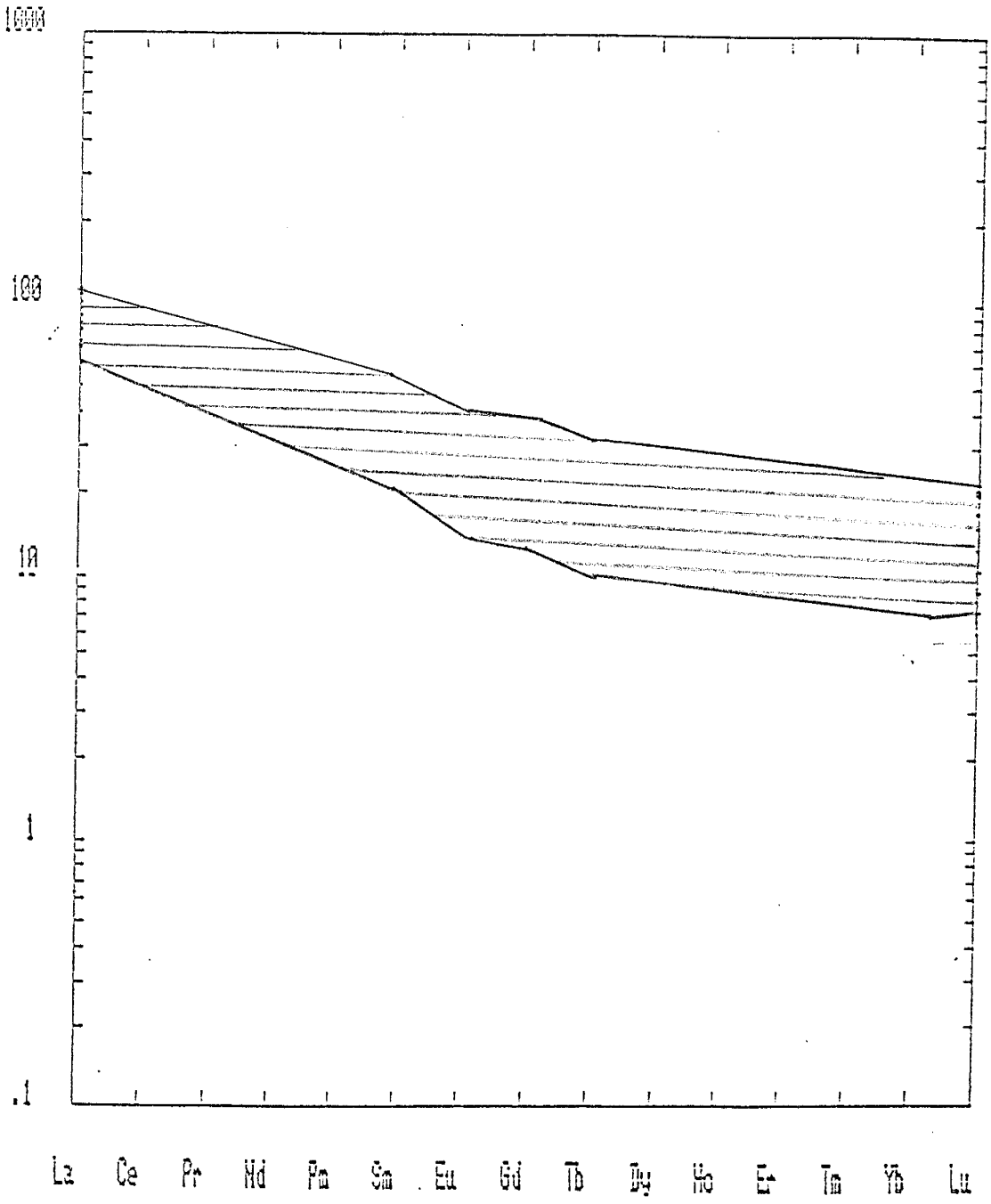

Figure 18. Chondrite-normalized REE patterns showing envelope of variation for intermediate rocks from the northern Sangre de Cristo Range.

Figure 19. MORB-normalized trace element patterns showing envelope of variation for intermediate rocks from the northern Sangre de Cristo Range.

andesites (Fig.20). This figure illustrates the similarity of the northern Sangre andesites to those of the New Hebrides and Japan and shows these andesites have similarities to andesites from continental margin arcs. The similarity seen in the northern Sangre andesites, to the average andesite from Japan, is not as close to the similarity seen with the New Hebrides andesites. The northern Sangre samples have significantly higher concentrations of the LIL elements then the Japan andesites.

Trace element diagrams to characterize andesites from different tectonic settings have been proposed by Bailey (1981) and Pearce (1983) . When the northern Sangre samples are plotted on these diagrams they tend to scatter among the various fields on the diagrams or fall outside the fields. Despite these problems some interpretations can be drawn from these diagrams. On the Ti/V vs. Zr/Y diagram of Bailey (1981) (Fig.21) two of the northern Sangre samples plot within the overlap area between the calc-alkaline continental margin arc and island arc fields. The other samples plot outside the boundaries of these fields but have Zr/Y ratios characteristic of andesites from these settings. Condie

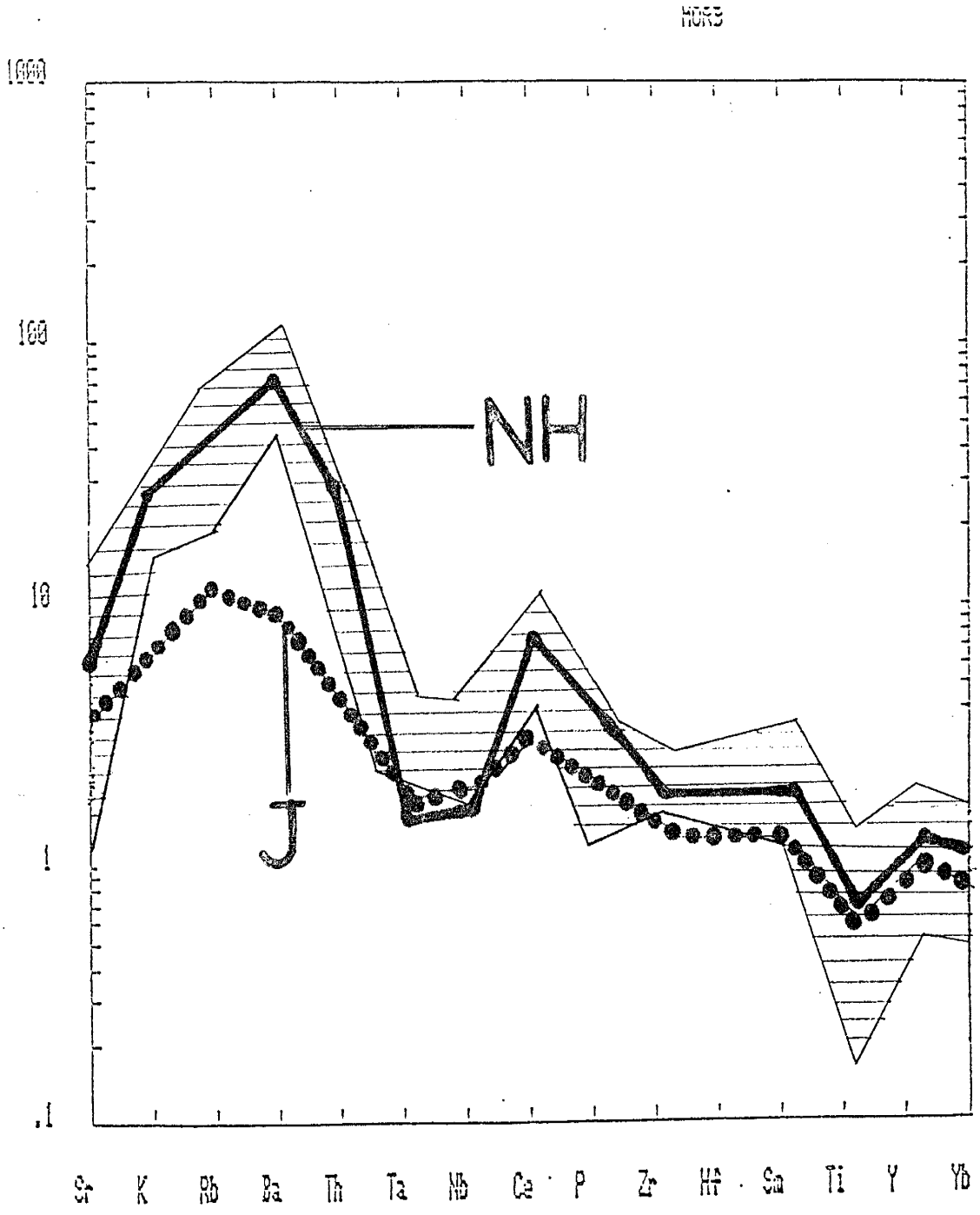

Figure 20. MORB-normalized trace element patterns for intermediate rocks from the northern Sange de Cristo Range compared to an andesite from NH: New Hebrides, J: Japan, (Basaltic Volcanism study project, 1981).

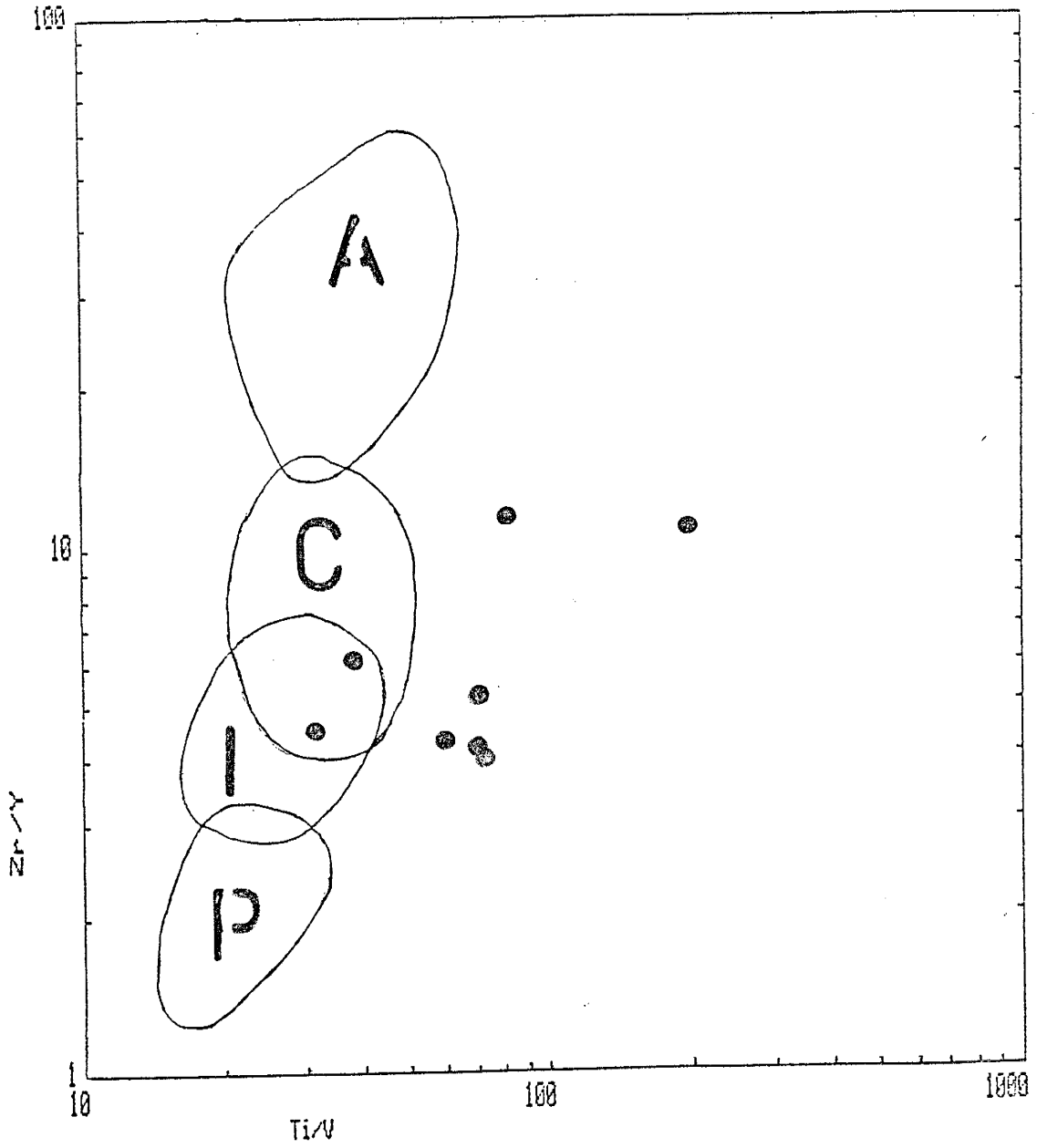

Figure 21. Distribution of northern Sangre de Cristo intermediate rocks on Ti/V vs. Zr/Y diagram. Fields after Bailey (1981), A: Andean, C: calc-alkaline, continental margin, I: calc-alkaline, island arc, P: primitive arc.

has also proposed the Th/Yb vs. La/Yb (unpublished, 1985) for the classification of andesites (Fig.22) and again the samples plot in and around the fields for calc-alkaline continental margin arcs and island arcs. The most significant aspect of these diagrams is that the andesites from the northern Sangre succession do not plot in or near fields for primitive or Andean arcs. Table 4 compares trace element ratios charactersitic of andesites from various tectonic settings to those of the andesites from the northern Sangres. The northern Sangre andesites are similar in their trace element ratios to calc-alkaline andesites from continental margin and island arcs.

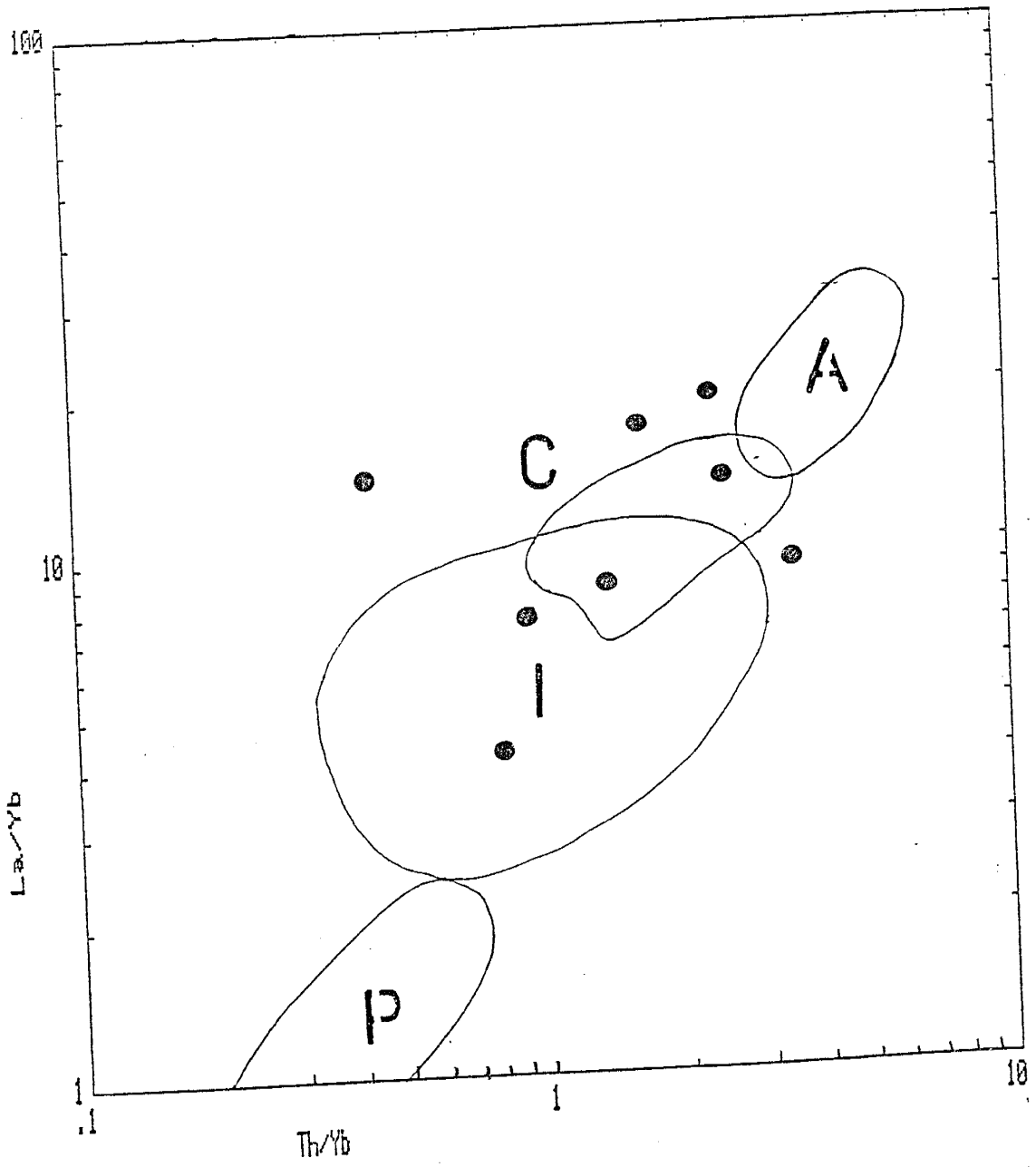

Figure 22. Distribution of northern Sangre de Cristo intermediate rocks on Th/Yb vs. La/Yb diagram. Fields same as in figure 21.

Table 4. Ranges of trace element ratios for andesites from various modern tectonic setting in comparison to andesites from the northern Sangre de Cristo area.

element ratio	Sangre samples	Primitive arc	calc-alk Island Arc	calc-alk Continental Margin Arc	Andean
La/Yb	5-17	1-2.5	3-10	5-15	12-30
Th/Yb	1-2.5	<0.8	0.5-3	1-4	3-7
Zr/Y	4-12	<3	3-7	4-12	12-50
Ti/V	60-80	<30	20-40	20-50	20-70
Hf/Yb	1-3	<1	1-3	1-3	>3
Ti/Zr	8-33	>50	40-50	40-50	<40

FELSIC ROCKS

As previously mentioned because of metamorphism and deformation it is difficult to distinguish of various populations of felsic rocks. This is also evidenced by chemical variation within the felsic rocks (Table 2), which may be partially the result of mechanical concentration of crystalclasts or non-volcanogenic sediment. Field characteristics suggest two populations of felsic rocks: massive ash flow tuffs and felsic volcaniclastics. The two groups do not show enough chemical distinction to be recognized on the various geochemical discrimination diagrams and will be treated together in this discussion.

The felsic rocks range from 66% - 78% SiO2 and show a high degree of variation in many of the major and trace elements (Table 3). All the felsic rocks are light REE enriched (~ 100 x chondrites), have small negative Eu anomalies and nearly flat heavy REE paterns (Fig.23). When considered on a MORB-normalized trace element diagram (Fig.24) the felsic rocks show considerable enrichment in the LIL elements relative to the HFS elements. All of the felsic rocks are characterized by negative P and Ti anomalies probably due to minor phases such as apatite, ilmenite, or rutile in the source. When the MORB-normalized trace element patterns for the Sangre felsic rocks are compared to those form modern rhyolites

TABLE 3 : Chemical Composition of Felsic Rocks from the northern Sangre de Cristo Range

	FELSIC	FELSIC	FELSIC	FELSIC	FELSIC	FELSIC
SAMPLE	TSG2-7	TSG2-2	TSG2-6	TSG2-5	TEB-1	TEB-3
SiO2	73.2	75.6	78.3	76.7	72.3	76.1
TiO2	0.1	0.1	0.1	0.1	0.2	0.2
Al2O3	12.3	12.2	11.8	12.4	13.7	12.2
Fe2O3-T	5.4	2.6	1.3	1.9	3.2	1.8
MgO	1.8	2.5	1.3	1.4	1.2	1.4
CaO	0.4	0.5	0.6	1.0	1.1	1.3
Na2O	4.8	3.4	5.9	5.8	4.9	4.6
K2O	0.9	1.7	0.2	0.6	2.4	1.7
MnO	0.0	0.0	0.0	0.0	0.0	0.0
P2O5	0.0	0.0	0.0	0.0	0.0	0.0
LOI	0.2	1.5	0.4	0.4	1.3	1.1
TOTAL	99.7	100.5	100.4	100.6	100.7	100.8
Rb	17.1	21.5	0.0	5.7	28.7	24.2
Ba	779.4	875.5	46.6	191.9	1974.9	681.8
Cs	0.4	0.1	0.0	0.5	0.5	0.0
Sr	44.8	75.2	59.9	121.2	98.0	75.9
Pb	11.2	16.4	12.4	12.0	11.5	14.2
Th	8.6	8.9	11.4	5.2	7.3	9.4
U	4.1	3.6	3.7	2.3	2.4	4.0
Sc	3.9	5.6	3.8	4.6	11.7	5.5
V	0.2	2.2	ND	ND	9.4	1.9
Cr	0.5	0.3	ND	0.6	4.2	ND
Co	1.9	1.7	1.6	3.4	1.5	0.6
Ni	ND	ND	ND	ND	ND	ND
Y	87.8	68.8	72.8	57.2	29.4	49.2
Zr	366.0	293.9	278.4	301.0	248.2	306.7
Nb	22.1	17.6	16.7	12.2	12.6	14.7
Hf	9.5	9.9	7.7	8.6	8.2	6.4
Ta	1.4	1.2	1.1	1.0	1.2	0.9
La	42.8	47.0	42.9	30.7	35.1	36.5
Ce	102.9	107.6	100.5	71.2	75.7	75.6
Sm	12.7	10.6	11.3	8.2	6.5	8.4
Eu	1.4	1.6	0.9	1.1	1.4	0.9
Tb	2.3	1.7	1.6	1.9	1.0	1.2
Yb	8.6	8.6	6.2	8.6	4.2	4.4
Lu	1.4	1.3	1.0	1.3	0.7	0.7
Mg Number	43.2	68.3	69.5	62.5	46.3	63.2
K2O/Na2O	0.2	0.5	0.0	0.1	0.4	0.3
Na2O+K2O	5.8	5.1	6.2	6.4	7.4	6.3
Al2O3/TiO2	77.4	73.1	90.6	73.8	53.7	59.3
CaO/TiO2	2.8	3.2	4.7	5.9	4.4	6.3
Zr/TiO2	0.2	0.1	0.2	0.1	0.1	0.1
K/Rb	461.2	655.7	ERR	893.9	705.8	596.9

TABLE 3 : Chemical Composition of Felsic Rocks from the northern Sangre de Cristo Range

Ba/Sr	17.3	11.6	0.7	1.5	20.1	8.9
Rb/Sr	0.3	0.2	0.0	0.0	0.2	0.3
La/Yb	4.9	5.4	6.9	3.5	8.2	8.1
La/Sm	3.3	4.4	3.7	3.7	5.3	4.3
Sm/Eu	8.6	6.5	12.6	6.9	4.3	8.5
Ti/Zr	2.6	3.4	2.8	3.3	6.1	4.0
Zr/Nb	16.5	16.6	16.6	24.5	19.6	20.8
Nb/Y	0.2	0.2	0.2	0.2	0.4	0.3
Zr/Y	4.1	4.2	3.8	5.2	8.4	6.2
Nb/Ta	15.8	14.3	14.4	11.4	10.3	15.6
Nb/La	0.5	0.3	0.3	0.4	0.3	0.4
La/Ta	30.5	38.2	36.9	28.7	28.7	38.8
La/Th	4.9	5.2	3.7	5.8	4.8	3.8
Y/Tb	38.1	38.9	43.7	29.2	28.8	38.1
Th/Yb	1.0	1.0	1.8	0.6	1.7	2.1
Ta/Yb	0.1	0.1	0.1	0.1	0.2	0.2
Hf/Th	1.1	1.1	0.6	1.6	1.1	0.6
Ti/V	3555.5	441.4	ERR	ERR	161.9	646.8
U/Pb	0.3	0.2	0.3	0.2	0.2	0.2
FeO-T/MgO	0.3	0.2	0.3	0.2	0.2	0.2
Sm/Yb	2.6	0.9	0.8	1.2	2.3	1.1
Eu/Eu*	1.4	1.2	1.8	0.9	1.5	1.9

Fe2O3-T ==> Total Fe as Fe2O3
NO ENTRY ==> No determination OR below detectability limit
MAJOR ELEMENTS ==> In weight percent
TRACE ELEMENTS ==> In parts per million

TABLE 3 : Chemical Composition of Felsic Rocks from the northern Sangre de Cristo Range

	FELSIC	FELSIC	FELSIC	FELSIC	FELSIC	FELSIC
SAMPLE	TEB-5	TSC-8	TSC-10	TSC-15	TSC-16	TBC-13
SiO2	77.7	74.3	76.5	66.7	74.7	77.5
TiO2	0.1	0.2	0.1	0.2	0.1	0.1
Al2O3	12.0	13.1	11.6	16.3	12.0	11.9
Fe2O3-T	0.9	3.0	2.4	4.0	3.2	2.3
MgO	1.3	1.1	1.1	2.4	2.8	0.7
CaO	0.7	0.6	1.4	0.8	0.0	0.9
Na2O	4.9	5.6	4.2	3.7	0.3	5.1
K2O	1.6	1.6	1.3	7.5	4.3	1.1
MnO	0.0	0.0	0.3	0.1	0.1	0.0
P2O5	0.0	0.0	0.0	0.0	0.0	0.0
LOI	0.3	0.3	0.5	0.4	1.3	0.5
TOTAL	99.9	100.3	99.9	102.7	99.2	100.5
Rb	19.7	38.3	14.6	110.6	94.7	10.6
Ba	497.6	844.4	1610.5	2225.8	803.7	1435.2
Cs	0.1	0.1	0.1	0.5	0.4	0.4
Sr	70.6	66.3	184.4	103.2	5.0	73.8
Pb	12.8	12.4	12.6	20.9	12.0	9.5
Th	8.9	4.3	8.3	10.3	9.0	7.9
U	4.5	2.1	3.6	4.3	3.3	2.3
Sc	5.0	5.7	5.7	6.2	5.1	3.3
V	1.9	1.9	6.8	33.2	5.0	1.9
Cr	1.2	2.1	0.5	4.3	3.3	0.2
Co	1.1	0.7	3.6	5.9	1.8	1.6
Ni	ND	ND	ND	0.6	ND	ND
Y	34.1	59.1	41.5	56.6	69.7	63.5
Zr	324.6	290.0	289.6	337.8	251.9	276.2
Nb	13.2	13.1	14.2	23.9	17.6	21.8
Hf	7.0	10.5	8.7	8.5	8.7	10.3
Ta	0.8	0.9	0.8	1.6	1.3	1.4
La	15.1	59.70	22.4	33.3	52.0	37.4
Ce	33.8	132.70	48.3	73.5	117.8	79.6
Sm	3.7	14.65	9.2	7.4	11.1	12.6
Eu	0.6	3.34	0.6	0.8	0.7	1.5
Tb	0.6	2.23	0.9	1.3	1.9	2.0
Yb	3.7	6.44	5.0	5.7	8.6	7.6
Lu	0.6	1.02	0.8	0.9	1.3	1.3
Mg Number	76.5	45.4	51.0	57.6	66.3	42.1
K2O/Na2O	0.3	0.3	0.3	2.0	14.0	0.2
Na2O+K2O	6.6	7.3	5.6	11.2	4.6	6.2
Al2O3/TiO2	79.5	64.5	60.4	63.7	77.8	102.1
CaO/TiO2	4.9	3.3	7.4	3.4	0.2	8.4
Zr/TiO2	0.2	0.1	0.1	0.1	0.1	0.2
K/Rb	695.7	364.5	761.9	563.1	379.3	922.2

TABLE 3 : Chemical Composition of Felsic Rocks from the northern Sangre de Cristo Range

Ba/Sr	7.0	12.7	8.7	21.5	157.9	19.4
Rb/Sr	0.2	0.5	0.0	1.0	18.6	0.1
La/Yb	4.0	9.2	4.4	5.7	6.0	4.9
La/Sm	4.0	4.0	2.4	4.4	4.6	2.9
Sm/Eu	5.8	4.3	14.4	8.9	15.3	8.3
Ti/Zr	2.7	4.2	4.0	4.5	3.6	2.5
Zr/Nb	24.4	22.0	20.3	14.1	14.2	12.6
Nb/Y	0.3	0.2	0.3	0.4	0.2	0.3
Zr/Y	9.5	4.9	6.9	5.9	3.6	4.3
Nb/Ta	16.1	13.4	16.5	14.6	12.8	15.5
Nb/La	0.8	0.2	0.6	0.7	0.3	0.5
La/Ta	18.4	60.9	26.0	20.3	37.6	26.7
La/Th	1.6	13.6	2.7	3.2	5.7	4.7
Y/Tb	51.6	26.5	46.1	40.7	35.7	30.9
Th/Yb	2.3	0.6	1.6	1.7	1.0	1.0
Ta/Yb	0.2	0.1	0.1	0.2	0.1	0.1
Hf/Th	0.7	2.4	1.0	0.8	0.9	1.3
Ti/V	459.9	637.7	168.3	46.1	183.4	360.0
U/Pb	0.3	0.1	0.2	0.2	0.2	0.2
FeO-T/MgO	0.3	0.1	0.2	0.2	0.2	0.2
Sm/Yb	0.6	2.4	1.9	1.4	1.0	2.7
Eu/Eu*	1.0	2.2	1.8	1.2	1.2	1.6

Fe2O3-T ==> Total Fe as Fe2O3
NO ENTRY ==> No determination OR below detectability limit
MAJOR ELEMENTS ==> In weight percent
TRACE ELEMENTS ==> In parts per million
==========

TABLE 3 : Chemical Composition of Felsic Rocks from the northern Sangre de Cristo Range

SAMPLE	FELSIC AVG	FELSIC STD
SiO2	75.0	3.0
TiO2	0.1	0.0
Al2O3	12.6	1.2
Fe2O3-T	2.7	1.1
MgO	1.6	0.6
CaO	0.8	0.3
Na2O	4.4	1.4
K2O	2.1	1.9
MnO	0.0	0.0
P2O5	0.0	0.0
LOI	0.7	0.4
TOTAL	100.4	0.8
Rb	32.1	33.1
Ba	997.3	649.2
Cs	0.2	0.1
Sr	81.5	41.8
Pb	13.2	2.8
Th	8.3	1.9
U	3.3	0.8
Sc	5.5	2.0
V	5.4	8.8
Cr	1.4	1.5
Co	2.1	1.4
Ni	0.0	0.1
Y	57.5	16.1
Zr	297.0	32.4
Nb	16.6	3.8
Hf	8.7	1.2
Ta	1.1	0.2
La	37.9	11.7
Ce	84.9	27.2
Sm	9.7	2.9
Eu	1.2	0.7
Tb	1.6	0.5
Yb	6.5	1.8
Lu	1.0	0.2
Mg Number	57.7	11.2
K2O/Na2O	1.5	3.7
Na2O+K2O	6.5	3.3
Al2O3/TiO2	73.0	13.2
CaO/TiO2	4.6	2.1
Zr/TiO2	0.1	0.0
K/Rb	ERR	ERR

TABLE 3 : Chemical Composition of Felsic Rocks from the northern Sangre de Cristo Range

Ba/Sr	23.9	40.9
Rb/Sr	1.8	5.0
La/Yb	5.9	1.7
La/Sm	3.9	0.7
Sm/Eu	8.7	3.4
Ti/Zr	3.6	0.9
Zr/Nb	18.5	3.8
Nb/Y	0.3	0.0
Zr/Y	5.6	1.8
Nb/Ta	14.2	1.8
Nb/La	0.4	0.1
La/Ta	32.6	10.7
La/Th	5.0	2.8
Y/Tb	37.4	7.2
Th/Yb	1.4	0.5
Ta/Yb	0.1	0.0
Hf/Th	1.1	0.4
Ti/V	ND	ND
U/Pb	0.2	0.0
FeO-T/MgO	0.2	0.2
Sm/Yb	1.5	1.7
Eu/Eu*	1.5	1.6

Fe2O3-T ==> Total Fe as Fe2O3
NO ENTRY ==> No determination OR below detectability limit
MAJOR ELEMENTS ==> In weight percent
TRACE ELEMENTS ==> In parts per million
==========

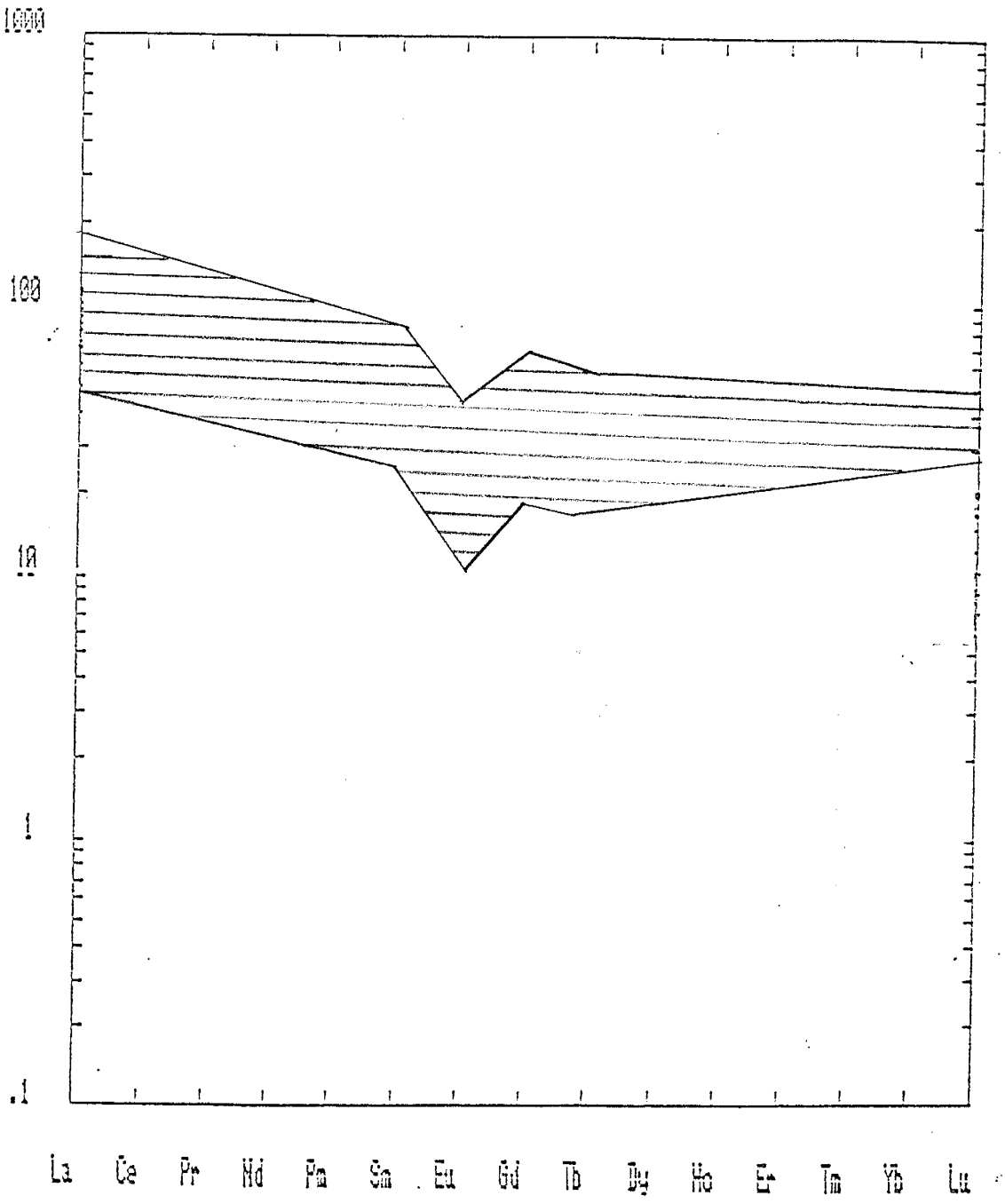

Figure 23. Chondrite-normalized REE patterns envelope variation for felsic rocks from the northern Sangre de Cristo Range.

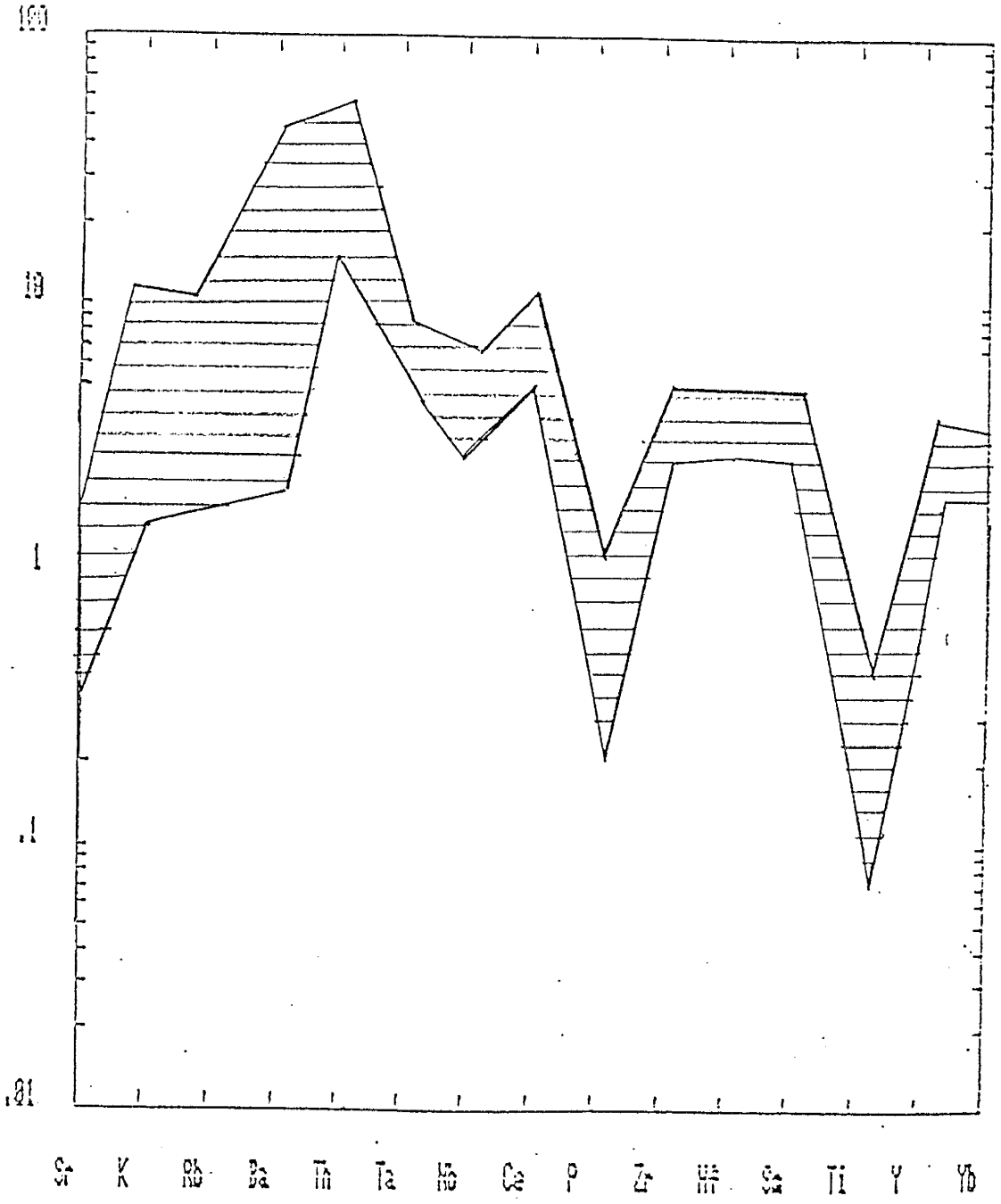

Figure 24. MORB-normalized trace element patterns showing envelope of variation for felsic rocks from the northern Sangre de Cristo Ranage.

from intracratonic rifts, continental margin arcs and primitive oceanic arcs (Ewart, 1979; and references therein) they show the greatest similarities to rhyolites from intracratonic rifts and continental margin arcs (Fig.25). Close agreement is seen between the patterns except for some of the more mobile LIL elements. The felsic rocks show the least similarities to modern rhyolites from oceanic island arcs that tend to have lower concentrations of both the LIL and HFS elements (Fig.26).

To further characterize the felsic rocks they are plotted on various trace element tectonic discrimination diagrams. On the Zr vs. Hf diagram the felsic rocks fall exclusively in the extensional basins field (Fig.27). Samples which plot in this field are from continental rifts or back arc basin tectonic settings. When considered on the Y vs. TiO2 diagram, the samples plot in the continental arc and rift field (Fig.28) and on the Zr vs. Y diagram (Fig.29) they fall within the extensional basin field. Other binary plots such as Zr vs. TiO2 , Zr vs.Y and Y vs. La/Yb record similar results. As a further test, the samples were plotted on the Y+Nb vs. Rb and Y vs. Nb diagrams of Pearce et al. (1984), for granitic rocks (Figures 30 and 31). On these diagrams, the samples also fall dominantly in the within- plate field. Hence felsic rocks of the northern Sangre de Cristo area show a

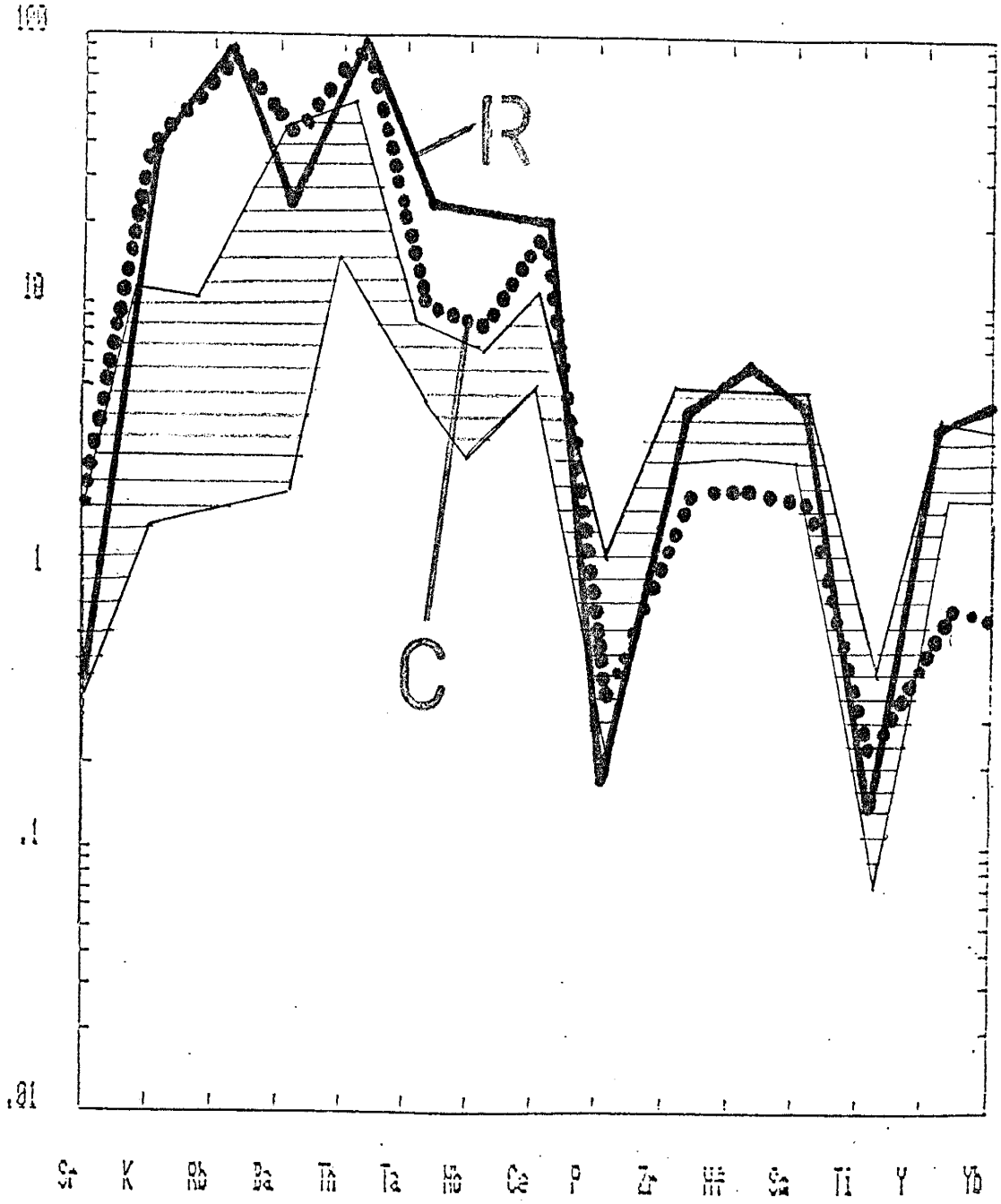

Figure 25. MORB-normalized trace element patterns for felsic rocks from the northern Sangre de Cristo Range compared to modern rhyolites from R: rift settings, C: continental arcs.

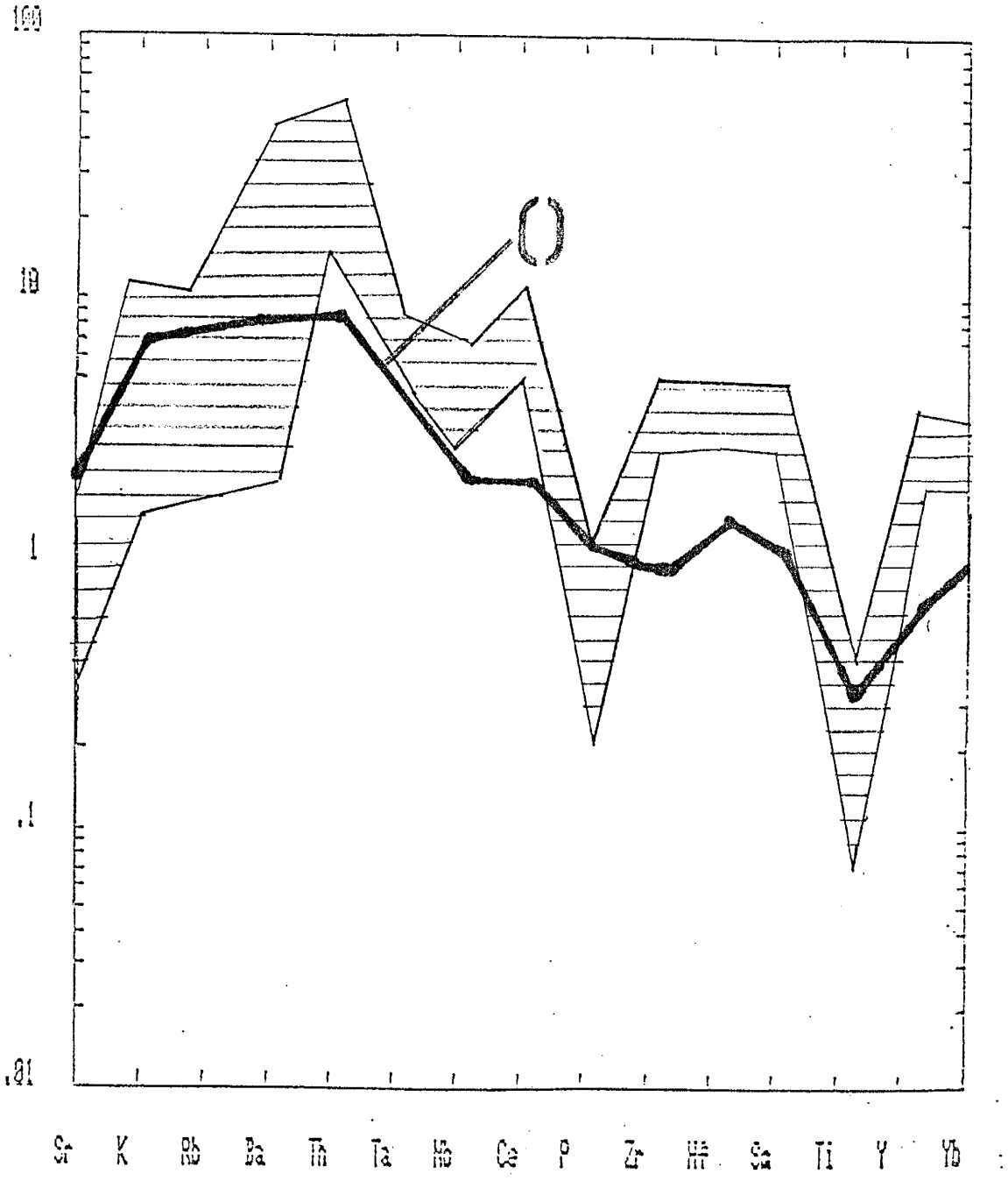

Figure 26. MORB-normalized trace element patterns for felsic rocks from the northern Sangre de Cristo Range compared to modern rhyolites from O: oceanic arcs.

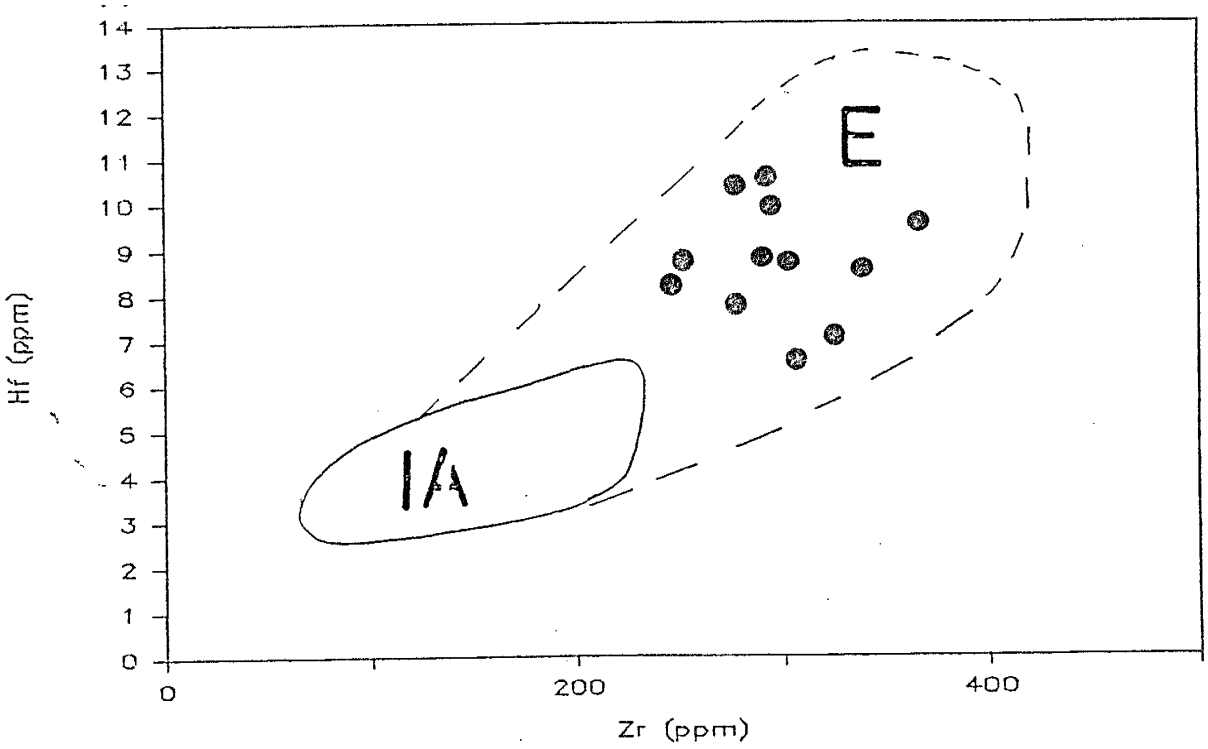

Figure 27. Distribution of felsic rocks from the norther Sangre de Cristo Range on Zr vs. Hf diagram , E: extensional basin settings including continental rifts and back-arc basins, IA: island arc settings.

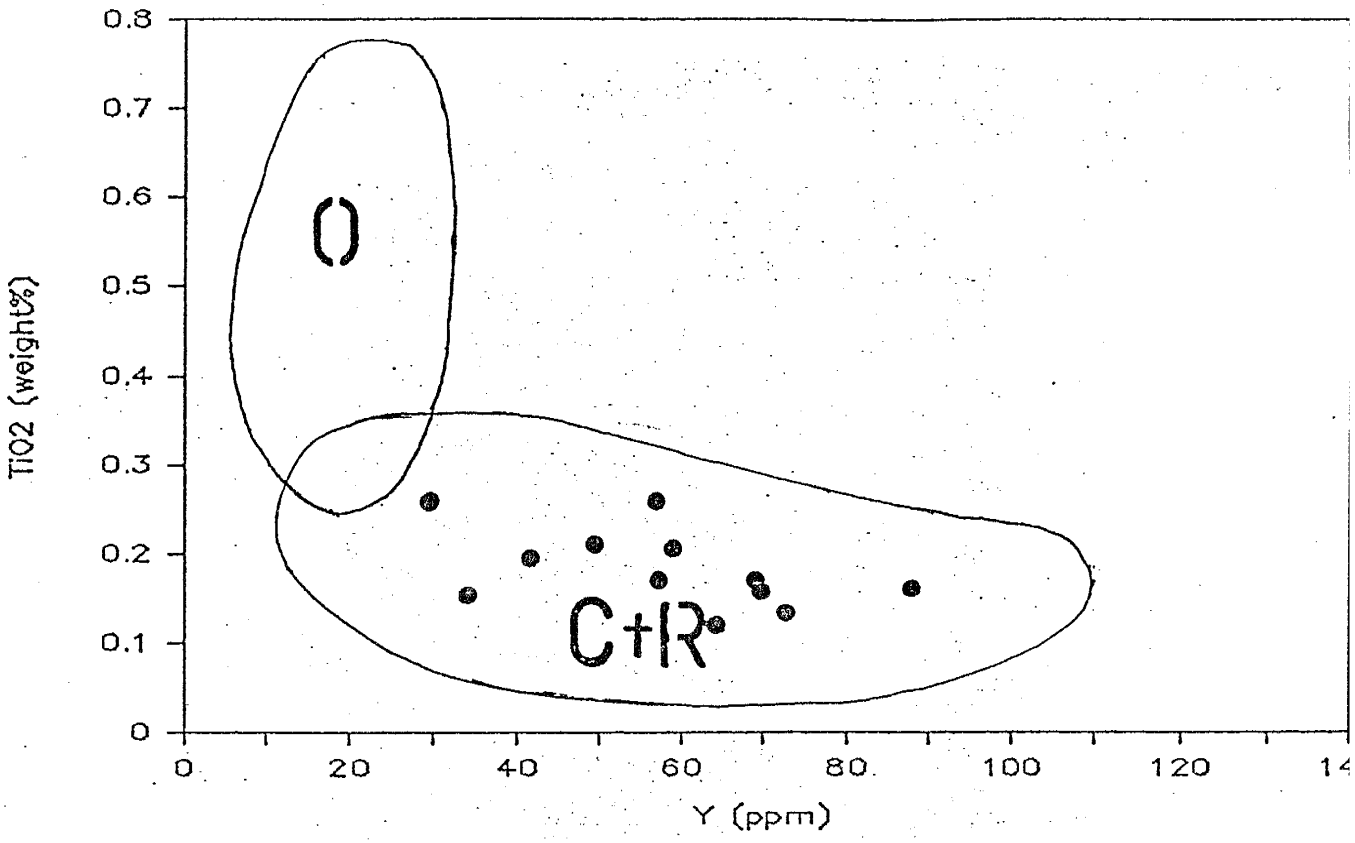

Figure 28. Distribution of felsic rocks from the northern Sangre de Cristo Range on Y vs. TiO2 diagram, C+R: continental arcs and rifts, O: oceanic arc settings.

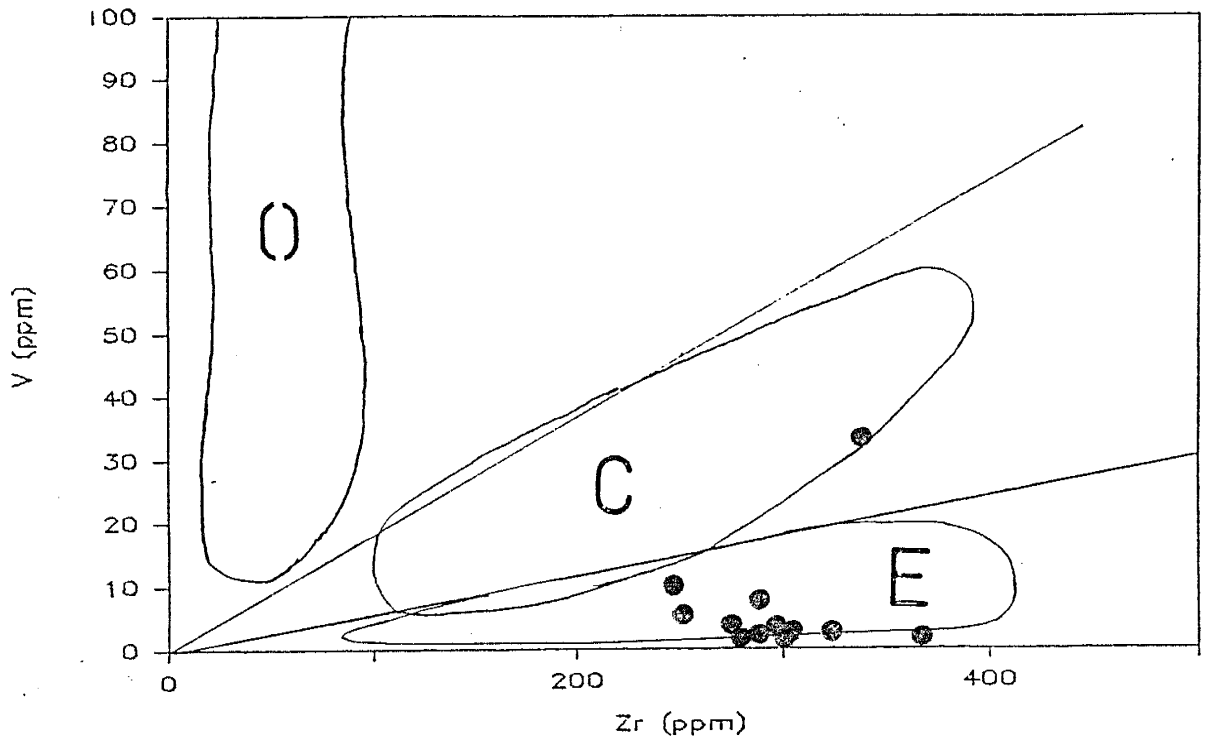

Figure 29: Distribution of felsic rocks from the norther Sangre de Cristo Range on Zr vs. V diagram, E: extensional basin settings including continental rifts and back-arc basins, C: continental arcs, O: oceanic arcs.

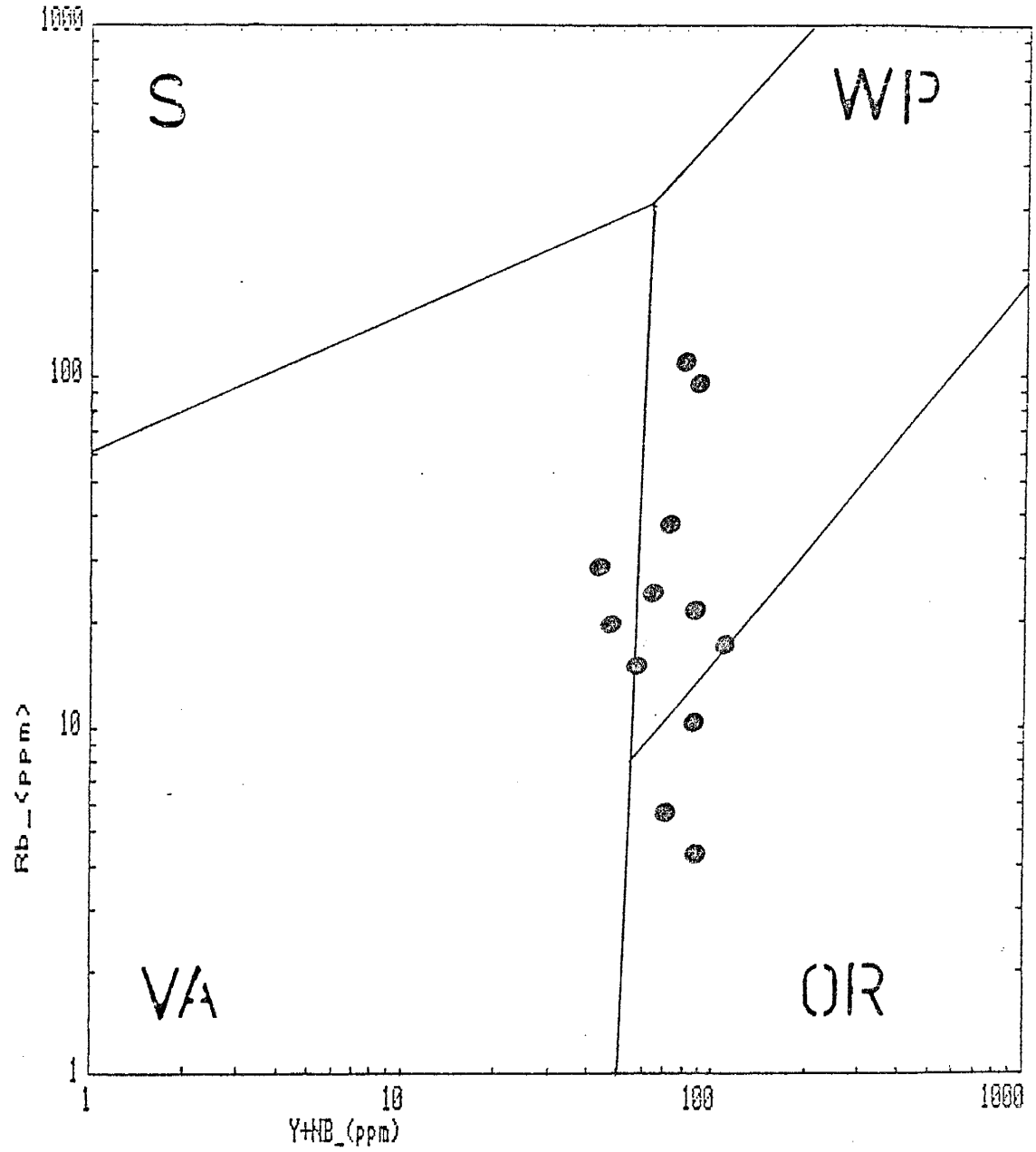

Figure 30. Distribution of felsic rocks from the northern Sangre de Cristo Range on Y+Nb vs. Rb diagram for granitic rocks. Fields after Pearce et al. (1984), VA: volcanic arcs, S: syncollisional settings, WP: within-plate settings; OR: ocean ridge settings.

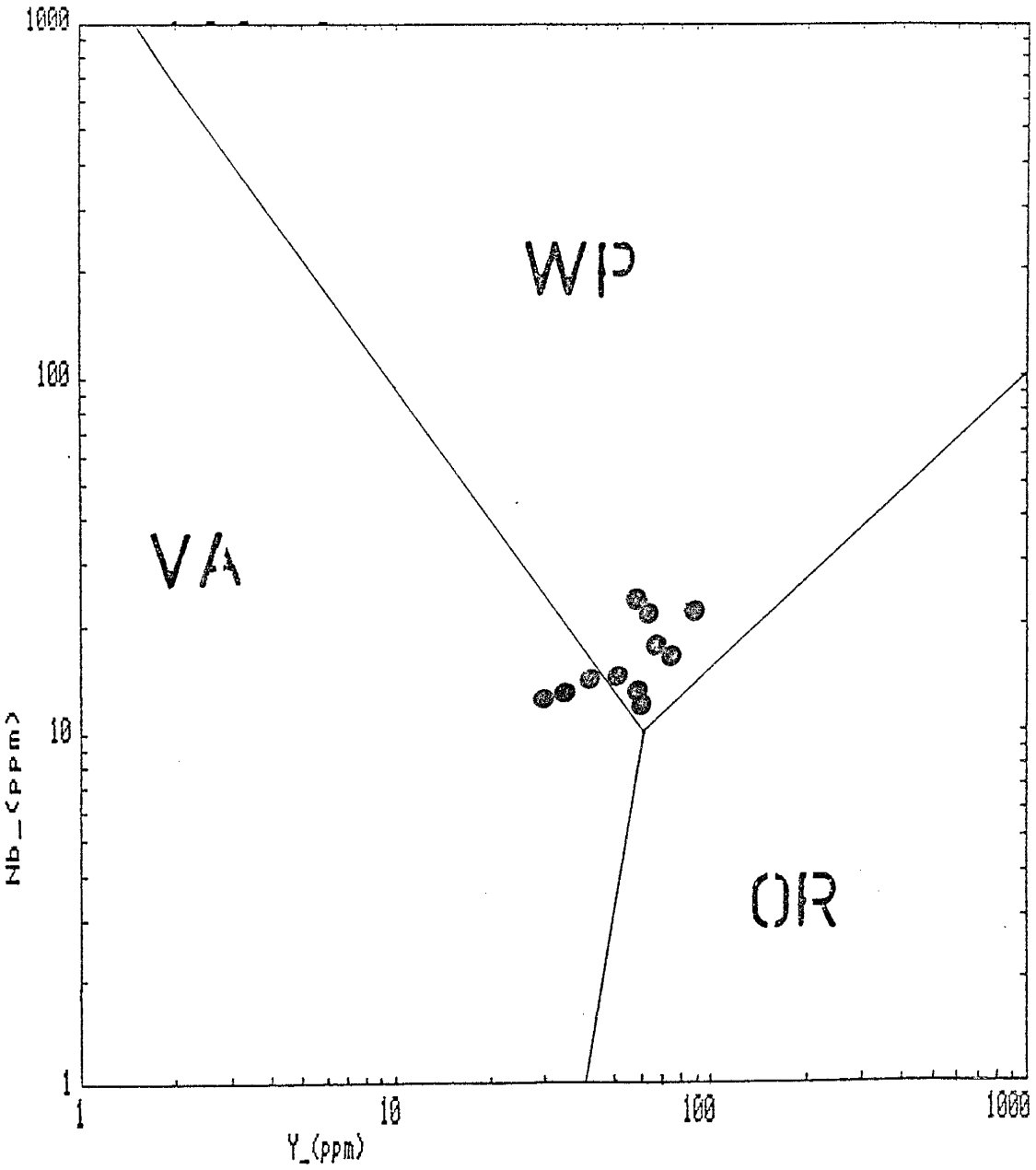

Figure 31. Distribution of felsic rocks from the northern Sangre de Cristo Range on Y vs. Nb diagram for granitic rocks. Fields same as in figure 30.

significant within-plate character on several different geochemical discriminant diagrams.

DISCUSSION

GEOCHEMICAL MODELING

To better determine the petrogenesis of the northern Sangre volcanic rocks, geochemical modeling using both major and trace elements has been investigated. The models tested include batch melting, incremental melting, open system fractional crystallization, and closed system fractional crystallization. A brief discussion of each model and the assumptions used in that model follows.

During batch melting a starting composition is assumed for the source from which magmas are derived so that the composition of the batch is that of the source. The composition of the liquid and residual solid are assumed to remain in equilibrium at all times. For the purposes of modeling it is also assumed that modal batch melting occurs. Modal batch melting assumes that the modes of mineral phases in the source are the same as those entering the magma, so that the mass fraction of a mineral in the source rock is equal to the mass fraction of a mineral entering the melt.

Incremental melting also requires assuming a starting composition for the source. During melting it is assumed that small batches of melt are removed from the source after small increments of melting. The composition of the source changes as each batch is removed so that

the residue left behind is the source for the next batch melt. The amount of melt must be assumed along with the amount removed in each batch.

In closed system fractional crystallization, a starting composition of the parent magma is assumed from which the rocks are derived. As crystallization occurs the composition of the magma changes and the solids separate from the magma as fast as crystallization occurs. It is assumed that the composition of the parent magma would be equal to that of the residual liquid and aggregate solids at any point. The amount of crystallization is assumed and adjusted to best fit the model.

In open system fractional crystallization, a starting composition of the parent magma is assumed. During crystallization new injections of primary magma into the fractionation chamber occurs so that the composition of the parent magma at any point is equal to the residual liquid and the aggregate solids plus the injected magma. During open system fractional crystallization, the amount of injection of new primary magma along with its composition is assumed. Again the amount of crystallization is assumed and adjusted to best fit the model.

To model the rocks of the northern Sangres, first the major element least squares computer modeling program MIXFRAC (after Wright and Doherty, 1970) by Knoper

(1987a) was used. This program computes by least squares approximation using fractional crystallization, the mineral proportions that would be seen in the daughter using the major element composition of a hypothetical parent and daughter. The hypothetical parent and daughter are assumed from actual samples from the field area. likely Mineral compositions are taken from the literature (Deer et al., 1966; Frey and Prinz, 1978; Coolen, 1982; Janardhan et al., 1982; Ramsey et al., 1984). Starting mineral modes and melt proportions were taken from a compilation by Condie (1985). The model calculates the major element concentrations that would be expected in the daughter given the major element concentrations in the hypothetical parent chosen for the model. These concentrations are compared to the concentrations of the hypothetical daughter chosen for the model. The model is adjusted using different starting compositions for both the parent and daughter, and different degrees of fractionation until a reasonable fit betweem the calculated and hypothetical daughters is accomplished and a value as close to zero is calculated.

Once a satisfactory model is found using the major elements it is used as a start to begin trace element modeling. Trace element modeling involves using modeling programs on MODULUS (Knoper, 1987b). MODULUS includes models designed to test both open and closed system fractional crystallization, modal and non-modal

equilibrium (batch) melting, and incremental melting. The calculated daughter mineral proportions from the major element modeling are input as a starting point for trace element modeling. The modeling involves assuming source and daughter trace element concentrations which are taken from likely candidates from the study area to start and from the literature if initial assumptions prove incorrect. The trace element concentrations are input into the model and the amount of fractional crystallization or melting is assumed. The trace element concentrations that would be expected in the daughter, given the concentrations input for the hypothetical parent, are calculated and listed along side the observed daughter concentrations for comparison (Appendix E). Further modeling involves trying different parent daughter combinations, changing mineral proportions, amount of minor phases, and degree of fractional crystalization or partial melting to obtain a better fit between the calculated and observed daughter trace element cooncentrations. The equations used for Rayleigh fractional crystallization and batch melting are listed in Appendix F.

MODELS TESTED

The possible modeling scenarios described in the previous section were tested for the rocks of the Sangre de Cristos and adjacent areas. The results and conclusions of the modeling are presented in this section.

As mentioned in the geochemistry section the mafic rocks have moderate to high MG numbers (40 - 67) and most are classified as primitive (Fig.17). The similarities in the composition of the mafic rocks in the area is interpretted to reflect a cogenetic suite. These similarities along with the trends of both the major and trace element versus MG number (Figures 8 and 9) suggest fractional crystallization for the petrogenesis of the mafic rocks. The absence of very high MG numbers (>70) suggests that the mafic rocks were derived from melts that were not in equilibrium with mantle material.

The first step in modeling the mafic rocks was to try and characterize the mantle source for the mafic magmas. This mantle source composition was calculated using the most primitive mafic sample (TEB-2). This sample is considered to represent the composition of the most primitive magma based on its high Ni content (165 ppm) and high MG number (67). The sample showed no evidence of being a cummulate and was representative of

a large mafic body found in the northeastern section of the study area. For the purpose of modeling this sample was considered to represent a 10% - 20% fractionation of a mafic magma, as would be typical for a gabbro. A simple mineralogy of olivine, orthopyroxene, and clinopyroxene was also assumed.

The calculated trace element concentrations of the hypothetical parent magma (Cl), that for a 10% fractional crystallization would produce TEB-2, is shown in Table 5, column 1. Using these trace element concentrations the hypothetical mantle source (Co) was calculated assuming the calculated magma (Cl) represented a 20% melt of this source (Table 5, Column 2). The trace element concentrations calculated for this mantle source (Co) are compared to the trace element concentrations seen in Lherzolites and Wood's primordial mantle for comparison (Table 5, columns 3-5).

Table 5 illustrates that using the most primitive sample to calculate the mantle source for the northern Sangre de Cristo area mafic rocks does not generate a composition for the source that shows much similarity to either Lherzolite or primordial mantle. Various models were tested using different samples to represent the daughter aggregate, more complex mineralogies, and varying degrees of fractional crystallization with inconsistent results. The simplest model is represented in Table 5 and suggests that the petrogenesis of the

mafic rocks involved a more complex history and that they are not the fractionation products of a magma that was in equilibrium with Lherzolite or primordial mantle.

The relationship of the mafic rocks to the intermediate and felsics was also tested using fractional crystallization modeling. The composition of the most primitive gabbro from the study area (TEB-2) was used to represent the composition of the mafic magma. Major element modeling for the production of the intermediates from a mafic source was first tested, Table 6a shows the results of this modeling. The major element composition of the assumed daughter andesite and source magma along with an assumed mineralogy is input. The modeling program calculates by least squares approximation the estimated source magma major element composition and compares it to the composition that was input to represent the source. A simple mineralogy of plagioclase, clinopyroxene, olivine and magnetite was input for the source. The observed and estimated major element concentrations of the mafic source are in fair agreement (the sum of the squared residuals = 0.1376), but an unreasonable amount of fractionation (90%) is calculated using this model. Table 6a also shows that a reasonably good fit can be obtained using another gabbro (TSP-1, MG number = 55) with the sum of the squared residuals = 0.5932 and a more reasonable amount of fractionation (70%). Table 6a represents the best fit obtained between observed and

Table 5. Calculated trace element concentrations in calculated ultramafic source for Sangre gabbro TEB-2 compared to average Lherzolites and Primordial Mantle.

element: (ppm) :	calc. Mafic Cl F=.1	calc. Mafic Co F=.2	(1) avg. Mantle Lherz.	(1) avg. K.H. Lherz.	(2) P.M.
Rb :	2.7	1.1	-	-	0.9
Ba :	47.4	19.6	-	-	7.6
Sr :	73.4	31.2	-	-	23
Th :	0.2	0.1	0.3	0.2	0.1
Y :	2.2	1.1	-	-	1.9
Zr :	7.7	3.3	-	-	11
Nb :	0.7	0.3	-	-	0.6
La :	1.2	0.5	2.1	0.2	0.7
Ce :	3.1	1.3	5.3	0.4	1.9
Sm :	0.45	0.19	0.4	0.3	0.4
Eu :	0.15	0.06	0.1	0.1	-
Tb :	0.9	0.4	-	-	0.1
Yb :	0.23	0.11	-	0.3	-
Lu :	0.04	0.02	0.01	0.06	-

using :	mode(%)	melt(%)
olivine:	60	25
opx :	25	20
cpx :	15	55

F = 0.2

opx - orthopyroxene
cpx - clinopyroxene
Lherz - Lherzolite
P.M.- Primordial Mantle
K.H. - Kilbourne Hole

References:
(1) Basaltic Volcanism study project (1981)
(2) Wood (1979)

Table 6a. Calculated parent basalt major element concentrations in comparison to observed concentrations for FXL from basalt to andesite.

major element (%)	observed parent (TSP-1)	estimated parent using (TSC-20)	observed parent (TEB-2)	estimated parent using (THP-P1)
SiO2	52.31	52.35	48.68	48.66
TiO2	0.91	0.82	0.79	0.99
Al2O3	18.87	18.93	16.29	16.29
Fe2O3-T	8.37	8.38	10.56	10.53
MnO	0.14	0.02	0.17	0.01
MgO	4.47	4.44	9.45	9.47
CaO	9.41	9.35	11.31	11.35
Na2O	4.05	3.31	2.17	2.40
K2O	1.22	1.33	0.44	0.55
P2O5	0.25	0.30	0.13	0.10
	squared residuals = 0.5932		squared residuals = 0.1376	
	F = 0.7		F = 0.9	

using	estimated mode (%)
plag	65
cpx	18
ol	6
mag	10

using	estimated mode (%)
plag	53
cpx	23
ol	13
mag	10

plag - plagioclase
cpx - clinopyroxene
ol - olivine
mag - magnetite

estimated sources but this senario can yield approximately the same results using many intermediate rocks from the study area to represent the daughter.

Modeling the possibility of the felsic rocks representing the fractional crystallizatiion products of the few remaining percent of a mafic magma was tested. The andesite TSC-20 was used as the starting composition of the remaining magma. This sample was chosen because it was representative of a large body found along the crest of the Sangre de Cristo Range and did not have textures indicative of a metasedimentary rock. Major element modeling using many different samples from the study area to represent source and daughter concentrations, trying all reasonable combinations of mineralogy, degree of fractionation, and two step fractionation for andesite to dacite, and dacite to rhyolite gave no acceptable results. In each case the sum of the squared residuals was too high and the mineral proportion and degree of fractionation unreasonable.

Results from major element modeling showed that relating the andesites and the mafic rocks through fractional crystallization is not unreasonable. Modeling the production of the felsic rocks from a mafic magma using fractional crystallization does not prove realistic. Modeling results using major elements were not conclusive, and were used to begin trace element modeling.

Trace element modeling investigating the production of the andesites from a mafic magma using fractional crystallization shows that the andesites may be related to the basalts but the results are not conclusive. Table 6b shows the calculated trace element concentrations for andesites using the trace element concentrations of two different gabbros from the study area as starting compositions for the mafic magma. For comparison trace element concentrations in two different andesites from the field area are also listed. The agreement between the calculated and observed andesites is not precise but for elements such as Y, Nb, Sm, Eu, Lu and Hf the agreement is not unrealistic given the variation seen among the bulk composition of these rocks.

Trace element modeling of the felsic rocks was also tested. Based on the results of both the major and trace element modeling the production of the felsic rocks by fractional crystallization from a mafic source proved unrealistic. A model involving partial melting was then tested.

Major element modeling was first tested using the composition of a sample (TEB-1) from the study area to represent the composition for the daughter liquid (C1) produced from a partial melt. This sample was chosen because it had the textural features of a massive tuff and was representative of extensive flows found throughout the northern part of the study area. Assuming

Table 6b. Calculated andesite trace element concentrations in comparison to observed concentrations for FXL from basalt to andesite.

using TEB-2 as a parent

element (ppm)	calculated andesite	observed andesite TSG-11	observed andesite THP-P1
Ba	181.8	164.6	-
Sr	453.6	215.7	89.2
Y	19.4	19.5	27.4
Zr	58.9	89.7	-
Nb	5.8	6.6	11.8
Ce	23.0	37.3	-
Sm	4.13	4.44	5.15
Eu	1.51	1.44	1.23
Tb	0.57	0.57	0.74
Yb	2.15	1.67	1.72
Lu	0.34	0.30	0.29
Hf	2.81	2.78	3.35
V	129.5	108.7	52.4
Pb	9.8	10.3	13.0

using TSP-1 as parent

element (ppm)	calculated andesite	observed andesite TSG-11	observed andesite THP-P1
Ba	643.2	164.6	-
Sr	777.9	215.7	89.2
Y	20.8	19.5	27.4
Zr	101.2	89.7	-
Nb	8.1	6.6	11.8
Ce	41.7	37.3	-
Sm	5.14	4.44	5.15
Eu	1.64	1.44	1.23
Tb	1.00	0.57	0.74
Yb	2.15	1.67	1.72
Lu	0.36	0.34	0.29
Hf	2.81	2.78	3.35
V	157.9	108.7	52.4
Pb	10.6	10.3	13.0

using	mode (%)
olivine	10
clinopyroxene	50
plagioclase	30
magnetite	10

F = 0.7

the simple mineralogy listed in table 7a and that TEB-1 represented the daughter produced by a 30% partial melt, the major element concentrations for the granitic source (Co) were calculated (Table 7a). This model was tested using several felsic rocks from the study area, and produced similar results.

For comparison to this calculated felsic source, the major element concentrations of other felsic rocks are listed. Except for SiO2, the calculated felsic source is most similar to an average Archean tonalite in its major element concentrations, but the fit is not excellent and the degree of partial melting to achieve this fit (30%) is perhaps slightly higher than what would be expected (20%).

The same model was tested using trace elements (Table 7b). Again sample TEB-1 was used to represent the daughter produced from the partial melt, the model gives similar results for many of the samples tested. Table 7b lists the calculated trace element concentrations for the granitic source and for comparison trace element concentrations of Archean and modern continental crust are also listed. Major element modeling showed the calculated felsic source to be most similar to an average Archean tonalite but trace element modeling does not show nearly as close a correlation between these two sources. The calculated felsic source shows little resemblance to any of the compositions listed in Table 7b. Many

Table 7a. Calculated granitic source major element concentrations in comparison to estimated felsic rocks and continental crust.

major element (%)	calculated granitic source	(1) avgerage Archean Tonalite	(1) avgerage Archean Granite
SiO2	71.98	69.2	72.5
TiO2	0.28	0.35	0.36
Al2O3	15.88	15.80	13.5
Fe2O3-T	0.83	3.0	2.5
MnO	0.02	0.04	0.05
MgO	1.17	1.10	0.5
CaO	2.62	3.30	1.6
Na2O	4.94	5.0	3.4
K2O	2.09	1.5	5.2
P2O5	0.04	0.10	0.15

major element (%)	(2) avgerage continental crust	(3) avgerage upper crust	(4) avgerage. canadian shield
SiO2	63.2	66.0	65.2
TiO2	0.6	0.5	0.6
Al2O3	16.1	15.2	15.8
Fe2O3-T	-	-	-
MnO	0.08	-	-
MgO	2.8	2.2	2.2
CaO	4.7	4.2	3.3
Na2O	4.2	3.9	3.7
K2O	2.1	3.4	3.2
P2O5	0.19	-	-

phase	mode (%)	melt (%)	
plagioclase	59	31	
biotite	4	4	
quartz	17	30	F = 0.3
magnetite	1	1	
k-spar	17	34	

References:

(1) Condie (1985)
(2) Weaver and Tarney (1984)
(3) Taylor and Mclennon (1985)
(4) Eade and Fahrig (1971)

Table 7b. Calculated granitic source trace element concentrations in comparison to estimated Archean and continental crust.

element (ppm)	calculated granitic source	(1) average Archean Tonalite	(2) upper continental crust	(3) India middle crust	(3) India lower crust	(4) Archean lower crust
Rb	7.7	500	112	62	13	11
Ba	647.5	400	550	937	499	757
Sr	119.8	460	350	602	509	569
Th	4.63	6	11	8	1.4	0.4
Y	21.5	7	22	15	13	7
Zr	1641.2	140	190	179	134	202
Nb	2.9	6	25	8	5	5
La	9.8	30	30	43	31	22
Ce	20.1	50	64	79	60	44
Sm	1.66	2.9	4.5	5	5	3
Eu	0.6	0.7	0.9	1.5	1.3	1.2
Tb	0.67	0.28	0.6	0.5	0.5	0.4
Yb	5.83	0.5	2.2	1.3	1.1	1.2
Lu	1.2	0.1	0.3	0.2	0.2	0.2

using	mode (%)	melt (%)
orthopyroxene.	5	0
clinopyroxene.	4	0
plagioclase	57	30
biotite	5	4
k-spar	8	34
quartz	18	30
magnetite	2	1
zircon	1	1

F = 0.2

References:

(1) Condie (1985)
(2) Taylor and Mclennon (1985)
(3) Allen (1985)
(4) Weaver and Tarney (1984)

combinations of mineralogy, including minor phases, were tested without obtaining conclusive results. Incremental batch melting was also tested but unrealistic results were obtained.

The calculated granitic source may not be representative of the actual source of the felsic rocks from the study area. Based on the results of the geochemical modeling the felsic rocks of the northern Sangre de Cristo area probably have not been produced by partial melts of a source we see represented today. Significant contamination of the felsic magma may have occurred during their petrogenesis but this cannot be substantiated based on their composition or the various models tested. A partial melting model proved more realistic than one involving fractional crystallization of a mafic source but results are not conclusive.

PETROGENESIS

In this section results from the petrography, geochemistry, and geochemical modeling sections will be discussed relative to the petrogenesis of the volcanic and volcaniclastic rocks of the northern Sangre de Cristo Mountains and adjacent areas. This section is divided into mafic and intermediate rocks, felsic rocks, and the relationship of the Sangre de Cristo Supracrustal rocks to adjacent areas.

Mafic and Intermediate rocks

The mafic rocks of the northern Sangre de Cristo area have primary textures representative of both flows and dikes, and show many similarities in their composition. Relative age correlation can be made based on field characteristics but no changes in composition can be correlated with relative age. Mafic rocks occur intruding and interlayered with intermediate and felsic rocks thrroughout the field area.

Compositionally the mafic rocks range from being evolved to primitive (MG No. 40-67), with the majority showing a slightly primitive character. The mean value for most of the major and trace elements are very similar for the gabbros and basalts and based on the findings

presented in the geochemistry section they are believed to be cogenetic. The major and trace elements further suggest that the mafic igneous rocks underwent fractional crystallization involving primarily olivine and plagioclase (Figures 8 and 9). Geochemical modeling favors fractional crystallization for the petrogenesis of the mafic rocks and indicates that the source of the mafic rocks was not in equilibrium with Lherzolite or primordial mantle.

The intermediate rocks of the nothern Sange de Cristo area consist of andesitic flows and metasediments which are often undistinguishable or only distinguishable by careful field, petrographic and geochemical studies. Throughout southern Colorado and northern New Mexico, the 1800-1700 Ma volcanigenic rocks are distinctly bimodal (Boardman and Condie, 1985) so that the scarcity of andesites in similar terranes throughout the Southwest makes their comparison to other Proterozoic andesites problematic.

More than one model for the petrogenesis for the andesites must be considered. Geochemical modeling indicates that some of the intermediate rocks may be genetically related to the mafic rocks through fractional crystallization, but models are not conclusive. The andesites could have been produced by fractional crystallization of a mafic source in a subduction related regime and represent the fractionation trend seen in a

typical tholeiitic complex which produce intermediate to felsic liquids only when there is a few percent of the original magma remaining (Carmichel et al., 1974). This model can explain the relative scarcity of andesites seen in the area (<10%). The greatest difficulty in determining the petrogenesis of the imtermediate rocks is distinguishing sediments from andesitic flows. One mechanism for the production of rocks of andesitic character is from the mixing of sediments and MORB. Sediments typically have a positive Eu anomaly and 10% appears to be the upper limit of sediment contribution before the characteristic Eu appears. None of the andesitic rocks from the study area have a positive Eu anomaly though field studies show that some of the andesites have textures indicative of metasediments. The possibility of the mixing of mafic magma with sediments to produce the andesites cannot be disregarded based on their chemistry but the percent of sediment would have been less than 10%. Contamination of mafic magma with continental crust can also produce rocks of intermediate character. The intermediate rocks from the area do not show similarities to Andean andesites (Figures 21 and 22) which are typically LREE enriched and HREE depleted, and do not have high concentrations of LIL elements which are typically concentrated in the continental crust. Another possible mechanism for the production of the andesites is by the mixing of bimodal endmembers. If this were the

case in the Sangre area the continental influence seen in the felsic rocks would be expected to be seen in the intermediates and it is not.

The andesites from the nothern Sangre de Cristo area show more similarities in their composition to the mafic rocks than the felsic rocks. Andesites formed by fractional crystallization of a mafic source will retain a memory of that source. MORB-normalized trace element patterns for the mafic igneous rocks show strong similarities to modern basalts from continental margin arcs or evolved island arcs and their associated back-arc basins. The andesites show the greatest similarities in their MORB-normalized trace element patterns to modern andesites from continental margin arcs. The mafic rocks show arc affinities on all the trace element discriminatory diagrams (Figures 15-17), and although the andesites show considerable scatter on most plots they also plot in or near arc fields. Neither basalts nor andesites show within-plate characteristics on any of the various discriminatory diagrams. Some of the rocks of andesitic character found in the area probably represent metasediments while others represent true andesites that are genetically related to the mafic rocks. This necessitates that both eruptive and depositional histories were similar and based on their composition, it suggests that they were deposited in a setting similar to that of a modern continental margin or evolved island arc.

Felsic rocks

The felsic volcanic rocks of the northern Sangre de Cristo area do not appear to be genetically related to the mafic and intermediate rocks although they occur interlayered in the same successions. Geochemical modeling does not favor the production of the felsic volcanic rocks from a mafic source by fractional crystallization. Little correlation can be seen between the calculated felsic magma produced by successive fractional crystallization of a mafic source and the actual composition of felsic samples analyzed. Besides the geochemical evidence against this origin for the felsic volcanic rocks, there is a significant volume problem. If the felsic rocks represent fractional cryatallization products of the last remaining mafic magma, how can the relative abundance of the felsic rocks (~30% of the section) be explained? The amount of mafic magma needed to produce the amount of felsic rocks observed is much greater than the amount represented by the mafic rocks in the area. It is possible that a significant volume of mafic rock is not exposed but its composition would have to be different than the mafic rocks analyzed to serve as a parent for the felsic volcanic rocks.

Geochemical modeling shows that the calculated granitic source for the felsic volcanic rocks does show some similarities to tonalite but the results are not conclusive. MORB-normalized patterns of the felsic volcanic rocks are similar to those of modern rhyolites from continental margin-arc and rift settings. Trace element discriminatory diagrams also suggest significant continental influence in the petrogenesis of the felsic volcanic rocks. They show concentrations of elements such as Zr, Hf, and Y that are higher than those characteristic of felsic volcanics from oceanic settings. The felsic volcanic and volcaniclastic rocks are all similar in their composition and appear to have been formed in a continental margin-arc or rift setting. The composition of the felsic rocks, their abundance and field relationships to other rocks in the area, and geochemical modeling suggest that these rocks were derived by partial melting of a tonalitic parent in the lower crust.

Relationship of the Sangre de Cristo Supracrustal rocks to adjacent areas

As discussed in the preceeding sections the supracrustal rocks of the northern Sangre de Cristo area appear to have been formed in a continental margin or evolved island arc setting. The mafic and intermediate volcanic rocks appear to have been derived by fractional crystallization and are believed to be genetically related, both have arc characteristics. The felsic volcanic rocks appear to have been derived by partial melting of a continent source.

The northern Sange de Cristo succession is bound by supracrustal rocks of the Salida Greenstone belt to the west and the Wet Mountains Succession to the east. The relationship of these successions to the Sangre succession can be inferred based on available zircon age dates, geochemistry, and field relations.

The Salida Greenstone belt is a well preserved Early Proterozoic bimodal volcanogenic complex. The felsic volcanic rocks have been dated at 1730 Ma (Bickford and Boardman, 1984) and occur as massive submarine ash-flows and volcaniclastic sedimentary rocks (Rossen, Pearcy and Boardman, 1982). The Mafic volcanic rocks occur as gabbro sheets, basalt flows and volcaniclastic rocks (Boardman, 1982). Minor pelitic and

semi-pelitic rocks are found in the section. Primary textures are much more well preserved in the Salida section than the Sangre succession but both successions show strong similarities in the composition and occurence of their volcanic rocks. Both successions are intruded by the Garrel Peak-Cotapaxi (GPC) batholith (1670 Ma) so that their lithologic boundary is no longer expressed.

The Sangre sucession appears to be younger (1670-1710 Ma) than the Salida succession (1730 Ma). Pendants and inclusions found along the western margin of the GCP batholith appear to represent those of the Sangre succession but a correlation based on age dates needs to be made do to the metamorphic deformation of these inclusions and the similarities between the rock types seen in both the Sangre and Salida successions. It is possible that the supracrustal rocks exposed along the northern side of the Arkansas River and extending as inclusions into the western boundary of the GCP batholith may belong to the Salida succession. Age dates from the two sucessions show the Sangre sucession to be younger but based on similarities in compositions, depositional histories and the fact that these rocks represent the most easterly occurence of metavolcanics in the area they are believed to be related to the Salida succession.

The Wet Mountain succession to the east is composed of a migmitite-gneiss terrane believed to be representative of a clastic sediment association

(Lanzirotti and Condie, 1986). Intrusive amphibolites and leucogranites are also found throughout the area. The amphibolites appear to exhibit arc-related affinities similar to the mafic volcanic rocks of the Sangre succession. Granites from the area have been dated and provide a minimum age of approximately 1740 Ma for the Wet Mountain gneisses. Although age dates are not conclusive it appears that the Wet Mountain succession is older than the Sangre succession.

The GCP batholith appears to have intruded along a major early Proterozoic lithologic boundary with a volcanic association on the west and a clastic sediment association on the east. The nature of the boundary may be preserved in the GCP batholith. As the batholith is traversed from west to east the nature of the inclusions changes from being dominantly volcanic/volcaniclastic to more gneissic in character. Futher to the east the inclusions are dominantly gneissic and migmititic in nature. Inclusion and pendent populations are not prevalent enough to make a clear distinction of this boundary but an area where the boundary may occur can be inferred (Fig.1a). Both field and geochemical evidence show that the northern Sangre de Cristo succession is volcanic in origin and the Wet Mountain succession is dominantly clastic in origin. Both successions had different depositional histories and data suggest they represent different tectonic settings. The Sangre

succession appears to represent a younger continental margin-arc association and the Wet Mountain succession appears to represent an older dominantly clastic sediment association which may have been formed in a back-arc basin developed within or near continental crust (Lanzirotti and Condie, 1986).

CONCLUSIONS

Based on the field and geochemical evidence presented, the northern Sangre de Cristo succession appears to have been formed in a continental margic-arc, with its associated back-arc basin, tectonic setting. Eruption of both mafic/intermediate and felsic magmas took place at the same time, although eruptive centers may have been separated by many kilometers. Deposition of both mafic/intermediate and felsic volcanics was synchronious within the basin, producing the interlayered relationships represented in the rocks. Pelitic sediments were also deposited in the basin but not in significant quantities compared to the mafic and felsic volcanic rocks. This type of association is typical of Early Proterozoic rocks of southern Colorado (Afifi,1981; Barker,1969; Bickford and Boardman,1984; Bennett,1984; Condie and Nuter,1981) and northern New Mexico (Bowring et al.,1984; Condie,1984; Condie and Budding,1979; Wobus,1984).

The Sangre and Salida successions appear to have had similar depositional histories. Both successions are believed to be related although age dates indicate that at least parts of the Sangre succession are younger. If there is a lithologic boundary with the Sangre succession representing a younger (1670-1710 Ma) volcanic terrrane

and the Salida succession representing a similar older (1730-1740 Ma) volcanic terrane, this boundary no longer is exposed or has been destroyed by the intrusion of the GPC batholith. Further age dates are necessary to determine the actual relationship of the two terranes.

The Sangre and Wet Mountain terranes do not appear to have been formed in similar tectonic settings. Field evidence, age dates and geochemistry point to separate depostional histories for the two terranes. The Sangre terrane represents the most easterly extent of a volcanic association and the Wet Mountain terrane represents a clastic sedimentary association. The lithologic boundary separating these two terranes is no longer identifiable. Field evidence suggests an area within the GPC batholith where xenoliths of both populations may exist but further study is required to confirm this.

Afifi, A. M., 1981. Precambrian Geology of the Iris Area, Gunnison and Saguache counties, Colorado. Unpub. M.S. Thesis, Colorado School of Mines, Golden, CO. 197p.

Basaltic Volcanism Study Project, 1981. Basaltic Volcanism on the Terrestrial Planets: New York, Pergamon Press, 1286p.

Barker, F., 1969. Precambrian Geology of the Needle Mountains, southwestern Colorado. U. S. Geol. Survey, Prof. paper 644-A, 35p.

Bowling, G.P., 1987. Geology and Geochemistry of Early Proterozoic Supracrustal Rocks from the western Dos Cabezas Mountains, Cochise County, Arizona, unpub. M.S. Thesis, New Mexico Institute of Mining and Technology.

Boardman, S.J., 1985. Early Proterozoic Subaqueous Bimodal Volcanic Rocks in central Colorado, part I, 51p., part II 29p.

Bickford, M.E., and S.J. Boardman, 1984. A Proterozoic Volcanic-Plutonic Terrane, Gunnison and Salida areas, Colorado. Jour. Geol., 92, p. 657-666.

Bowering, S.A., J.C. Reed, and K.C. Condie, 1984. U-Pb Geochronology of Proterozoic Volcanic and Plutonic Rocks, Sangre de Cristo Mountains, NM Geol. Soc. Am., Abstract with programs, 16, p.216.

Carmichael, I.S.E., F.J. Turner, and J. Verhoogan, 1974. Igneous Petrology. McGraw-Hill, New York, NY, 739p.

Condie, K.C., 1986. Plate-tectonics Model for Continental Accretion in the southwestern United States: Geology, Vol. 10, pp. 37-42.

Condie, K.C., 1986. Geochemistry and Tectonic Setting of Early Proterozoic Supracrustal Rocks in the southwestern United States: Jour. Geol., Vol. 94, pp. 845-864.

Condie, K.C. and A.J. Budding, 1979. Geology and Geochemistry of Precambrian Rocks, central and south-central New Mexico: New Mexico Bureau of Mines and Mineral Resources, Memoir 35, 58p.

Condie, K.C. and T. McCrink, 1982. Geochemistry of Proterozoic Volcanic and Granitic Rocks from the Gold Hill-Wheeler Peak area, northern New Mexico. Precamb. Res., 19, pp. 141-166.

Condie, K.C. and J.A. Nuter, 1981. Geochemistry of the DuBois Greenstone Succession: An Early Proterozoic Bimodal Volcanic Association in West-Central Colorado. Precamb. Res., 15, pp. 131-155.

Condie, K.C., 1982. Plate Tectonic Model for Proterozoic Continental Accretion in the southwestern United States: Geology, Vol. 10, pp. 37-42.

Condie, K.C., P.G. Bouling, and K.R. Vance, 1985. Geochemistry and Origin of Early Proterozoic Supracrustal Rocks, Dos Cabezas Mountains southeastern Arizona: Geololical Society of America Bulletin, Vol. 96, pp. 622-655.

Copeland, P., 1986. Geochemistry and Geology of the Pinal Schist, Cochise and Pina counties, Arizona: unpub. M.S. Thesis, New Mexico Institute of Mining and Technology, 176p.

Deer, W.A., R.A. Howie, and J. Zussman, 1966. An Introduction to the Rock Forming Minerals: London, Longman Group Ltd., 528p.

De Malas, J.P., 1983. The Geology, Petrology, and Provenance of the Pinal Schist: unpub. M.S. Thesis, New Mexico Institute of Mining and Technology, Socorro, NM, 128p.

Ehlers, E.G., and H. Blatt, 1982. Petrology: Igneous, Sedimentary, and Metamorphic, W.H. Freeman and Co., 732p.

Gordon, E.E., K. Randie, G.G. Goles, J.B. Corlis, M.H. Beeson, and S.S. Oxley, 1968. Instrumental Neutron Activation Analysis of Standard Rocks with High Resolution Gamma-Ray Detectors. Geochem. Cosmochem. Acta, Vol. 32, pp. 369-396.

Irvine, T.N. and W.R.A. Barager, 1971. A Guide to the Chemical Classification of Common Volcanic Rocks: Canadian Journal of Earth Science, Vol. 8, pp.523-548.

Jensen, L.S., 1976. A New Cation Plot for Classifying Subalkaline Volcanic Rocks. Ontario Division of Mines Misc., paper 66, 22p.

Karlstrom, K.E., and R.S. Houston, 1984. The Cheyenne Belt: Analysis of a Proterozoic Suture in southern Wyoming: Precamb. Res., Vol. 25, pp.415-446.

Kroner, A., 1981. Precambrian Plate Tectonics, in Kroner A. Ced., Precambrian plate tectonics: Amsterdam, Elsevier, pp.57-90.

Pearce, J.A., 1982. Trace Element Characteristics of Lavas from Destructive Plate Boundaries, in Thorpe, R.S. Ced., Andesite: John Wiley and Sons, pp.525-548.

Pearce, J.A., 1983. Role of the Subcontinental Lithosphere in Magma genesis at Active Continental Margins, in Continental Basalts and Mantle Xenoliths, Hawksworth, C.J., and Narry, M.J., (eds.): Shiva Publishing Ltd., Nantwich, U.K., pp.230-249.

Pearce, J.A., and J.R. Cann, 1973. Tectonic Setting of Basic Volcanic Rocks Determined Using Trace Element Analysis: Earth Plan. Sci. Lett., Vol. 19, pp. 290-300.

Pearce, J.A. and M.J. Narry, 1979, Petrogenetic Implications of Ti, Zr, Y, and Nb Variations in Volcanic Rocks: Contrib. Mineral Petrol., Vol. 69, pp. 33-47.

Pharaoh, T.C., and J.A. Pearce, 1984. Geochemical Evidence for the Geotectonic Setting of Early Proterozoic Metavolcanic Sequences in Lapland: Precamb. Res., Vol. 25, pp.283-308.

Robertson, J.M., 1984. Geology and Geochemistry of the Early Proterozoic Pecos Greenstone Belt, southern Sangre de Cristo Mountains, New Mexico, [abs.]: Geol. Soc. America Abstracts with Programs, Vol. 16, no. 4, pp. 252.

Shadel, C.A., 1982. The Geology and Geochemistry of the Proterozoic Metavolcanic and Volcaniclastic Rocks of the Green Mountain Formation Sierra Madre Range, Wyoming: Unpub. M.S. Thesis, New Mexico Institute of Mining and Technology, 164p.

Taylor, S.R. and S.M. McLennan, 1985. The Continental Crust: Its Composition and Evolution: Oxford, Blackwell Sci. Pub., 312p.

Winchester, J.A. and P.A. Floyd, 1977. Geochemical Discrimination of Different Magma Series and Their Differentiation Products Using Immobile Elements: Chem. Geol., Vol. 20, pp. 325-343.

Wood, D.A., 1979. A Variably Veined Suboceanic Upper Mantle - Genetic Significance for Mid-Ocean Ridge Basalts from Geochemical Evidence: Geology, Vol. 7, pp. 499-503.

Wright, T.L. and P.C. Doherty, 1970. A Linear Programming and Least Squares Computer Method for Solving Petrologic Mixing Problems: Geol. Soc. America Bull., Vol. 8, pp. 1995-2008.

Appendix A: SAMPLE LOCATIONS

Geographic location of northern Sangre samples used for chemical analysis and/or petrographic examination

TSC-4 38 21'47"N, 105 53'20"W, Bushnell Peak Quadrangle, 12800'

TSC-14 38 21'08"N, 105 53'02"W, Bushnell Peak Quadrangle, 12300'

TSC-3 38 21'37"N, 105 53'15"W, Bushnell Peak Quadrangle, 11900', Twin Sisters

TSC-19 38 20'34"N, 105 53'13"W, Bushnell Peak Quadrangle, 12600', Bushnell Peak

TSC-8 38 21'08"N, 105 54'05"W, Bushnell Peak Quadrangle, 13000', Twin Sisters

TSC-10 38 22'25"N, 105 54'55"W, Bushnell Peak Quadrangle, 12500', Red Mountain

TSC-15 38 21'00"N, 105 53'17"W, Bushnell Peak Quadrangle, 12400', Bushnell Peak

TSC-16 38 20'55"N, 105 53'25"W, Bushnell Peak Quadrangle, 12500', Bushnell Peak

TSC-2 38 21'17"N, 105 53'07"W, Bushnell Peak Quadrangle, 11500', below Stout Creek lakes, Twin Sisters

TSC-7 38 21'13"N, 105 51'18"W, Bushnell Peak Quadrangle, 12900', Twin Sisters

TSC-20 38 20'26"N, 105 53'16"W, Bushnell Peak Quadrangle, 13105', Bushnell Peak

TSG2-9 38 28'29"N, 105 48'27"W, Howard Quadrangle, 7650', Sand Gulch

TSG2-4 38 28'03"N, 105 48'10"W, Howard Quadrangle, 7425', Sand Gulch

TSG-5 38 29'36"N, 105 45'30"W, Howard Quadrangle, 9400', Sand Gulch

TSG-6 38 29'39"N, 105 45'42"W, Howard Quadrangle, 9575', Sand Gulch

TSG-15 38 29'38"N, 105 46'35"W, Howard Quadrangle, 9200', Sand Gulch

TSG-21 38 28'12"N, 105 45'20"W, Howard Quadrangle, 9650', Burned Timber Mountain

TSG-23 38 29'15"N, 195 44'10"W, Cotopaxi Quadrangle, 9259', Park Mountain

TSG2-7 38 27'47"N, 105 47'57"W, Howard Quadrangle, 8100', Sand Gulch

TSG2-2 38 28'00"N, 105 48'14"W, Howard Quadrangle, 7650', Sand Gulch

TSG2-6 38 27'55"N, 105 48'00"W, Howard Quadrangle, 7670', Sand Gulch

TSG2-5 38 27'50"N, 105 48'10"W, Howard Quadrangle, 7660', Sand Gulch

TSG-3D 38 29'58"N, 105 48'10"W, Howard Quadrangle, 9250', Sand Gulch

TSG-11 38 28'43"N, 105 46'15"W, Howard Quadrangle, 9200', Sand Gulch

TKG-1 38 25'25"N, 105 46'33"W, Howard Quadrangle, 7450', Kiln Gulch

TKG-2 38 25'22"N, 105 46'31"W, Howard Quadrangle, 7420', Kiln Gulch

TGP-4 38 23'56"N, 105 45'12"W, Howard Quadrangle, 7850'

THP-1 38 23'04"N, 105 55'55"W, Wellsville Quadrangle, 11400', Hunts Lake

THP-P1 38 23'00"N, 105 56'40"W, Wellsville Quadrangle, 13071', Hunts Peak

THP-P2 38 23'05"N, 105 56'34"W, Wellsville Quadrangle, 13050', Hunts Peak

THP-P3 38 22'58"N, 105 56'03"W, Wellsville Quadrangle, 11300', Hunts Lake

TBC-13 38 29'55"N, 105 57'02"W, Wellsville Quadrangle, 7350', Bear Creek

TSP-1 38 25'26"N, 105 59'03"W, Wellsville Quadrangle, 11900', Simmons Peak

TSP-7 38 24'56"N, 105 58'00"W, Wellsville Quadrangle, 11700', Simmons Peak

THC-5 38 24'04"N, 105 55'50"W, Wellsville Quadrangle, 10275', Porter Gulch

THC-7 38 24'10"N, 105 55'42"W, Wellsville Quadrangle, 10050', Porter Gulch

TTC-1 38 36'40"N, 105 48'40"W, Cameron Mountain Quadrangle, 9220'

TEB-1 38 35'00"N, 105 48'30"W, Cameron Mountain Quadrangle, 9025', East Badger Creek

TEB-2 38 35'08"N, 105 48'53"W Cameron Mountain Quadrangle, 9100', East Badger Creek

TEB-3 38 35'12"N, 105 48'55"W, Cameron Mountain Quadrangle, 9150', East Badger Creek

TEB-5 38 35'10"N, 105 49'50"W, Cameron Mountain Quadrangle, 8600', East Badger Creek

Appendix B: Sampling and Analytical Procedures

SAMPLING

During field work approximately 150 samples were collected in triplicate from the locations shown in Appendix A. One sample is kept for reference, one sample is used for thin section study, and one sample is used for geochemical analysis. Much care was taken to avoid all weathered surfaces and veining and to obtain fresh samples that were representative of the outcrop. Of the samples collected, 23 were selected for thin section study and a representative suite of 41 samples were selected for chemical analysis.

SAMPLE PREPARATION

One sample from each triplicate was chosen for geochemical study and crushed to thumbnail size using a large mechanical jaw crusher. Pieces that appeared to have any metal or oxidation on their surfaces were discarded. Samples were reduced to a fine powder using temamill and rotary porcelain grinders. These techniques are designed to avoid contaminating the samples.

INSTRUMENTAL NEUTRON ACTIVATION ANALYSIS

Trace elements analyzed by instrumental neutron activation were Ba, Ce, Co, Cr, Cs, Eu, Hf, La, Lu, Ni, Sc, Sm, Ta, Tb, Th, U and Zn. The methods used are similar to those described by Jacobs et al. (1977) and Gibson and Jacobs (1980). Polyethylene vials containing approximately 300 mg of samples are irradiated in the Annular core Research Reactor at Sandia National Laboratory, Albuquerque, New Mexico. The samples are subjected to a neutron flux of approximately 2.7×10^{13} for ten thousand seconds. To assure an even flux, air is supplies to the irradiation chamber. Seven and forty days after the samples are irradiated gamma rays are counted using a coaxial intrinsic Ge-crystal detector along with a Nuclear Data 6600 multichannel analyser and LSI-11 computer. Reference samples of approximately 200 mg of fly ash standard NBS-1633 are irradiated with the samples for reference. Other rock standards are irradiated and analyzed with the samples to determine the accuracy of the data. As a further test of accuracy five samples of TSG-3 were anayzed and critical values for the analytes were calculated. The data is reduces by using TEABAGS

(Trace Element Analysis By Automated Gamma-ray Spectrometry, Lindstom and Korotev, 1982) software.

X-RAY FLUORESCENCE

Major and trace elements Zr, Rb, Sr, Y, Nb, Ni, Zr, Ga, Pb, and V were determined by X-ray flouresecence (XRF) uing an automated Rigaku 3064 XRF spectrometer and PDP-11 computer and software at New Mexico Bureau of Mines and Mineral Resources. The analyses involved two techniques following the methods of Norrish and Hutton (1969) and Norrish and Chappel (1977). Fused disks were made from ~ 0.5 grams of powdered sample and ~ 2.7 grams of lithium borate flux by fusing them in a Pt crucible to ~ 900°C for 5 minutes, then placing the liquid into a mechanical press and mold to cool. These disks are then used to analyze for the major elements (SiO2, TiO2, Al2O3, Fe2O3-T, Mgo, Cao, Na2O, K2O, MnO, P2O5). Pressed pellets were made with a boric acid backing using one drop of polyvinyl alcohol as a binder per gram of sample and about 8 grams of powder. The mixture is exposed to a pressure of 10 tons for five minutes using a hydraulic press. These pellets are used to analyze for the trace elements (Zr, Rb, Sr, Y, Nb, Cu, Ni, Zn, Ga, Pb).

Appendix C: Accuracy of major and trace elements analyzed by XRF and INAA. Accuracy is determined by comparing the mean value of standards run in triplicate, to the known value from the literature and is expressed in a percentage of the variance of the mean to the actual value.

Accuracy = known value - instrumental value / known x 100

major element (%)	mean BLCR (n=3)	known BLCR	accuracy (%)
SiO2	55.6	55.65	0.09
TiO2	0.84	0.87	6.6
Al2O3	16.94	16.97	0.18
Fe2O3-T	7.21	7.43	2.96
MnO	0.12	0.13	6.15
MgO	6.02	5.86	2.7
CaO	7.79	7.9	1.4
Na2O	3.79	3.72	1.88
K2O	1.38	1.45	4.48
P2O5	0.162	0.16	1.25

trace element (ppm) XRF	mean BCR-1 (n=3)	known BCR-1	accuracy (%)
Rb	48.5	46.6	4.01
Sr	331.0	330.0	0.30
Y	37.6	37.1	1.35
Zr	184.4	190.0	2.95
Nb	12.77	13.5	5.40

INAA	mean BLCR (n-3)	known BLCR	accuracy (%)
Sc	32.85	32.0	5.78
Cr	142.15	160.0	11.15
Co	32.6	29.0	12.4
U	1.55	1.5	3.3
Ce	28.15	26.7	5.4
Sm	4.11	3.7	11.1
Eu	1.34	1.3	3.07
Tb	0.75	0.78	3.8
Yb	3.27	3.1	5.48
Lu	0.56	0.52	7.7
Hf	4.7	4.3	9.3
Ta	0.38	0.42	9.5
Th	4.04	4.1	1.22

Appendix D: Calculated Critical values (C.V.) for the five samples of TSG-3 analyzed to aid in the determination of accuracy of INAA data. The C.V. is a measure of the percentage the samples vary from the calculated mean of the five samples analyzed.

C.V. = standard deviation (STD.) / mean X 100

element (ppm)	mean TSG-3 (n=5)	STD.	C.V.(%)
Sc	10.56	1.29	12.2
Cr	2.04	0.96	47.0
Co	5.56	0.59	10.6
Cs	6.97	0.41	5.8
U	2.67	0.32	11.9
La	36.6	6.35	17.3
Ce	143.0	22.7	15.8
Sm	16.9	1.46	8.6
Eu	2.27	0.37	16.2
Tb	2.9	0.2	6.9
Yb	9.5	0.94	9.9
Lu	1.37	0.08	5.8
Hf	16.78	2.7	16.1
Ta	1.61	0.08	4.9
Th	3.3	0.49	14.8

Appendix D: Calculated Critical values of standards run to determine the accuracy of the major and trace element data determined by XRF.

major element (%)	mean BLCR (n=3)	STD.	C.V. (%)
SiO2	55.6	0.106	0.19
TiO2	0.84	0.002	0.23
Al2O3	16.94	0.026	0.15
Fe2O3-T	7.2	0.015	0.2
MgO	6.04	0.037	0.61
CaO	7.79	0.026	0.33
Na2O	3.79	0.057	1.5
K2O	1.38	0.002	0.18
MnO	0.122	0.001	1.23
P2O5	0.162	0.002	1.23

trace element (ppm)	mean ANG (n=3)	STD.	C.V. (%)
Rb	0.83	0.14	16.86
Ba	41.0	6.08	14.8
Sr	75.6	0.95	1.25
Pb	11.18	1.67	14.9
Y	9.7	0.2	2.06
Zr	13.2	1.1	8.3
Nb	2.5	0.49	19.6

Appendix E: Sample spread sheet from MIXFRAC for closed system fracti
crystallization.

MIXFRAC: Least-Squares Mixing Program
Attempt: 8

USING TEB-2

>> Input Data:

	AND1	CPX	PLG	MAG	OL	BAS1
SiO2	60.63	50.88	51.65	0.28	40.34	48.19
TiO2	1.00	0.52	0.08	0.00	0.01	0.78
Al2O3	15.03	1.72	29.40	0.21	0.00	16.13
Fe2O3	9.36	14.54	0.00	99.63	14.29	10.45
MnO	0.20	0.54	0.00	0.00	0.17	0.17
MgO	1.82	13.99	0.16	0.00	47.10	9.35
CaO	3.76	18.17	13.38	0.00	0.19	11.20
Na2O	4.93	0.00	3.68	0.00	0.00	2.15
K2O	2.38	0.00	0.18	0.00	0.00	0.44
P2O5	0.39	0.00	0.00	0.00	0.00	0.13
TOTAL	99.50	100.36	98.53	100.12	102.10	98.99

>> Output Data:

	Y.OBS.	Y.EST.	RESIDUALS
SiO2	48.19	48.20	-0.0110
TiO2	0.78	0.27	0.5120
Al2O3	16.13	16.10	0.0305
Fe2O3	10.45	10.45	-0.0000
MnO	0.17	0.17	-0.0008
MgO	9.35	9.34	0.0093
CaO	11.20	11.19	0.0060
Na2O	2.15	2.28	-0.1286
K2O	0.44	0.33	0.1067
P2O5	0.13	0.04	0.0896
TOTAL	98.99	98.38	SQUARED RESIDUALS = 0.2993

COMPONENT	PROPORTION
AND1	0.1037
CPX	0.2397
PLG	0.4803
MAG	0.0427
OL	0.1215

Appendix E: Sample spread sheet from MODULUS for open system fractiona crystallization.

ID for Cl: T3C-2.ANO
ID for Co: TE3-2.BAS

	INPUT: Co	Cl	MINERAL	MODE	OUTPUT: D	Obs Cl/Co	Calc Cl/Co	SRS
Rb	9.1	61.9	AMPHI	0.000	0.0748	6.825	9.368	0.357
Ba	131	1200	CPX	0.000	0.1829	9.234	2.386	0.458
K	0	0	OLIVI	0.140	0.0826	6.818	8.229	0.276
Sr	401	178	MGT	0.050	1.0711	0.445	0.340	1.231
Th	1.00	5.87	OPX	0.290	0.0846	5.870	9.680	0.199
U	0.72	3.09	PLAG	0.520	0.0513	4.292	8.542	0.081
La	6.21	36.70	ZIR	0.000	0.0997	5.910	9.191	0.212
Ce	16.60	84.40	APAT	0.000	0.0924	5.084	8.240	0.132
Nd	0.00	0.00	QTZ	0.000	0.1064	ERR	8.148	0.000
Sm	3.18	9.12	GAR	0.000	0.1518	2.914	2.879	.000
Eu	1.18	2.56	spare A	0.000	0.2394	2.169	2.236	0.001
Tb	0.44	1.40	spare B	0.000	0.1804	3.182	2.790	0.020
Yb	1.63	4.20			0.2132	2.435	2.576	0.001
Lu	0.27	0.69	TOTAL	1.000	0.1784	2.556	2.740	0.005
Y	15.0	43.2			0.1720	2.887	2.772	0.002
Sc	49	21			0.7428	0.431	1.281	8.878
Hf	2.10	5.58			0.1178	2.657	8.076	0.025
Ta	0.03	0.69			0.0674	7.667	8.418	0.307
Ti	1	1			0.4856	1.282	1.721	0.117
Zr	42.2	190.2			0.0406	4.275	8.629	0.028
Nb	4.2	11.7			0.0556	2.771	8.508	0.071
P	0	0			0.0000	8.000	4.000	0.111
Ni	165.2	0.0			4.2140	0.000	0.157	ERR
Co	60.1	9.6			1.8809	0.160	0.784	12.913
Cr	385.0	4.5			*******	0.018	0.015	0.017
V	274	86			1.6050	0.313	0.624	0.331

M. F. XTALS: X = 0.800
M. F. LEAK: Y = 0.100
M. F. INJECT: Z = 0.400
M. F. CONTAM: W = 0.000

Total Sqr Residuals = ERR
LILE Sqrd Residuals = 2.351
HFSE Sqrd Residuals = 9.654
REE Sqrd Residuals = 0.871
COMP Sqrd Residuals = ERR

Notes:

Appendix F: Equations Used in Geochemical Modeling

Fractional Crystallization

$$\frac{C_l}{C_o} = F^{(D-1)}$$

Batch Melting

$$\frac{C_l}{C_o} = \frac{1}{D+F(1-P)}$$

$$D = \sum m_i K_d$$

$$P = \sum p_i K_d$$

where

C_o = initial concentration of an element

C_l = instantaneous concentration of an element in the liquid

F = fraction of melt

D = bulk distribution coefficient

P = bulk distribution coefficient for melting

K_d = distribution coefficient for an element (mineral/liquid)

m_i = mass fraction of a mineral in source rock or solid cumulate

p_i = mass fraction of a mineral entering the melt

Appendix G: Recommendations for future work

Before the geology and geochemistry of the northern Sangre de Cristo area can be fully understood a thorough field, structural, geochemical, and geochronological survey is needed. Metamorphism has destroyed many of the primary textures in the volcanic rocks but a detailed field study will undoubtly reveal primary textures not observed in this study that will lend more insight into the eruptive and depositional history of these rocks. No detailed structural study has been undertaken in the area and the need for a detailed structural analysis of the rock units is neccesary to better understand their relationships to one another. Although no major folding is observed in the area the possibility of very large scale isoclinal folds exists so that the units may actually repeat themselves. The sample population analyzed in this study was minor in comparison to the variety of rock types observed in the area. A thorough geochemical study involving a large representative suite of samples is important to verify the findings of this study and shed further light on the geochemical classification of the volcanic rocks. Geochronology could perhaps provide the greatest insight into the relationships of the various terranes we see exposed today. Until more U-Pb zircon dates for the volcanic rocks are available subdivision of the Proterozoic

terranes in this area is not possible.